Causes and prevention of irrigation blockages in the bioleaching process

Case study: Terrafame mine

Author: Wojciech Strycharski

Delft

August 29, 2017

Causes and prevention of irrigation blockages in the bioleaching process. Case study: Terrafame mine.

By

Wojciech Strycharski

in partial fulfilment of the requirements for the degree of

Master of Science

in Applied Earth Sciences

at the Delft University of Technology,

to be defended publicly on Tuesday August 29, 2017 at 10:00 AM.

Thesis committee : Prof.dr.ir. Timo Heimovaara (TU Delft)
Dr. ir. Dominique Ngan-Tillard (TU Delft)
Dr. ir. Doris van Halem (TU Delft)
Dr inż. Agnieszka Pawłowska (Politechnika Wrocławska)
Dr. Ferenc Mádai (Miskolci Egyetem)
Antti Arpalahti (Terrafame Oy)

TU Delft Politechnika Wrocławska MISKOLCI EGYETEM Terrafame

Abstract

Blockages in irrigation during bioleaching operation cause additional production costs and might negatively influence metals yield. The main research question was to find out if the lifetime of the irrigation system can be extended. Production process was investigated from various angles in search of causes and patterns of solution flow blockages due to calcium sulfate precipitation which was identified as the main reason of clogging. Large number of process data was statistically analyzed. Clear correlation between the PLS temperature and calcium concentration in the solution was drawn and it was found that it is far different from any other research presented. Calcium solubility was experimentally tested – solution was cooled down to approx. 4 °C and agitated daily. Results were unclear, however, on average, calcium concentration decreased by approx. 100 mg/L. The ambiguity of the initial solubility trials led to designing a new experiment. Investigation of the system pointed out critical points and allowed for the formulation of clogging control strategy. Primary calcium sources were found within the ore and metals recovery plant; sulfate is produced during bioleaching process and added to the solution with sulfuric acid – pH control. Forced precipitation of gypsum was proposed as the most viable solution. Conceptual precipitation pond was proposed based on seeded batch crystallization of gypsum. Moreover, clogging was found more prominent in areas with lower pressure head thus redesigning of the irrigation system was suggested along with implementing pulsating pressure. The outcomes of this study set a new direction for the company to counter calcium precipitation problem.

Table of contents

ABSTRACT .... **I**

LIST OF TABLES .... **V**

ACKNOWLEDGMENTS .... **XI**

1. INTRODUCTION **1**

1.1. MOTIVATION 3
1.2. RESEARCH QUESTIONS 6

2. CONCEPTUAL MODEL OF THE SITE **9**

2.1. GEOLOGY AND ORE MINERALOGY 9
2.2. BIOLEACHING PROCESS 10
2.3. IRRIGATION SYSTEM 12
2.3.1. Emitters *13*
2.3.2. Laterals and mains *16*
2.3.3. Drip line type used in Terrafame *17*
2.3.4. Design of the irrigation system in Terrafame *19*
2.3.5. Leachate circulation *22*
2.4. METALS RECOVERY PLANT 24

3. CLOGGING PHENOMENA **25**

3.1. SOLIDS FOUND IN THE IRRIGATION SYSTEM 26
3.2. CALCIUM SULFATE SOLUBILITY 28
3.2.1. Theoretical background *28*
3.2.2. Solubility of calcium sulfate in pure water and standard conditions ... *33*
3.2.3. Solubility of calcium sulfate in hydrometallurgical process solutions .. *35*
3.3. CALCIUM SULFATE PRECIPITATION FROM SOLUTIONS 42
3.3.1. Scale formation *42*

3.3.2. Effect of process parameters on gypsum scale formation 43
3.4. EMITTER CLOGGING 48
3.4.1. Literature review 48
3.4.2. Emitter clogging in Terrafame 50

4. EXPERIMENTAL PART 51

4.1. CHARACTERIZATION OF THE SOLIDS 51
4.2. CALCIUM SULFATE SOLUBILITY TESTS 53
4.2.1. Motivation 53
4.2.2. Methodology for the initial tests 54
4.2.3. Results and conclusions from the initial tests 55
4.2.4. Methodology for concise tests 58
4.3. DRIPLINE TESTS 60
4.4. DRIP LINE INSPECTIONS 68
4.5. CONCLUSIONS 71

5. DATA ANALYSIS 72

5.1. DATA SETS 73
5.1.1. Leachate composition 73
5.1.2. Ambient temperature 76
5.1.3. Operational information 76
5.2. METHODOLOGY 77
5.3. RESULTS 78
5.3.1. Outliers analysis of the process data 78
5.3.2. Correlation analysis 82
5.3.3. Calcium concentration data 85
5.3.4. Operational data analysis 90
5.4. CONCLUSIONS 98

6. CLOGGING CONTROL STRATEGY 100

6.1. GYPSUM CONSTITUENT INFLUX CONTROL 100
6.2. REDUCTION OF CALCIUM IONS CONCENTRATION 102

6.2.1. Chemical precipitation 103
6.2.2. Physical precipitation 103
6.3. PROCESS RELATED SOLUTIONS 107
6.3.1. Irrigation section design 108
6.3.2. Alternative drip lines 108
6.3.3. Solution temperature control 109
6.3.4. Pulsating pressure and dripline flushing 111
6.3.5. Solution management 114
6.4. MOLECULAR OSCILLATION TECHNOLOGY 115
6.5. SUMMARY 117

7. CONCLUSIONS AND RECOMMENDATIONS 118

7.1. CONCLUSIONS 118
7.2. RECOMMENDATIONS 121

APPENDIX A 122

APPENDIX B 123

APPENDIX C 124

APPENDIX D 126

BIBLIOGRAPHY 129

List of Tables

TABLE 1. TECHNICAL PARAMETERS OF THE AZUD DRIP 16 DRIP LINE (AZUD SISTEMA S.A., 2017). 18

TABLE 2. GIBBS FREE ENERGIES OF FORMATION AT 298.15 K AND 1 BAR (WAGMAN ET AL., 1982). 34

TABLE 3. LIST OF THE MULTI-COMPONENT SYSTEMS FOR WHICH CALCIUM SULFATE SOLUBILITY HAS BEEN EXPERIMENTALLY ESTABLISHED BY DUTRIZAC (2002) AND USED FOR MODELING BY AZIMI ET AL. (2007). 40

TABLE 4. XRF ANALYSIS RESULTS. 53

TABLE 5. SAMPLING POINTS DESCRIPTION FOR THE INITIAL SOLUBILITY TESTS 54

TABLE 6. BASIC STATISTICS OF CALCIUM CONCENTRATION FROM THE INITIAL SOLUBILITY TEST IN MG/L. 55

TABLE 7. TECHNICAL PARAMETERS OF TESTED DRIP LINES. 62

TABLE 8. AVERAGE DRIP LINES LIFETIME ON LEACHING PAD 3. VALUES IN ITALIC REPRESENT AN AVERAGE LIFETIME OF CHANGED DRIP LINE ON EACH HEAP. THE LAST ROW REPRESENTS AVERAGE DRIP LINE LIFETIME PER ONE HOSE CHANGE ON ALL HEAPS; THE LAST COLUMN REPRESENTS AVERAGE DRIP LINE LIFETIME ON EACH HEAP. 91

TABLE 9. AVERAGE DRIP LINES LIFETIME ON LEACHING PAD 4. VALUES IN ITALIC REPRESENT AN AVERAGE LIFETIME OF CHANGED DRIP LINE ON EACH HEAP. THE LAST ROW REPRESENTS AVERAGE DRIP LINE LIFETIME PER ONE HOSE CHANGE ON ALL HEAPS; THE LAST COLUMN REPRESENTS AVERAGE DRIP LINE LIFETIME ON EACH HEAP. 92

List of Figures

FIGURE 1. MAP WITH LOCATION OF THE MINING SITE. SOURCE: WWW.MAPS.GOOGLE.FI. 2

FIGURE 2. DISCHARGE FROM AN EMITTER WORKING IN A SIGNIFICANTLY CLOGGED DRIP LINE. 4

FIGURE 3. ILLUSTRATION OF THE MAIN REACTIONS AND TRANSPORT PROCESSES IN BIOLEACHING OF METAL SULFIDE ORES. ADAPTED FROM: PETERSEN (2010). 11

FIGURE 4. CROSS-SECTION THROUGH A TYPICAL HEAP USED FOR LEACHING WITH PROCESSES INDICATED (PETERSEN & DIXON, 2007). 12

FIGURE 5. IN-LINE EMITTER ASSEMBLY IN THE LATERAL (DASBERG & OR, 1999)....... 13

FIGURE 6. TURBULENT WATER FLOW INSIDE THE LABYRINTH FLOW PATH WITH FLOW “TUNNEL” INDICATED BY THE BLUE ARROW. ADAPTED FROM: DASBERG AND OR (1999). 15

FIGURE 7. (A) AZUD DRIP EMITTER, (B) SOLUTION FLOW IN THE LABYRINTH – WARM COLOR REPRESENTS HIGH FLOW VELOCITY (AZUD SISTEMA S.A., 2017). 18

FIGURE 8. PRESSURE – FLOW RATE CHARACTERISTIC CURVE OF THE AZUD EMITTERS. THE RED CIRCLE INDICATES THE EMITTER USED IN TERRAFAME (AZUD SISTEMA S.A., 2017). 19

FIGURE 9. CROSS–SECTIONAL VIEW OF THE IRRIGATION SYSTEM IN TERRAFAME (NOT IN SCALE). 20

FIGURE 10. TOP VIEW OF THE IRRIGATION CELLS (NOT IN SCALE). BLUE LINES REPRESENT THE IRRIGATION DRIP LINES. 21

FIGURE 11. SIMPLIFIED FLOW CHART OF THE PLS FLOW PATHS IN THE SYSTEM 22

FIGURE 12. PLS FLOW PATH IN PRIMARY LEACHING STAGE (EXAMPLE FOR LEACHING PAD 1). 23

FIGURE 13. PHASE TRANSITION DIAGRAM OF $CaSO_4$ IN H_2O. THE SOLID LINE REPRESENTS STABLE PHASE, DASHED LINE META STABLE (AZIMI ET AL., 2007). . 36

FIGURE 14. EFFECT OF $ZnSO_4$ ON CALCIUM SULFATE SOLUBILITY IN 0.1M H2SO4 SOLUTIONS AT 40 AND 90 °C (DUTRIZAC, 2002). 38
FIGURE 15. PHASE TRANSITION DIAGRAM OF $CaSO_4$ IN H_2SO_4 SOLUTIONS (AZIMI ET AL., 2007). 39
FIGURE 16. $CaSO_4$ SOLUBILITY IN $CaSO_4$-(0.5M) H_2SO_4-H_2O SOLUTION AT 25,45,70 AND 90 °C (AZIMI & PAPANGELAKIS, 2010). 40
FIGURE 17. MASS OF GYPSUM SCALE FORMED DURING THE EXPERIMENT REGARDING THE SOLUTION'S TEMPERATURE. FLOW RATE: 30ML/MIN; RUN TIME: 3H; Ca^{2+} CONCENTRATION: 0.075 M (HOANG ET AL., 2008). 44
FIGURE 18. MASS OF GYPSUM SCALE FORMED DURING THE EXPERIMENT REGARDING THE SUPERSATURATION RATIO, S. FLOW RATE: 30 ML/MIN; RUN TIME: 3H, T=20 °C (HOANG ET AL., 2011). 45
FIGURE 19. MASS OF GYPSUM SCALE FORMED DURING THE EXPERIMENT REGARDING THE RUN TIME. FLOW RATE: 30 ML/MIN; S = 3.75; T=20 °C; PIPE DIAMETERS: (A) 0.7 CM, (B) 1.3 CM (HOANG ET AL., 2011). 46
FIGURE 20. MASS OF GYPSUM SCALE FORMED DURING THE EXPERIMENT REGARDING THE SOLUTION FLOW RATE. RUN TIME: 3H; S = 3.05; T=20 °C; PIPE DIAMETERS: (A) 0.3 CM, (B) 0.5 CM, (C) 0.7 CM, (D) 1.3 CM (HOANG ET AL., 2011). 47
FIGURE 21. XRD RESULTS TABLE 52
FIGURE 22. XRD SPECTRUM IMAGE. 52
FIGURE 23. THE DECREASE IN CALCIUM CONCENTRATION AGAINST THE INITIAL CONCENTRATION, GROUPED BY SAMPLING LOCATION, LEGEND COLOR CORRESPONDS TO THE PLS TEMPERATURE DURING SAMPLING, LINEAR REGRESSION MODEL USED WITH PARAMETERS DISPLAYED ON EACH PLOT. 57
FIGURE 24. LAYOUT OF THE DRIPLINES TEST; DIFFERENT TYPES MARKED ACCORDING TO COLOR. SOURCE: TERRAFAME'S MATERIALS. 61
FIGURE 25. IN-LINE EMITTER PLACED ON A WALL OF THE HOSE (CROSS SECTIONAL VIEW OF THE NETAFIM ARIES DRIP LINE). SOURCE WWW.NETAFIMUSA.COM. 61
FIGURE 26. THE AVERAGE DRIPPING RATE IN THE EASTERN PART OF THE TEST CELL. 64

FIGURE 27. THE NUMBER OF NO FLOW INSTANCES IN THE EASTERN PART OF THE TEST CELL. 65
FIGURE 28. THE AVERAGE DRIPPING RATE IN THE WESTERN PART OF THE TEST CELL. 65
FIGURE 29. THE NUMBER OF NO FLOW INSTANCES IN THE WESTERN PART OF THE TEST CELL. 66
FIGURE 30. THE AVERAGE DRIPPING RATE IN THE TEST CELLS. 66
FIGURE 31. THE TOTAL NUMBER OF NO-FLOW INSTANCES WITH THE AVERAGE VALUE PER HOSE. 67
FIGURE 32. THE OBSERVED DISTRIBUTION OF CLOGGED EMITTERS WITHIN THE SECTION OF IRRIGATION (WHITE COLOR REPRESENTS WORKING EMITTERS; BLACK COLOR REPRESENTS CLOGGED EMITTERS). 70
FIGURE 33. BOXPLOTS OF THE PLS TEMPERATURE IN PRIMARY LEACHING STAGE WITH 1.5IQR TOLERANCE APPLIED. 80
FIGURE 34. BOXPLOTS OF THE PLS TEMPERATURE IN PRIMARY LEACHING STAGE WITH 2.5IQR TOLERANCE APPLIED. 80
FIGURE 35. BOXPLOTS OF THE CALCIUM CONCENTRATION IN PRIMARY LEACHING DATA WITH 1.5IQR TOLERANCE APPLIED. 81
FIGURE 36. BOXPLOTS OF THE CALCIUM CONCENTRATION IN PRIMARY LEACHING DATA WITH 2.5IQR TOLERANCE APPLIED. 81
FIGURE 37. CORRELATION HEAT MAP OF ALL PROCESS DATA. VALUES IN BOXES REPRESENT THE PEARSON'S CORRELATION COEFFICIENT VALUE, BASED ON 28640 OBSERVATIONS, WITH CORRESPONDING SHADES APPLIED. 83
FIGURE 38. CORRELATION HEAT MAP OF THE PRIMARY LEACHING PROCESS DATA. VALUES IN BOXES REPRESENT THE PEARSON'S CORRELATION COEFFICIENT VALUE, BASED ON 19339 OBSERVATIONS, WITH CORRESPONDING SHADES APPLIED. 84
FIGURE 39. AMBIENT TEMPERATURE OBTAINED FROM THE WEATHER STATION IN SOTKAMO (~ 20 KM NE FROM THE SITE) AND RELATIONSHIP TO PLS

TEMPERATURES IN THE OUTFLOW FROM THE HEAPS. THE DISTINCTION BETWEEN TWO MINE OWNERS INDICATED ON THE GRAPH. 85
FIGURE 40. PLS TEMPERATURE IN THE IRRIGATION POND 3 AND THE AVERAGE AMBIENT TEMPERATURE. 86
FIGURE 41. PLS TEMPERATURE IN THE IRRIGATION POND 4 AND THE AVERAGE AMBIENT TEMPERATURE. 87
FIGURE 42. CALCIUM CONCENTRATION RELATIONSHIP TO THE PLS TEMPERATURE FOR ALL PROCESS DATA. REGRESSION LINE INDICATED WITH A RED COLOR; PEARSON'S COEFFICIENT AND P-VALUE IN TOP LEFT CORNER. 88
FIGURE 43. CALCIUM CONCENTRATION RELATIONSHIP TO THE PLS TEMPERATURE FOR PRIMARY LEACHING DATA. REGRESSION LINE INDICATED WITH A RED COLOR; PEARSON'S COEFFICIENT AND P-VALUE IN TOP LEFT CORNER............................. 89
FIGURE 44. TOTAL DISSOLVED IONS INFLUENCE ON CALCIUM CONCENTRATION IN THE SOLUTION (FOR LEACHING PAD 4). 90
FIGURE 45. AVERAGE DAILY TEMPERATURE AND DRIP LINE LIFETIME ON LEACHING PAD 3. 93
FIGURE 46. AVERAGE DRIP LINE LIFETIME ON LEACHING PAD 3 IN RELATION TO THE AVERAGE PLS TEMPERATURE DURING THE LIFETIME PERIOD OF THAT DRIP LINE. 94
FIGURE 47. AVERAGE DRIP LINE LIFETIME ON LEACHING PAD 3 IN RELATION TO THE AVERAGE Ca^{2+} IONS CONCENTRATION IN PLS DURING THE LIFETIME PERIOD OF THAT DRIP LINE.. 95
FIGURE 48. AVERAGE DAILY TEMPERATURE AND DRIP LINE LIFETIME ON LEACHING PAD 4. 96
FIGURE 49. AVERAGE DRIP LINE LIFETIME ON LEACHING PAD 4 IN RELATION TO THE AVERAGE PLS TEMPERATURE DURING THE LIFETIME PERIOD OF THAT DRIP LINE. 97
FIGURE 50 AVERAGE DRIP LINE LIFETIME ON LEACHING PAD 4 IN RELATION TO THE AVERAGE Ca^{2+} IONS CONCENTRATION IN PLS DURING THE LIFETIME PERIOD OF THAT DRIP LINE.. 97

FIGURE 51. MAIN SOURCES OF CALCIUM SULFATE CONSTITUENTS IN THE SYSTEM. . 101
FIGURE 52. OUTOTEC'S FORCED DRAUGHT COOLING TOWER. SOURCE: WWW.OUTOTEC.COM 106
FIGURE 53. FLOATING POND COVERS: HEXAGONAL (A) HEXA-COVER® AND SPHERICAL (B) SHADE BALLS. SOURCES: (A) WWW.HEXA-COVER.DK; (B) WWW.SHADE-BALLS.COM. 110
FIGURE 54. IRRIGATION PRESSURE AGAINST TIME (SOLID LINE – CONSTANT PRESSURE; DASHED LINE – PULSATING PRESSURE), USED IN THE EXPERIMENT BY ZHANG ET AL. (2017). 112
FIGURE 55. COMPARISON BETWEEN THE NUMBER OF CLOGGED EMITTERS IN RELATION TO THE NUMBER OF IRRIGATION EVENTS. BLUE COLOR – CONSTANT PRESSURE, RED COLOR – PULSATING PRESSURE ZHANG ET AL. (2017). 112
FIGURE 56. ON THE LEFT – BATTERY OPERATED CONTROL VALVE, ON THE RIGHT – PROGRAMMABLE CONTROLLER. SOURCE: WWW.NETAFIMUSA.COM 113
FIGURE 57. NETAFIM'S FLUSHING AND PRESSURE CONTROL VALVE INSTALLED ON THE SUB-MAIN PIPE. SOURCE: WWW.AQUAROYALSPRING.COM. 114
FIGURE 58. INSTALLATION OF MERUS RING ON THE PIPE (BARATI ET AL., 2014)...... 115
FIGURE 59. EFFECT OF THE MOLECULAR OSCILLATION RING ON SUBSTANCE FUNDAMENTAL OSCILLATION (A) 180^o PHASE-DELAYED, (B) IN-PHASE (BARATI ET AL., 2014). 116
FIGURE 60. TERRAFAME PRODUCTION FLOWCHART. SOURCE: TERRAFAME OY. 122

Acknowledgments

I would like to express my appreciation to the Terrafame Oy mining company for granting me this Master's Thesis Project. Specifically, I would like to thank Antti Arpalahti (Chief Production Officer) for his patience and knowledge input and Mikael Korte (Research Engineer) for countless conversations about important and not-so-important issues.

Furthermore, I would like to thank my Supervisor – Prof. Timo Heimovaara for his guidance and help regarding this project as well as to the entire Thesis Committee for their valuable comments.

Lastly, I wish to express my gratitude to my family, close ones and friends for supporting me throughout this Project and making the cold Finland feel a little bit warmer.

Author

Wojciech Strycharski

1. Introduction

Terrafame Oy (formerly Talvivaara Mining Company) is a nickel mine, located in central Finland approximately 300 km away from the Arctic Circle within the range of boreal type of climate. Metals are extracted from the ore by bacterially assisted hydrometallurgical process – bioleaching. Most of the metals leaching operations are usually performed in warm climates. These conditions make Terrafame a unique project on a worldwide scale. The mine changed ownership in August 2015 due to the bankruptcy of the previous company. Despite many challenges that this project is facing, production ramp up is ongoing.

Figure 1. Map with location of the mining site. Source: www.maps.google.fi.

Four main stages are distinguished in the process: open pit mining, materials handling, heap bioleaching and metals recovery. After mining stage, the ore is crushed down to approx. 8 mm, agglomerated for consolidation of the fines with coarser particles and at the end stacked onto heaps where it is aerated from the inside and irrigated from the top by drip irrigation system. This method delivers the solution to the top of each heap at a steady and uniform discharge rate. Leaching liquor – pregnant leachate solution (PLS) – is constantly recirculated in the system; it can be characterized as a concentrated multi-component sulfate solution with very low pH (~2). Primary leaching stage lasts for 18 months, and after it is finished, the material is transported and stacked on the secondary heap and leached until all metals are extracted. Secondary leaching area is also a place of the final deposition of the waste material.

1.1. Motivation

During the primary leaching stage, irrigation of the heaps becomes nonuniform in time due to gradual deposition of solid material in the hoses (drip lines). This phenomenon decreases the performance of irrigation system and eventually leads to a break in the irrigation caused by drip line replacement, creating an additional cost to the production.

The main precipitate found during the previous investigations of this problem was calcium sulfate (gypsum). It can clog the entire irrigation section in a very short time. Therefore, a further, in-depth investigation of this problem is required. The magnitude of this phenomenon is clearly visible at the top of heaps. In time, each drip line is covered with a variety of precipitates, usually having different colors. First solids form close to the orifices, where the solution exits the drip line. Not so long after the commencement of irrigation, solid matter begins to grow around the discharge points, successively covering entire hoses. However, precipitation occurs much sooner, inside the hoses and emitters – not visible from the outside. Gradually building up along the labyrinth flow path, eventually hindering the flow from an emitter. After part of emitters is clogged the flow from others increases (effects pictured in Figure 2). Not only does it apply to much PLS in these spots but it also speeds up the precipitation and eventually the entire irrigation section clogs with gypsum (domino like effect).

Figure 2. Discharge from an emitter working in a significantly clogged drip line.

Effects of irrigation inconsistencies on bioleaching performance are tough to assess explicitly. One can approximate that an uneven distribution of the PLS inside the heap body can inhibit bacterial activity and thus decrease ferrous and base metals production. In the book on Biomining, Rawlings and Johnson (2007) pointed out that reduced irrigation rates can be harmful to bacteria due to creating high osmotic potentials, caused by the accumulation of salts in a heap. Moreover, having zones with a very high flow and zones with no flow can significantly change flow paths inside the heap. Additionally, too high flow of the solution might lead to washing of the fine particles, which were agglomerated previously, and shifting them downwards to the bottom of the heap, causing the heap to clog literally.

Currently, this problem is countered with several processes related solutions such as:

- frequent drip line replacements,
- calcium monitoring and oversaturation prevention (PLS mixing between the ponds, diluting with fresh water),
- roughing of the heap's surface (making it uneven),
- drip line burial and covering (historical approach).

The replacement of hoses was identified as one of the negative effects which increased gypsum precipitation has on the production costs. With the lifetime of an average hose, averaging to approx. 1.5 month, the operation of drip line replacement requires a lot of workforce and materials. Although those preventive approaches generate additional production costs, lower nickel and zinc yields, due to uneven and retarded solution delivery, are probably generating even higher losses but those are hard to assess. Therefore, it is crucial for the operation to investigate this phenomenon and find solutions that could counter it in the future.

1.2. Research questions

The introduction to this project led to formulating the main research question which is as follows:

Is it possible to extend the lifetime of the irrigation system?

Several secondary questions and objectives should be formulated first, to give a correct answer to the main research question.

1. **How does the production system work at Terrafame?**
   Objectives:
   - ✓ Build a conceptual model of the site (describe each stage of the production)
   - ✓ Find sources of calcium sulfate constituents, introduced to the system

2. **What promotes precipitation in the irrigation system?**
   Objectives:
   - ✓ Literature study on calcium sulfate solubility and precipitation
   - ✓ Field observations
   - ✓ Process data analysis

3. **What is the calcium sulfate solubility in the PLS?**

   Objectives:

   - ✓ PLS sampling from the system
   - ✓ Perform solubility tests
   - ✓ Relate the results to literature study on calcium sulfate

4. **What are the technical possibilities to counter the clogging problem?**

   Objectives:

   - ✓ Review the possible technical solutions that could help solve the problem
   - ✓ Relate the findings to Terrafame process and propose viable solution

1.3. Thesis outline

Chapter 2 : Conceptual model of the site

- ➢ description of metals production cycle
- ➢ description of the irrigation system

Chapter 3 : Clogging phenomenon

- ➢ gypsum solubility literature review

Chapter 4 : Experimental part

- ➢ identification of solids in the irrigation system

- gypsum solubility tests in the pregnant leachate solution (PLS)
- different drip lines tests
- description of clogging distribution

Chapter 5 : Data analysis

- statistical analysis of process data
- clogging patterns investigation
- search for critical parameters triggering gypsum precipitation

Chapter 6 : Clogging control strategy

- proposition of methods leading to extension of the drip lines operation time
- review of the possible technical solutions

Chapter 7 : Conclusions and recommendations

- conclusions from the conducted research
- recommendations for further research of this topic
- proposition of improvements in the company

2. Conceptual model of the site

This Section will cover most important elements of the production cycle related to the PLS flow system. The full conceptual model of the site cannot be presented in this Thesis as it contains sensitive information. However, it was fully utilized by the author to understand the process and find relevant answers to the research questions formulated previously.

2.1. Geology and ore mineralogy

Terrafame deposits, Kuusilampi and Kolmisoppi, are situated in the southern part of Kainuu Schist Belt. The resources of nickel sulfide are amongst the largest in the world. The metamorphosed black schist hosts mineralization of nickel and other metals. Main minerals occurring within the ore are quartz, micas, graphite, and sulfides which are represented mostly by pyrrhotite (Fe_7S_8) and pyrite (FeS_2). Among the rest of sulfides sphalerite (Zn,Fe)S, pentlandite $(Ni,Fe)_{4.5}S_8$, alabandite MnS and chalcopyrite $(Cu,Fe)S_2$ can be listed (Riekkola-Vanhanen, 2013; Saari & Riekkola-Vanhanen, 2012).

2.2. Bioleaching process

Leaching of metal sulfides is based on the conversion of these insoluble minerals into water-soluble metal sulfides by electrochemical processes taking place at the mineral's surface. Sulfide minerals are predominantly leached thanks to the ferric ions found in the solution and their oxidative action. Leaching process begins with the reduction of iron (III) to iron (II) by interacting with metal sulfide. This results in the release of metal cations (M^{2+}) and water-soluble sulfur compounds (thiosulfate which then oxidizes to sulfate). The bioleaching process is based on the same principle and is assisted by bacteria added to the solution. The fundamental role of microorganisms in this process is the production of leaching chemicals. The two most occurring bacteria known as *Acidithiobacillus ferrooxidans* and *Leptospirillum ferrooxidans* can recover iron (III) – required for sulfides leaching – by oxidizing iron (II) formed in the leaching process. Furthermore, it is important to stress that bioleaching is an exothermic process. (Donati & Sand, 2007; Free, 2013; Rohwerder *et al.*, 2003). The schematic illustration of the bioleaching process is depicted in Figure 3.

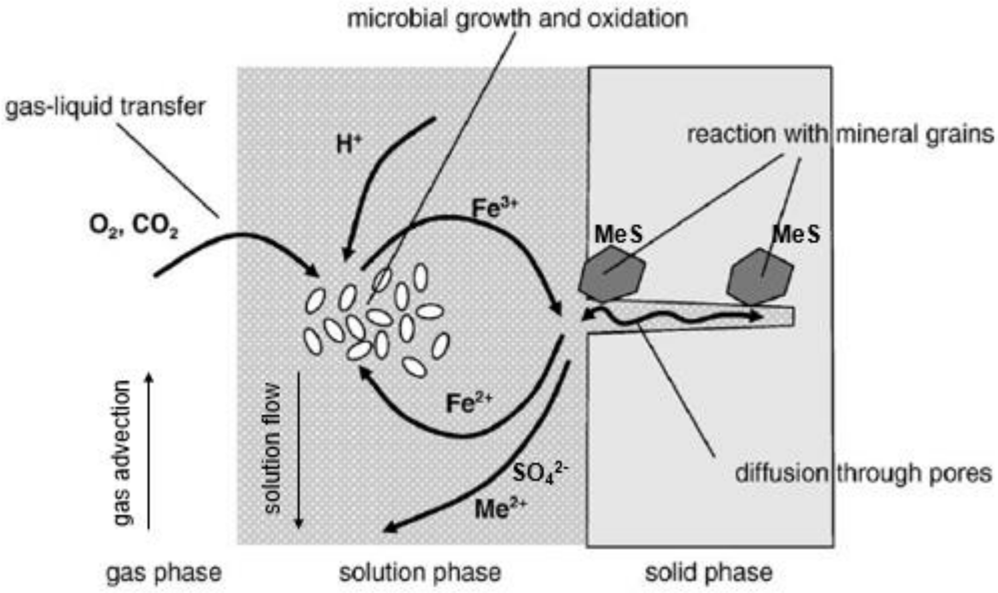

Figure 3. Illustration of the main reactions and transport processes in bioleaching of metal sulfide ores. Adapted from: Petersen (2010).

For the bioleaching process to occur, three phases must be present: solid (ore), liquid (solution) and gas (air) phase, all interacting with each other. These conditions imply the unsaturated flow conditions within the heap; application of the solution is made from the top at a steady discharge rate, air is pumped from aeration tubes placed inside the heap, and appropriate drainage is supplied. Schematic cross-section through a typical heap is depicted in Figure 4. The solution is transported downwards by gravity and capillary action whereas air travels upwards due to convection. These requirements entail good flow properties in the heap's structure to allow those three phases to meet and bioleaching process to occur. Solution application rate is one of the most important factors determining the success of bioleaching operation (Bartlett, 1997; Lu & Likos, 2004).

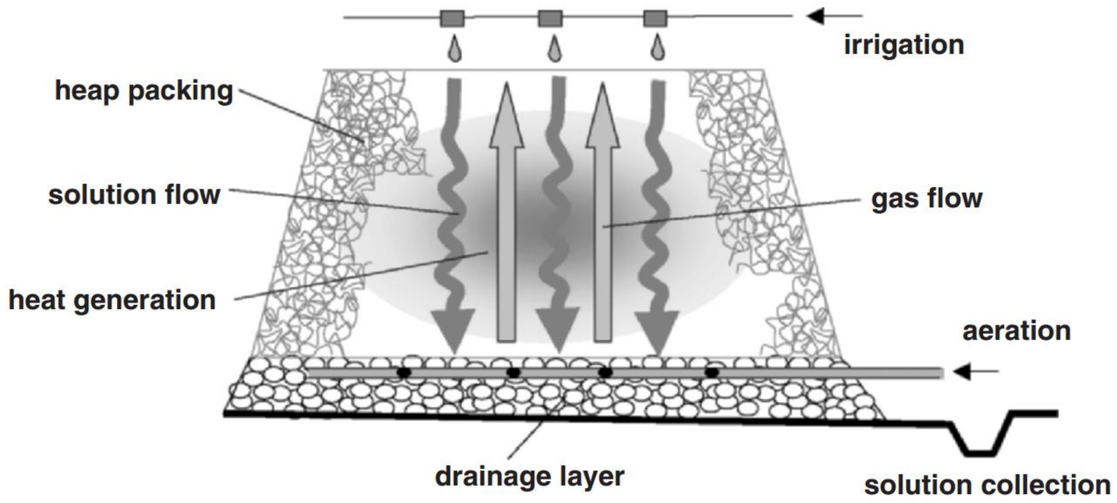

Figure 4. Cross-section through a typical heap used for leaching with processes indicated (Petersen & Dixon, 2007).

2.3. Irrigation system

Variety of irrigation methods is available nowadays: spray, drip or flood (furrow) irrigation (USGS, 2016). Most of them had been developed to serve for agricultural purposes and then incorporated by the mining industry. Terrafame is currently using the drip irrigation system. This method was selected because of its suitable parameters, not only meeting the requirements of bioleaching process (as mentioned above) but also environmental restrictions. Tough weather conditions, which are typical for the boreal type of climate, have also influenced the decision making regarding the irrigation method. Selection of the spray irrigation method, which is accomplished by using sprinklers, would cause the solution to freeze during the winter period before it could reach the surface of the heap. Furthermore, the solution, rich in heavy metals and acid, could be blown away by the wind and contaminate adjacent terrains as the sprinklers produce mist.

2.3.1. Emitters

The drip line consists of an in-line, factory pre-installed emitter which slowly and regularly applies the solution on the heaps and a network of plastic hoses – laterals, in which those emitters are embedded (Liu & Huang, 2009). We can differentiate a number of emitter types, according to the following classification criteria given by (Dasberg & Or, 1999; Karmeli, 1977): flow rate, form of pressure dissipation and construction details such as: flow path regime (laminar – long flow path, tortuous – labyrinth flow path), place of installation (on-line, in-line) and pressure compensation (Savva & Frenken, 2001).

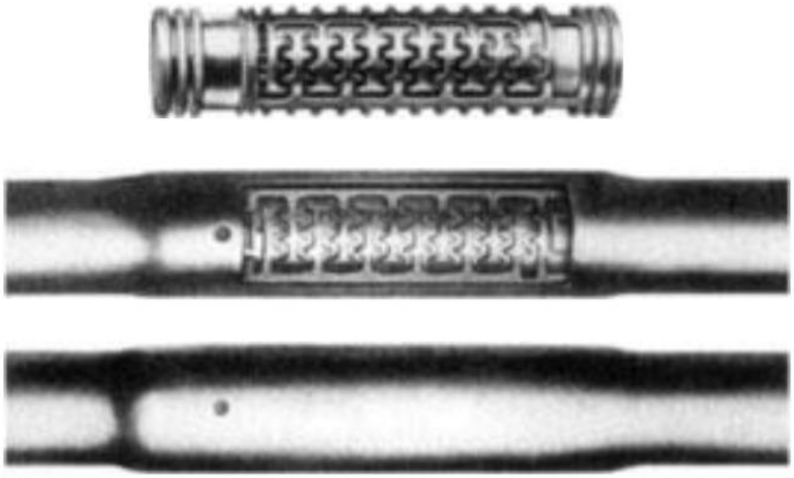

Figure 5. In-line emitter assembly in the lateral (Dasberg & Or, 1999).

Essentially, the task of an emitter is to dissipate the energy from the flowing solution. Fulfilling that mission provides uniformity of irrigation rate by low and steady discharge, uniform along the entire lateral. Most of the commercially used drip lines work under higher than atmospheric pressure, causing the turbulent flow regime inside the hoses and emitters. The flow regimes are characterized by non-dimensional Reynolds number, which for a cylindrical flow path can be written as:

$$Re = \frac{4Q}{\pi d\eta} \ [-] \tag{1}$$

where Q is the emitter discharge rate, m^3/h, η the kinematic viscosity of water and d, cross–section diameter, mm.

Dasberg and Or (1999) have identified the three major flow regimes being:

- laminar (for $Re < 2\ 000$),
- unstable (partially turbulent for $2\ 000 < Re < 4\ 500$),
- turbulent (for $Re > 4\ 500$).

The tortuous flow emitter type adopts the “labyrinth” solution flow channels (Figure 6), which have considerably smaller flow sections – typically less than 1.0 mm (Qingsong *et al.*, 2008). The labyrinth in the emitters is usually constructed by making the flow path surface dentate (Figure 6). The teeth could be of different shape and layout, along the flow path, and the design differs by manufacturer. The flow path in the emitter governs the efficiency and accuracy of the drip irrigation system. Liquid enters the flow path of the dripper at calculated pressure, and the process of friction in the flow path decreases that pressure gradually so producing the accurate flow rate at the output of the dripper. The distance between the teeth and special angles in the labyrinth produces turbulence which doesn't allow sedimentation of particles and dirt in the dripper. The liquid flows continuously between the teeth of the labyrinth. At the corners, there is a calm area where a concentration of water is like big molecules to produce a friction process for the accurate flow rate of the dripper. Many companies have their own technologies (secret) of the labyrinth design and thus flow properties. For instance, the "DS Technology" developed by AZUD company that allows the solution to flow in between the teeth by placing them in a way that prevents from overlapping of the teeth along the flow path – creates a straight-line flow path (see blue arrow in Figure 6).

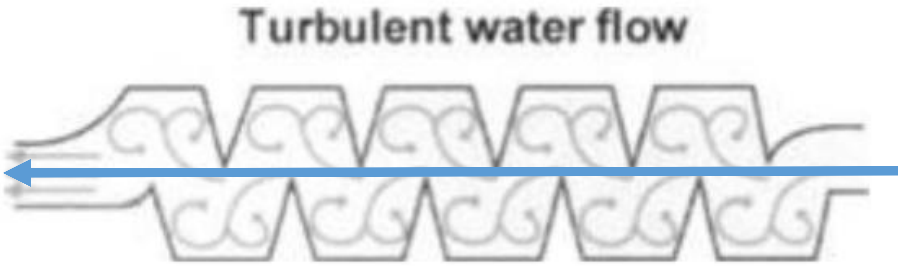

Figure 6. Turbulent water flow inside the labyrinth flow path with flow "tunnel" indicated by the blue arrow. Adapted from: Dasberg and Or (1999).

Flow rate characteristics of emitters are described by the following equation, given by Karmeli (1977):

$$q = kH^{x} \tag{2}$$

where q is the discharge from an individual emitter, usually given in L/h, k is the discharge coefficient of an emitter and H is the hydraulic head at the inlet of an emitter, in m; x is the emitter discharge exponent, characterized by flow regime (Li Yang 2005). The producer typically gives the factors for calculating emitter's flow rate. For the turbulent flow conditions, discharge exponent x has a value of approximately 0.5 (Karmeli, 1977).

2.3.2. Laterals and mains

Emitters are embedded in the laterals or drip lines. These tubes, often made of polyethylene, provide flexibility and no corrosion. Inner diameter of the laterals is usually 12–32 mm and walls that are capable of withstanding pressures in the range of 4 – 6 bars, depending on design. One of the critical parameters that should be calculated when describing the lateral is the pressure head loss along the length of this tube. The most commonly used formula to calculate it, given by (Dasberg & Or, 1999), is that of Hazen–Williams and follows:

$$H_L = 2 \cdot 78 \cdot 10^{-6} \cdot FLD^{-4.87} \left(\frac{N\bar{Q}}{C}\right)^{1.85} \tag{3}$$

where H_L stands for the head loss in laterals, in m; L is the lateral length, in m; D is the inside diameter of the lateral, in m; N is the number of emitters on the lateral; Q is the average emitter discharge along the lateral, in m^3/h; C is the Hazen–Williams roughness coefficient, dimensionless. The main and sub-main lines supply the leachate to the laterals. These pipes are manufactured from a rigid plastic such as polyethylene or PVC.

Hoses are placed directly on the heaps or buried to prevent the PLS from freezing. Bioleaching is an exothermic process, and the temperature on the top of the heaps is usually above the freezing point. Another reason for using drip system is the environmental concern. The solution delivered by sprinklers could easily be blown away by the wind and not only contaminate adjacent terrains but also reduce the uniformity of irrigation.

2.3.3. Drip line type used in Terrafame

Currently, Terrafame uses the multi–seasonal drip line manufactured by a Spanish company – Sistema AZUD S.A. The emitters selected for the process have a nominal discharge rate of 4 L/h. Table 1 presents the technical details of the dripline selected for the Terrafame process. AZUD emitters are a non-pressure compensating, turbulent flow, long-path emitters. The liquid travels through a specially designed labyrinth path. The feature worth noticing is the exclusive design of the teeth, creating a flow channel with anti-clogging properties (DS Technology). The solution flows in between the teeth, pushing out the solid particles that could contribute to emitter clogging. Moreover, this type of drip line has one solution entry point, through a fine mesh (entry through the entire inner perimeter of the emitter, approx. 1 mm wide) and two discharge orifices placed on the opposite sides of the drip line.

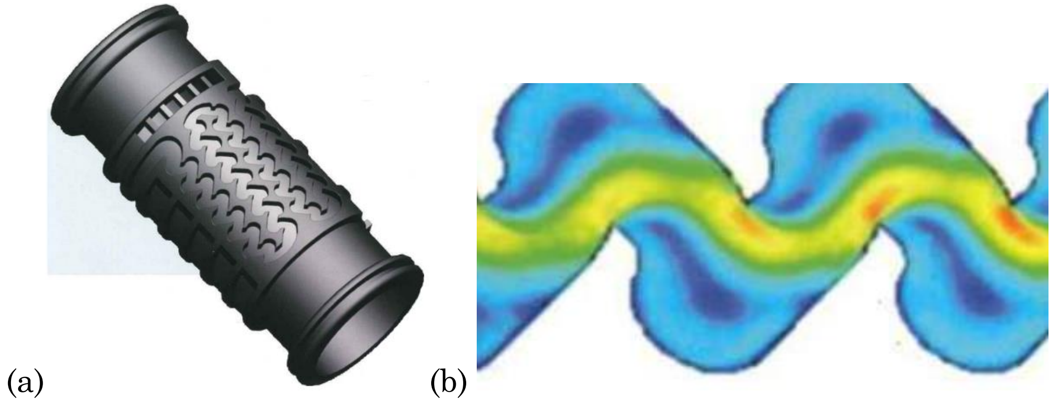

Figure 7. (a) AZUD Drip emitter, (b) solution flow in the labyrinth – warm color represents high flow velocity (Azud Sistema S.A., 2017).

Table 1. Technical parameters of the AZUD DRIP 16 drip line (Azud Sistema S.A., 2017).

Manufacturer:	AZUD Sistema S.A.	**Unit**
Model:	AZUD DRIP 16	
Nominal flow:	4	L/h
Nominal thickness:	0.9 – 1.0	mm
Inner diameter:	13.6	mm
Maximum pressure:	3 – 3.5	bar
Discharge coefficient (k):	1.34	–
Discharge exponent (x):	0.47	–
ΔQ*:	5	%

* ΔQ – difference in the flow rate between the first and last dripper in line for 52 m long drip line, 0.6 m spacing between emitters and 1 bar entry pressure.

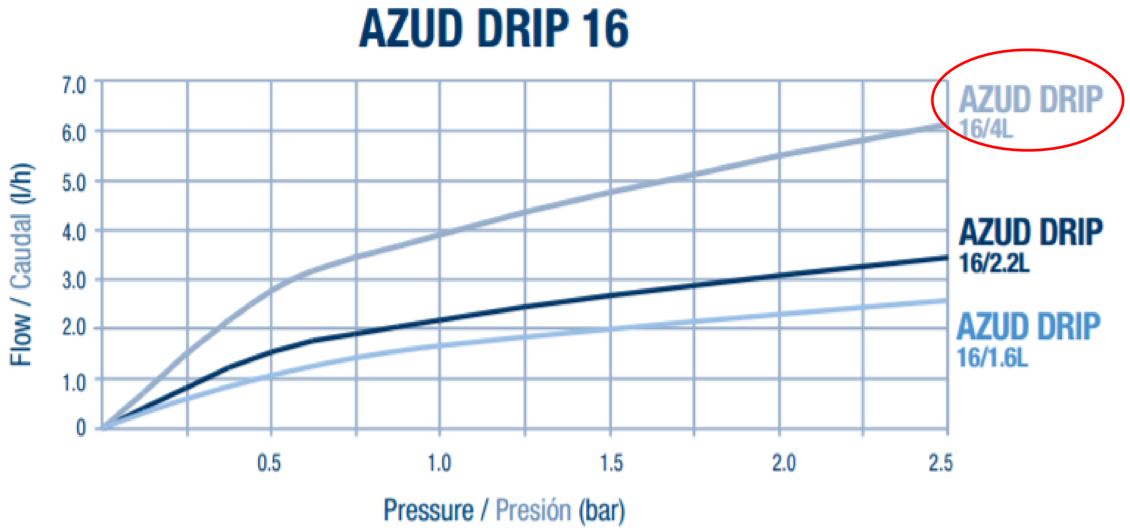

Figure 8. Pressure – flow rate characteristic curve of the AZUD emitters. The red circle indicates the emitter used in Terrafame (Azud Sistema S.A., 2017).

The total number of installed irrigation hoses, and thus emitters, can easily be calculated from the design parameters of each irrigation cells by multiplication. For example, in the 165 m long and 35 m wide cell, the number of drip lines is: 275 and the total amount of emitters is over 16 000 (assuming 0.6 m spacing between drip lines and emitters). The entire length of the laterals per heap is over 550 km which means that almost 1 000 000 emitters are working on one heap.

2.3.4. Design of the irrigation system in Terrafame

The system was designed to fit both the hydraulic properties of the heap and its dimensions to provide efficient solution distribution. Irrigation was designed to work under the pressure of 1 bar. To make the system design straightforward, discussion of the layout is necessary.

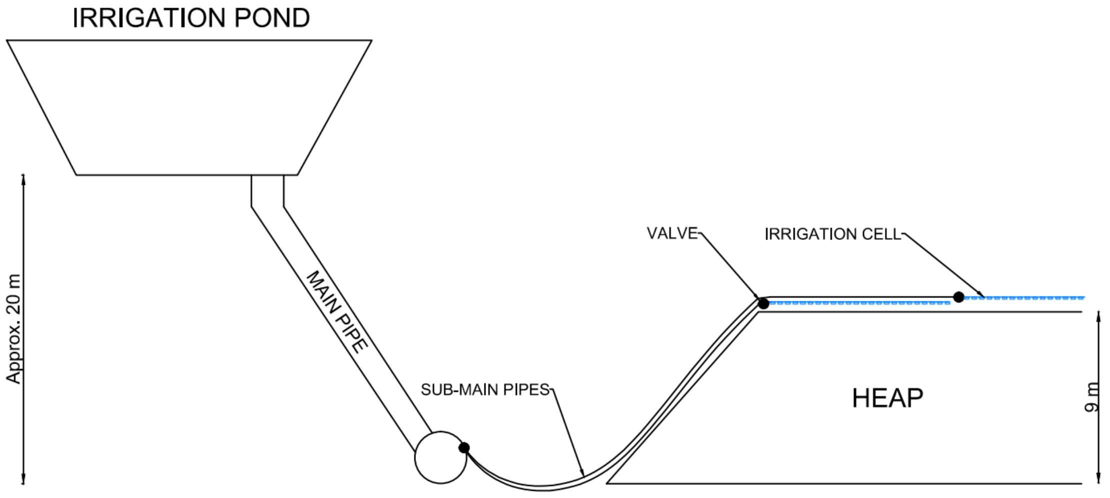

Figure 9. Cross–sectional view of the irrigation system in Terrafame (not in scale).

Depending on the size, every heap has from five to six irrigation sectors, each being 35 m wide, 300 m long and consisting of two irrigation cells. The solution is delivered to the irrigation cells from the irrigation ponds by gravity (see Figure 9). Every leaching pad has its appointed pond thus there are four in total. Ponds are located approximately 20 meters above the primary leaching pads. The solution travels towards the heaps along the slope in 1 m diameter, PVC main pipe. After that, the main pipe continues along the leaching pad horizontally. Every irrigation cell, depicted in Figure 10, is connected to the main pipe through a 110 mm diameter sub–pipe that delivers the solution to the top of the heap (nine meters higher than the main pipe). This design was employed to provide accurate pressure conditions to the drip lines. Having only one large section would cause a significant pressure to drop between the beginning and end of the irrigation cell.

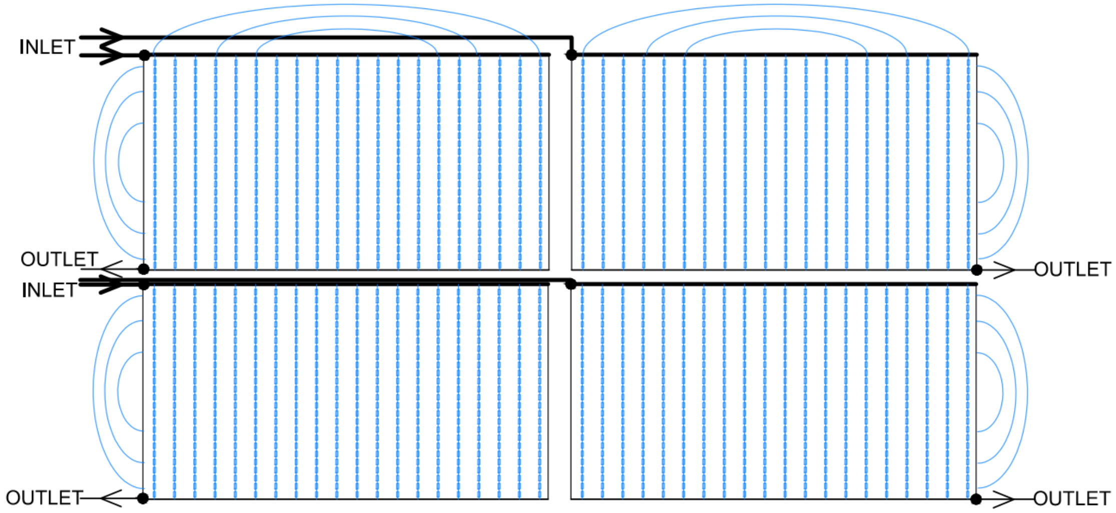

Figure 10. Top view of the irrigation cells (not in scale). Blue lines represent the irrigation drip lines.

Within the irrigation cell, we can distinguish an inlet and an outlet of the solution with valves installed for flow control. However, the outlet is only opened during the winter period (very low temperatures) to prevent the solution from freezing. That design feature allows for flushing of the pipes by opening both valves at the same time as well. Drip lines are connected to the sub-main pipes at 60 cm intervals. There is no pressure measurement employed in any part of the system thus assumption must be made when regarding this system, that a uniform pressure of 1 bar is present within the irrigation cells. The only mean of control is the flow rate that enters the irrigation cell. There are special valves installed on the main pipe and flow is set to the value of 35 m^3/h per each sub-main pipe. Flow measurements, done by an ultrasonic flow meter, give an overview of the total amount of PLS discharged from each irrigation cell.

2.3.5. Leachate circulation

Leachate circulation system in Terrafame is closed and was presented in the Appendix A. Solution from the primary leaching stage is either redirected to the irrigation ponds (IP) or partially sent to the metals recovery plant (approx. 25% of the flow). After all of the metals are recovered, solution undergoes treatment in the reversed osmosis process. Purified water is used as process water whereas the effluent – containing a high amount of calcium ions – goes to the Raffinate Pond and eventually back into the system. Moreover, part of the solution from the secondary leaching stage is also transported to the primary leaching circulation through the Raffinate Pond. The simplified flowchart has been depicted in Figure 11. During day-to-day operation, flows between the major production stages vary and are adjusted to maintain the flow balance.

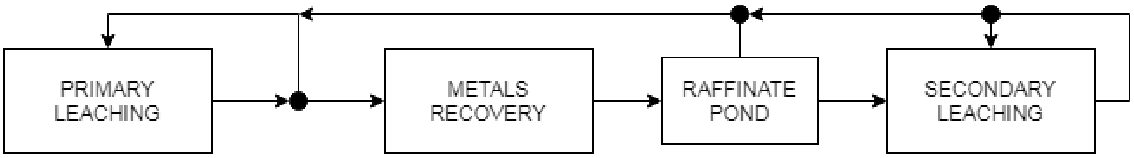

Figure 11. Simplified flow chart of the PLS flow paths in the system

In the primary leaching stage, the solution is delivered to the irrigation system by gravity and then collected at the outflow from heaps. Consecutively, the PLS flows to the pH adjustment pond, sulfuric acid is added at that stage, and after that, it is directed to the PLS pond. From there the solution can be either directed to other PLS ponds, moved to the Metals Recovery Plant or pumped back into the Irrigation Pond. Additionally, the feed to the Irrigation Ponds can be mixed with the solution coming from secondary leaching stage/metals recovery plant (this system is depicted in Figure 12).

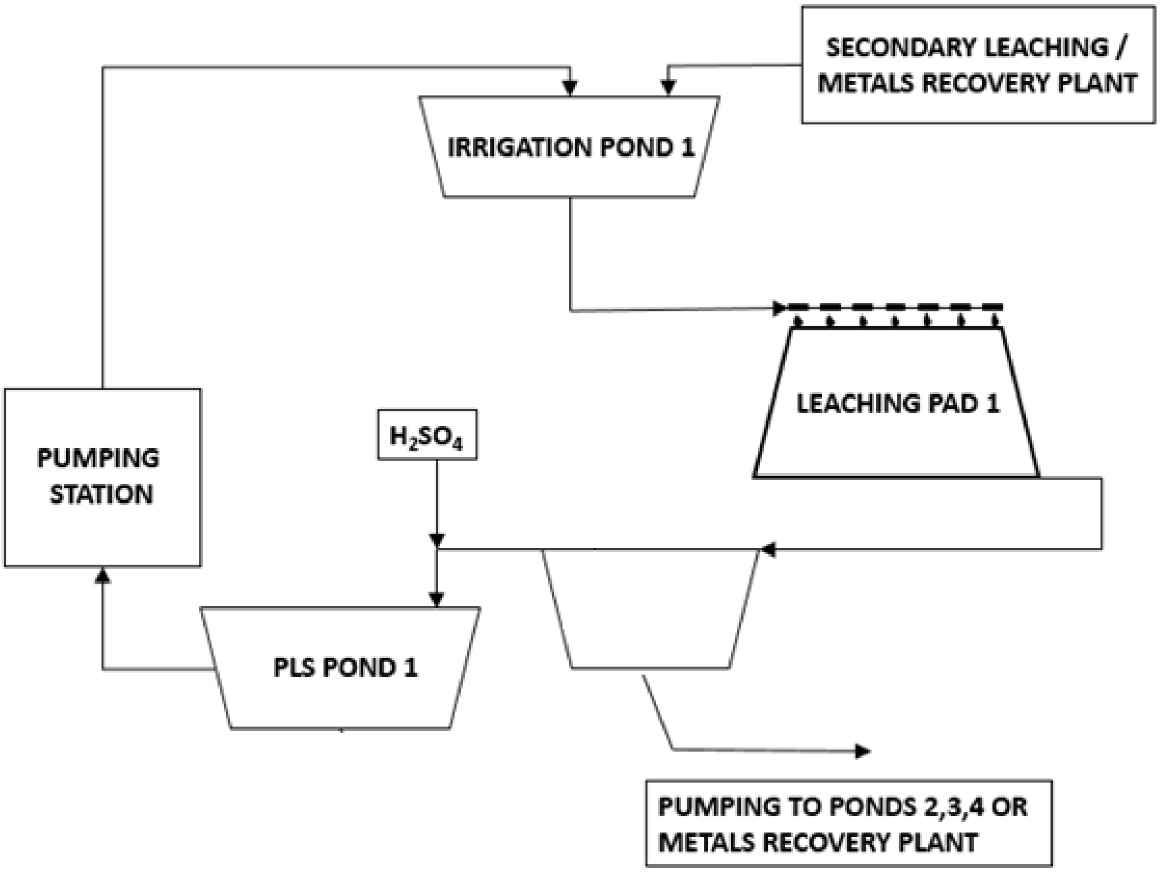

Figure 12. PLS flow path in primary leaching stage (example for leaching pad 1).

2.4. Metals recovery plant

The product of the bioleaching process is a highly saturated solution, containing large quantities of dissolved metals and other chemical compounds. Metals are separated from the liquid phase by precipitation induced by addition of hydrogen sulfide and a change in solution's acidity. Different metal sulfides precipitate in different pH environments (Lewis, 2010). All stages of metals production are depicted in Appendix A. The pH is increased by the addition of lime slurry ($CaCO_3$) and milk of lime ($Ca(OH)_2$) in different stages of the process. This increases calcium concentration in the solution and promotes precipitation of gypsum which is then placed on the secondary heaps for additional leaching. At the end of metals production, the solution undergoes treatment in the reverse osmosis process.

3. Clogging phenomenon

The purpose of this project was to investigate the problem of excessive solid matter precipitation, hindering the solution flow and leading to clogging of the emitters in primary bioleaching stage. The magnitude of this phenomenon has been identified for every single leaching pad. Thus it might be considered as a global problem. As the production ramp-up proceeds, it is expected to cause even bigger issues in the future.

3.1. Solids found in the irrigation system

There are three main groups of solid material suspected to precipitate in and on the drip lines. We can distinguish calcium sulfate, iron hydroxides, and nickel/iron sulfate precipitates (see Appendix B).

a) Calcium sulfate

Calcium sulfate, identified as the primary precipitate found in the drip lines, obstructs the solution flow. This inorganic salt occurs in nature in more than one crystalline form, depending on solution's composition and temperature. Each crystalline phase can be stable, meta stable or unstable (Azimi & Papangelakis, 2010). Three main hydrates can be distinguished:

- Anhydrite ($CaSO_4$)
- Hemihydrate ($CaSO_4 \cdot 0.5\ H_2O$)
- Dihydrate (gypsum) ($CaSO_4 \cdot 2\ H_2O$)

The dominance of gypsum has been confirmed by XRD analysis of the solid material collected from the irrigation system and described in Section 4.1. However, it is probable that at higher temperatures also anhydrite can be formed as well as hemihydrate. The mentioned analysis didn't recognize any of those two hydrates present in the solid material.

b) Iron precipitates

Iron precipitation concerns mostly ferric iron and essentially is driven by the changes in pH (starts to occur at $pH < 3$). Ferrous iron present in the solution doesn't precipitate by itself, but due to exposure to air is oxidized to iron (III) and can contribute to overall solid production. The main Fe-containing solids recognized are:

- Goethite ($FeOOH$)
- Jarosite (one of the forms: $KFe_3(SO_4)_2(OH)_6$)

Goethite is fairly soluble in diluted acids – such as the PLS (Schwertmann, 1991); however, it is relatively stable in the heaps. This mineral usually shows up as a first iron precipitate. Because of its moderate solubility, it doesn't create any problem as most probably will be washed away by rain or melted snow. Jarosite, on the other hand, is a stable precipitate. It takes much more time for it to precipitate and the reaction requires heat. These formation conditions result in jarosite being present in the form of hard and dry particles. Jarosite precipitation is beneficial to the process as it helps with sodium (or potassium) and sulfate removal from the solution. Majority of the solids mentioned above are present outside of the drip lines, around the discharge points (as marked in Appendix B) but some are also found in the solids formed inside of the drip lines.

c) Metal sulfates

These precipitates are visible around most of the discharge points. Typically, they form very quickly and have a specific green hue. These precipitates are not recognized to have a negative influence on solution flow through the emitters since they are very well soluble in water – containing water molecule in their structure. The general formula is written as follows: $MeSO_4 \cdot xH_2O$ (Me – being either Ni^{2+}, Fe^{2+} or Cu^{2+} ions and x the amount of water molecules).

3.2. Calcium sulfate solubility

This sub-chapter will summarize literature study on calcium sulfate formation and its solubility in solutions with an emphasis on the hydrometallurgical processes as well as give the underlying theory.

3.2.1. Theoretical background

The solution is as a mixture of at least two components. The substance dissolved in another is called solute whereas the other is known as a solvent. In hydrometallurgical processes, we are dealing with liquid solutions, where the role of solvent is typically played by pure water (H_2O).

The following theoretical description of basic concepts in aqueous solutions was adapted from Appelo and Postma (2005). Fundamental law, required for any description of equilibrium in aquatic solutions is the *law of mass action*.

It can be represented by the equilibrium constant *K,* which for generalized reaction type given by Eq. 4 can be written as shown in Eq. 5. The bracketed values represent the *activities* or the “effective concentrations”.

$$aA + bB \ \leftrightarrow cC + dD \tag{4}$$

$$K_{eq} = \frac{[C]^c[D]^d}{[A]^a[B]^b} \tag{5}$$

When the system is at equilibrium then both sides of Eq. 5 are equal. Another way of expressing the equilibrium constant is by using the Gibbs free energy for calculation as follows:

$$K_{eq} = e^{-\left(\frac{\Delta G^0}{RT}\right)} \tag{6}$$

There are many ways of expressing the solute/solvent ratio by incorporating concentration term. Most commonly used are:

- mass concentration – mass of solute per unit of volume,
- molarity, M – moles of solute per unit of volume,
- molality, m – moles of solute per unit weight of solvent.

Furthermore, knowledge about the density of solution and Total Dissolved Solids (TDS) is of importance for calculating the molal concentrations.

In solutions, ions interact with each other and other molecules. At higher concentrations, ions tend to behave as they are less concentrated than they are in reality. With higher ionic strength in solution and thus higher concentration of ions, those interactions are interrupted. The activity of an ion i can be therefore expressed by the molal concentration (m_i) of that ion, corrected with the activity coefficient (γ_i). The activity can be thought of as an "active concentration" – concentration available for the reaction.

$$[i] = \gamma_i \cdot m_i \tag{7}$$

The activity coefficient can be calculated for dilute pure solutions with the Debye–Hückel theory which states that the electrical charges, present in the solution, should be known therefore the *ionic strength* of the solution needs to be calculated as follows in Eq. 8.

$$I = \frac{1}{2} \sum (m_i \cdot z_i^2) \tag{8}$$

After the ionic strength is known, activity coefficient can be determined. However, this step is simple for dilute electrolyte solutions, establishing it for concentrated, multi-component solutions is very difficult. For the dilute solutions (i.e. brackish water), Debye–Hückel equation can be applied but for solutions with higher ionic strength (i.e. sea waters), we can use the modified version of that equation, given by Davis. Those empirical formulas don't represent the activities of ions in concentrated solutions well (Fitts, 2013; Havli□k, 2008)

The value of activity coefficient depends on the thermal conditions of the solution thus thermodynamics should also be discussed. Chemical reactions can be exo– or endothermic therefore each reaction will be associated with some change in energy. Gibbs energy is a value that can be used to represent this energy which can be used to do work. It combines enthalpy (H), entropy (S) and temperature (T).

$$G = H - TS \tag{9}$$

Change in that energy is of importance to describe the chemical reactions. For general reaction written in Eq. 4, page 29, change in Gibbs free energy ΔG_r can be written as follows:

$$\Delta G_r = \Delta G_r^0 + RT \ln K_{eq} \tag{10}$$

where ΔG_r^0 represents the standard Gibbs free energy of the reaction (calculated as a sum of energies of all reactants), R is the gas constant, T absolute temperature in Kelvins and K – equilibrium constant of the reaction. By the value of change in Gibbs free energy we can assess towards which direction the reaction will evolve. For a negative value of Gibbs free energy reaction is spontaneous and will proceed to the right, for positive to the left (Ryan, 2014).

The solubility of a species is the amount of that species able to dissolve to form a saturated solution. This value is expressed by the solubility product K_{sp} which is derived from the equilibrium constant $K_{eq.}$ The activity of a solid is 1. Therefore every dissolution reaction will involve only the numerator activities from the equilibrium constant, unlike for the precipitation reactions, placing the solid phase in the denominator. Saturation state (Ω) of the solution is represented by the relationship between ionic activity product (IAP) and $K_{sp.}$ IAP represents the real activities of ions in the solution.

$$\Omega = \frac{IAP}{K_{sp}} \tag{11}$$

The outcome of the Eq. 11 can tell in what state the solution is, as follows:

- when $\Omega > 1$, the solution is supersaturated,
- when $\Omega = 1$, the solution is at saturation,
- when $\Omega < 1$, the solution is undersaturated.

Additionally, we can translate the saturation state to the saturation index by using a logarithm as shown in Eq. 12.

$$SI = log\,\Omega = \log\left(\frac{IAP}{K_{sp}}\right) \tag{12}$$

Negative saturation index informs about the under saturated solution whereas a positive one will mean a supersaturated state. SI equal to zero tells that the solution is at equilibrium.

3.2.2. Solubility of calcium sulfate in pure water and standard conditions

The solubility of calcium sulfate in water was studied previously. Maximum solubility value has been reported to be at approximately 50 °C. Gypsum is the solid saturating phase in water up to 100 °C (Dutrizac, 2002). General case of calcium sulfate hydrates solubility in pure water will first be described. For equilibrium state in the water we can write the following equation:

$$CaSO_4 \cdot nH_2O \rightarrow Ca^{2+} + SO_4^{2-} + nH_2O \tag{13}$$

where n = (0, 0.5, 2)

Mass action expression can be written as shown in Eq. 5, page 29. The activity of pure solid is equal to unity and for dilute electrolyte solutions [H_2O] = 1. Therefore, this expression reduces to:

$$K_{gypsum} = [Ca^{2+}][SO_4^{2-}] = 10^{-4.60} \quad at\ 25^{o}C \tag{14}$$

Changing the molal concentrations from Eq. 5 to activity yields leads to:

$$K_{gypsum} = (\gamma_{Ca^{2+}} \cdot m_{Ca^{2+}})(\gamma_{SO_4^{2-}} \cdot m_{SO_4^{2-}}) = 10^{-4.60} \tag{15}$$

Gypsum is an equimolar mineral thus Eq. 15 can be simplified by assuming that the molal concentrations and activities of calcium and sulfate are equal to:

$$m_{Ca^{2+}} = \frac{5.01 \cdot 10^{-3}}{\gamma_{Ca^{2+}}} \tag{16}$$

Additionally, solubility product might be obtained from the Gibbs free energy data. For the dissolution reaction given by the Eq. 4, page 29, we can write the standard Gibbs free energy of the reaction, using the data of free energy of formation ΔG_f^0 , given in Table 2, following the Eq. 17.

Table 2. Gibbs free energies of formation at 298.15 K and 1 bar (Wagman et al., 1982).

Specimen	$\boldsymbol{\Delta G_f^0}$ [kJ/mol]
$CaSO_4 \cdot 2H_2O$	–1796.4
H_2O	–237.2
Ca^{2+}	–553.8
SO_4^{2-}	–742.0

$$\Delta G_r^0 = \Delta G_{fCa^{2+}}^0 + \Delta G_{fSO_4^{2-}}^0 + \Delta G_{fH_2O}^0 - \Delta G_{fCaSO_4}^0 \tag{17}$$

$$\Delta G_r^0 = -553.8 - 742.0 - 2 \cdot (237.2) + 1796.4 = 26.3\ kJ/mol$$

Using the formula given by Eq. 6, page 29, the solubility product of gypsum can be calculated as follows (using the gas constant 0.008314 kJ/mol):

$$K_{gypsum} = e^{\frac{-26.3}{0.008314 \cdot 298.15}} = e^{-10.61} = 10^{-4.61}$$

The obtained values of gypsum solubility constant are valid for an ideal situation, but it shows that it can be calculated using different approaches. However, the value of this constant is highly dependent on the values used for the Gibbs free energy calculations.

3.2.3. Solubility of calcium sulfate in hydrometallurgical process solutions

Calcium is one of the most abundant elements in the Earth's crust, with 4–5% in total mass. Minerals containing calcium as one of the main constituents are found in the heavy metal ores frequently. Thus inevitably, hydrometallurgical processes liquids, which most commonly are sulfate solutions, will involve an influx of calcium ions. Whenever those two ions occur together in aqueous solutions, calcium sulfate deposits due to its relative insolubility. This mineral has been recognized as one of most frequently inorganic salts, found in the hydrometallurgical processes. (Azimi *et al.*, 2007).

Crystallization kinetics of this calcium sulfate is believed to be influenced by the temperature, concentrations of both heavy metal sulfates and sulfuric acid, as well as the type of crystals present in the solution (Wang *et al.*, 2012). As mentioned before, calcium sulfate can occur in the form of three different hydrates (dihydrate, hemihydrate and anhydrite). Each crystalline phase can be stable, meta stable or unstable, depending on the solution's conditions, as depicted in Figure 13. Transformation of gypsum to anhydrite leads to a decrease in solubility level. This phenomenon makes predicting and controlling of $CaSO_4$ formation complicated (Azimi & Papangelakis, 2010). Below the temperature of ~ 40 °C, gypsum has the lowest solubility, thus can be considered as the most stable one. The point at which gypsum transitions to anhydrite and hemihydrate can be found at 40 ± 2 °C and 99 ± 2 °C respectively. Gypsum remains metastable in between these temperature ranges; however, it depends on the solution's properties. For some cases, it might be that heating the solution up to 100 °C will not trigger the gypsum–anhydrite transition, for others, can be rapid above 60 °C (i.e. in concentrated acid-salt solutions). The transition point between hemihydrate and anhydrite has not yet been experimentally proven and is believed to lie at relatively high temperatures (Azimi *et al.*, 2007).

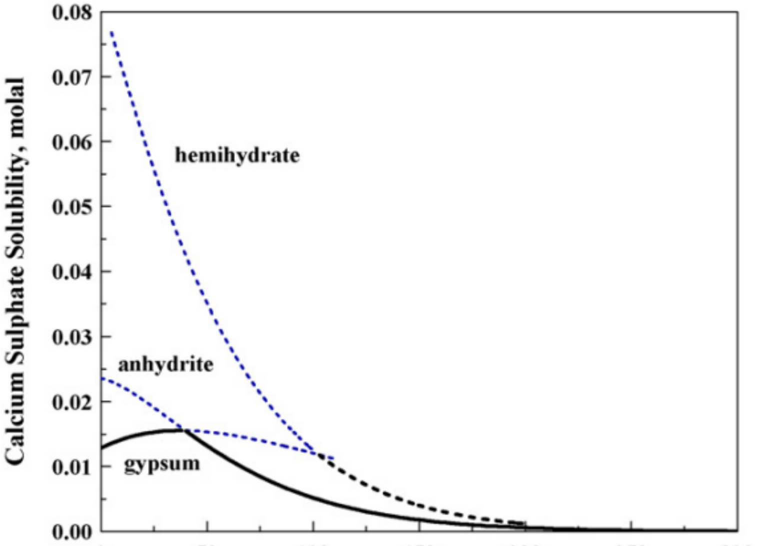

Figure 13. Phase transition diagram of $CaSO_4$ in H_2O. The solid line represents stable phase, dashed line meta stable (Azimi et al., 2007).

Many researchers attempted to test and model calcium sulfide solubility in multi–component sulfate solutions, rich in $MeSO_4$ where Me = (Ni, Zn, Fe, Mn, Mg) and H_2SO_4. Campbell and Yanick (1932) had discovered that solubility of calcium sulfate could be different in the presence of $NiSO_4$ salts in solution. After that revelation, science has focused on finding the link between solution properties and calcium sulfate solubility. There are several experimental data sets available concerning solubility in binary, ternary and multi-component systems, tested in the temperature range from room temperature (~ 25 °C) to over 100 °C. Zeng and Wang (2011) reviewed the available data on calcium sulfate solubility in quaternary systems involving heavy metal sulfates and sulfuric acid. They concluded that concentration of acid and sulfates influences solubility of gypsum. Usually, in the data, there was a peak solubility visible for a certain temperature and amount of constituent under analysis. After reaching the maximum value, solubility decreased. Wollmann and Voigt (2008) tested the binary systems of $MeSO_4$ where Me = (Mg, Mn, Co, Ni, Cu, Zn) and $CaSO_4$ at 25 and 40 °C, finding that at low concentrations of $MeSO_4$, solubility of gypsum decreased until it reached minimum; further increase of the bivalent metal sulfate led to an increase in solubility of gypsum.

Dutrizac (2002) tested the solubility of gypsum in simulated zinc processing solutions which in some way are similar the solution of Terrafame. However the $ZnSO_4$ content was significantly larger (1.5 M – 2.5 M), but the acid contribution from H_2SO_4 was considered. Experiments were carried in the temperature ranges from room temperature to 95 °C on the systems listed in Table 3. From Figure 14 it can be seen that increase in the metal sulfide concentration led to a decrease in $CaSO_4$ solubility. Azimi *et al.* (2007) tried to model those dependencies. Addition of sulfuric acid to the $CaSO_4$–H_2O system, had been reported to influence calcium sulfate solubility; initially increasing it with increasing concentration of acid up to ~1.8 M H_2SO_4 and further decrease above that value. Additionally, modeled values depicted in Figure 15 showed that at very high and low temperatures and high acid concentration, increase in solubility can also be visible.

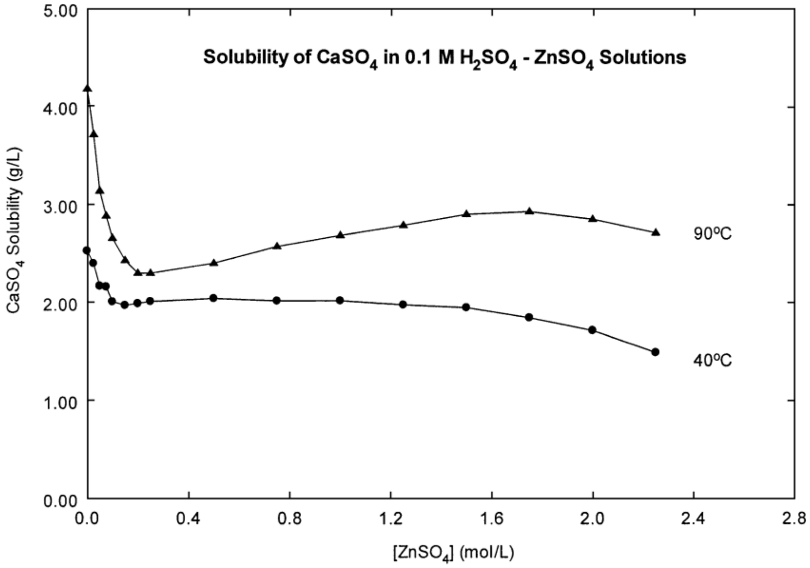

Figure 14. Effect of $ZnSO_4$ on calcium sulfate solubility in 0.1M H2SO4 solutions at 40 and 90 °C (Dutrizac, 2002).

Later on, Azimi and Papangelakis (2010) tested the effect of different electrolytes on $CaSO_4$ solubility. The solubility of calcium sulfate was found to be the same for all metal sulfate solutions with different cations. Initially, at low $MeSO_4$ concentration, solubility dropped due to common ion effect and then increased due to neutral calcium sulfate species formation. After passing maximum value, solubility decreased due to salting-out (decreasing number of free water molecules in solution). The study has also showed higher calcium sulfate solubility when instead of sulfuric acid, hydrochloric acid (HCl) was used. The important conclusion from this study is that cations have a little effect on calcium sulfate solubility and anions are the main constituents defining it (when the electrolyte's anion is the same as in the product, in this case – SO_4^{2-}) (Figure 16).

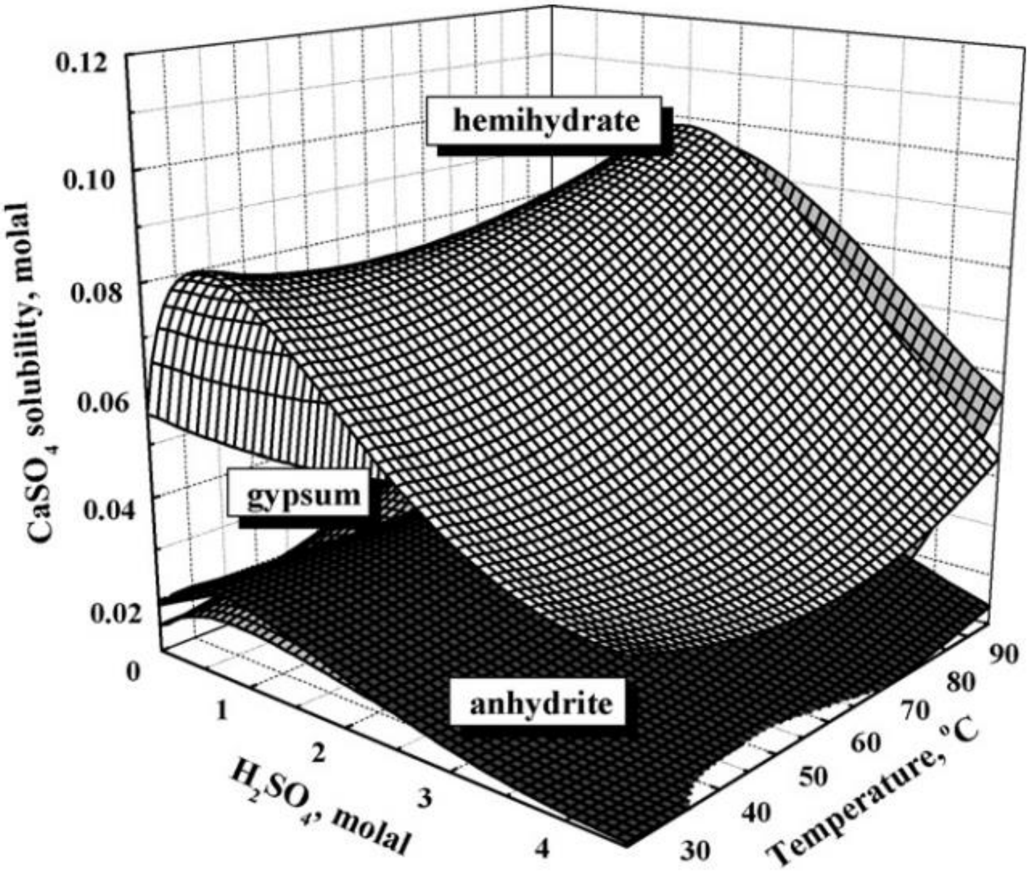

Figure 15. Phase transition diagram of $CaSO_4$ in H_2SO_4 solutions (Azimi et al., 2007).

Table 3. List of the multi-component systems for which calcium sulfate solubility has been experimentally established by Dutrizac (2002) and used for modeling by Azimi et al. (2007).

System	**Temp. range [°C]**	**Solid phase**
$CaSO_4 – ZnSO_4 – H_2SO_4$ (0.1 M) – H_2O	25 – 90	$CaSO_4 \cdot 2H_2O$
$CaSO_4 – H_2SO_4 – ZnSO_4$ (1.5 M) – H_2O	25 – 90	
$CaSO_4 – Na_2SO_4 – H_2SO_4 – H_2O$	45 – 80	
$CaSO_4 – MgSO_4 – ZnSO_4$ (1.5 M) – H_2SO_4 (0.1 M) – H_2O	25 – 90	
$CaSO_4 – MgSO_4 – ZnSO_4$ (1.5 M) – H_2SO_4 (0.3 M) – H_2O	25 – 90	
$CaSO_4 – Fe_2(SO_4)_3 – ZnSO_4$ (1.5 M) – H_2SO_4 (0.3 M) – H_2O	25 – 90	
$CaSO_4 – Na_2SO_4 – ZnSO_4$ (2.5 M) – $MgSO_4$ (0.41 M) – $MnSO_4$ (0.18 M) – H_2SO_4 (pH 3.8) – H_2O	25 – 90	
$CaSO_4 – ZnSO_4$ (2.5 M) – $MgSO_4$ (0.41 M) – $MnSO_4$ (0.18 M) – $H_2SO_4 – H_2O$	25 – 90	
$CaSO_4 – (NH_4)_2SO_4 – ZnSO_4$ (2.5 M) – $MgSO_4$ (0.41 M) – $MnSO_4$ (0.18 M) – H_2SO_4 (pH 3.8) – H_2O	25 – 90	

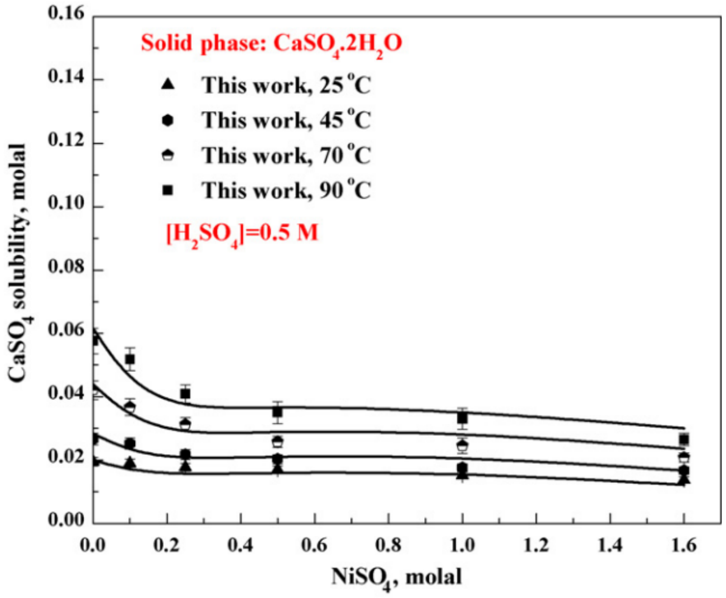

Figure 16. $CaSO_4$ solubility in $CaSO_4$-(0.5M) H_2SO_4-H_2O solution at 25,45,70 and 90 °C (Azimi & Papangelakis, 2010).

Anderko *et al.* (2002) pointed out that the knowledge of thermodynamic properties, phase equilibria and solubility of inorganic salts in electrolyte solutions is essential for the design and maintenance of hydrometallurgical operations. Azimi *et al.* (2007) recommended using the Mixed Solvent Electrolyte model (MSE) for describing those parameters of solutions. This model includes Pitzer method for describing the activities, based on the Debye–Hückel limiting law. It factors in both the long and short-range interactions between ions. Recently developed MSE model can calculate thermodynamic properties over the entire range of concentrations. The activity is modeled by factoring in the nonideality of electrolyte solutions and defined by the excess Gibbs free energy, G^E, of the solution as follows:

$$\ln \gamma_i = \left(\frac{\partial (G^E/RT)}{\partial n_i}\right)_{T,P,n_{i\neq j}} \tag{18}$$

where γ_i is the activity coefficient, n_i is the number of moles of the solution constituents (species i), and j is any other species; R is the gas constant and T represents the temperature.

$$\frac{G^E}{RT} = \frac{G^E_{LR}}{RT} + \frac{G^E_{MR}}{RT} + \frac{G^E_{SR}}{RT} \tag{19}$$

The excess Gibbs free energy in that model consists of three components, as can be seen in Eq. 9: the long-range electrostatic interactions described by the Pitzer-Debye-Hückel equation (G^E_{LR}), the middle-range interactions (G^E_{MR}) and the short-range interactions (G^E_{SR}), coming from molecule-molecule, molecule-ion and ion-ion interactions which can be calculated by the UNIQUAC model (Azimi *et al.*, 2007; Wang *et al.*, 2012). This model is implemented into the OLI Software platform which is commercial software, used for chemical modelling of hydrometallurgical solutions.

3.3. Calcium sulfate precipitation from solutions

3.3.1. Scale formation

Chemical precipitation from solutions, resulting in a fast formation of the solid phase is a process induced by physical or chemical changes within the solution. Essentially, it is the crystallization process of forming a solid particle with crystalline structure from the liquid. The main driving force for precipitation is the presence of supersaturation state in the solution (Dohring & Dixon, 2012). Gypsum precipitation phenomenon and resulting scaling process can be described by incorporating the approach of scale formation in pipe flow systems. Although the flow properties in the labyrinth path way and pipes are different, this type of approach is a good enough approximation of what is happening inside the emitters. Scaling proceeds through the following stages/phases (Ang *et al.*, 2011; Dohring & Dixon, 2012):

a) **nucleation** that results in the formation of minuscule solid particles due to a high condensation of ions in supersaturated solutions; can occur either in the bulk of solution or on the solid surface (i.e. pipe's wall),

b) **diffusion** transport mechanism of the solvated ions, crystalline matter, and other molecules from solution to the solid surface (which can be a pipe wall or larger crystals),

c) **crystal growth** resulting in an increase of tiny particle size until the point of supersaturation,

d) **flocculation** when solids start to interact with each other, forming larger aggregates

e) **deposition** previously transported components are adsorbed directly on the solid surface or other crystals which are already attached to the solid thus propagating the scale formation.

3.3.2. Effect of process parameters on gypsum scale formation

Hoang *et al.* (2008); (2011) tested process parameters and their influence on gypsum scale formation in pipes. Below a conclusion of their research work is listed:

a) Effects of temperature on scale formation

The temperature had a significant effect on the amount of gypsum scale deposited on the walls of test pipes (Figure 17). Tested solution contained 0.075M Ca^{2+}. Higher temperatures seemed to promote the scaling potential of gypsum significantly. However, it is important to note that the solubility of gypsum in this range of temperatures doesn't change significantly (Figure 13). Hoang *et al.* (2008) concluded that temperature wasn't the only parameter causing an increase in scaling rate. Elevated temperatures provided required energy to the molecules that allowed them to overcome activation energy of the precipitation reaction. The scaling phenomenon is thus happening quicker at higher temperatures.

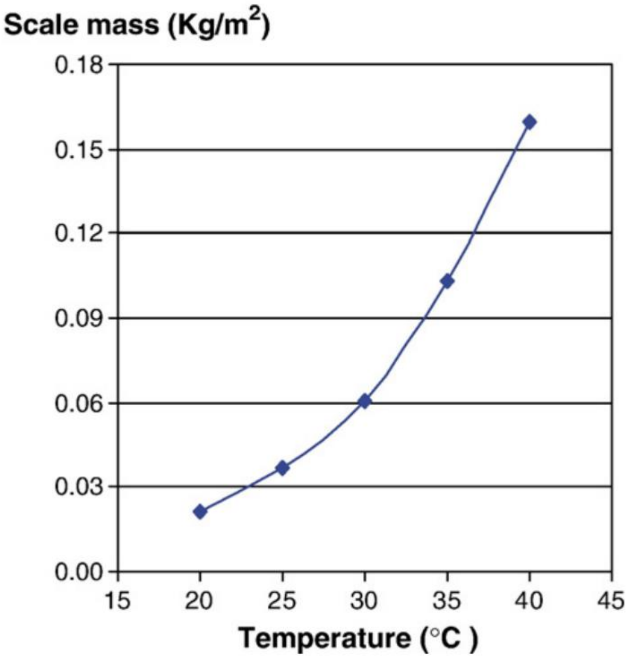

Figure 17. Mass of gypsum scale formed during the experiment regarding the solution's temperature. Flow rate: 30mL/min; run time: 3h; Ca^{2+} *concentration: 0.075 M (Hoang et al., 2008).*

b) Effect of supersaturation

The main driving force of precipitation from solutions was identified previously to be the presence of supersaturation state. The supersaturation ratio S is the ratio between the solution concentration C and concentration of saturated solution C^*, determined by the solubility curve. As can be seen from the Figure 18, at low supersaturation ratios, there was very little scale formed unlike for the higher values of S, where the scale formation was so great that it blocked the flow in the pipe. Authors also point out that below some supersaturation ratio the nucleation tempo is very low thus less scale is formed. Another conclusion from this study was that deposition of calcium sulfate on the pipe walls is a surface attachment controlled process.

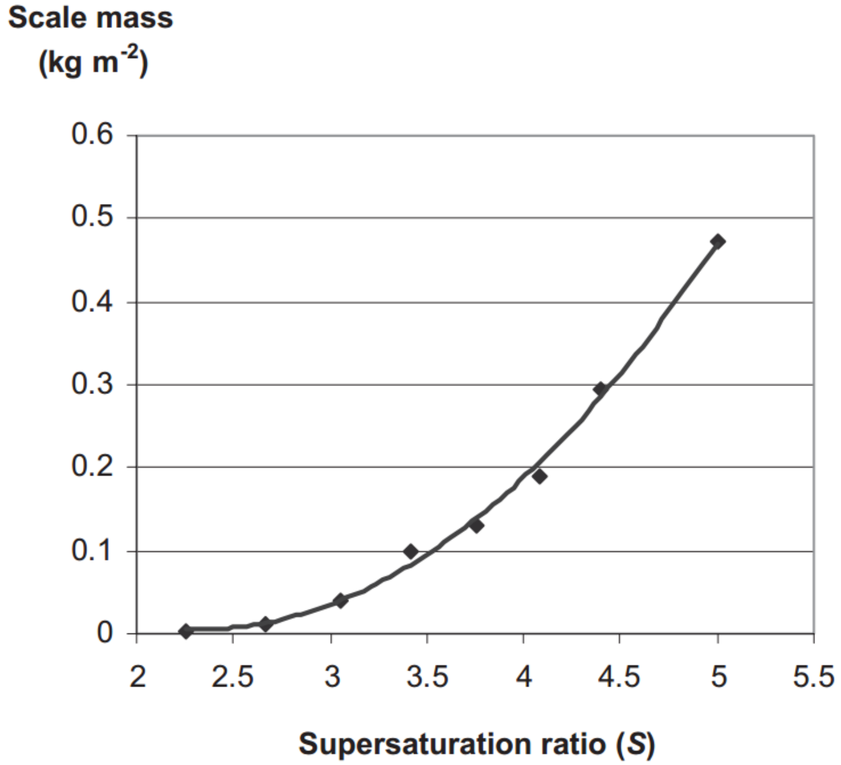

Figure 18. Mass of gypsum scale formed during the experiment regarding the supersaturation ratio, S. Flow rate: 30 mL/min; run time: 3h, T=20 °C (Hoang *et al.*, 2011).

c) Effects of the run time

Presence of supersaturation state in solution alone doesn't lead to scaling. Before solid material can develop, there is a need for many active nucleation centers. As soon as the nuclei are formed (either on the surface of the pipe or in bulk solution), the accumulation of deposits – gypsum – starts. Hoang *et al.* (2011) illustrated the dependency of scale mass formation regarding the duration of flow. They tested the two differently sized pipes with diameters of 0.7 and 1.3 cm which by size are like the irrigation hoses used by Terrafame. The conclusion from this study, depicted in Figure 19, clearly indicated that the amount of deposited calcium sulfate increased in time. Furthermore, linear relationship between the scaled mass and time was reported, however, initial hour of runtime was excluded from this regression due to small scale deposition.

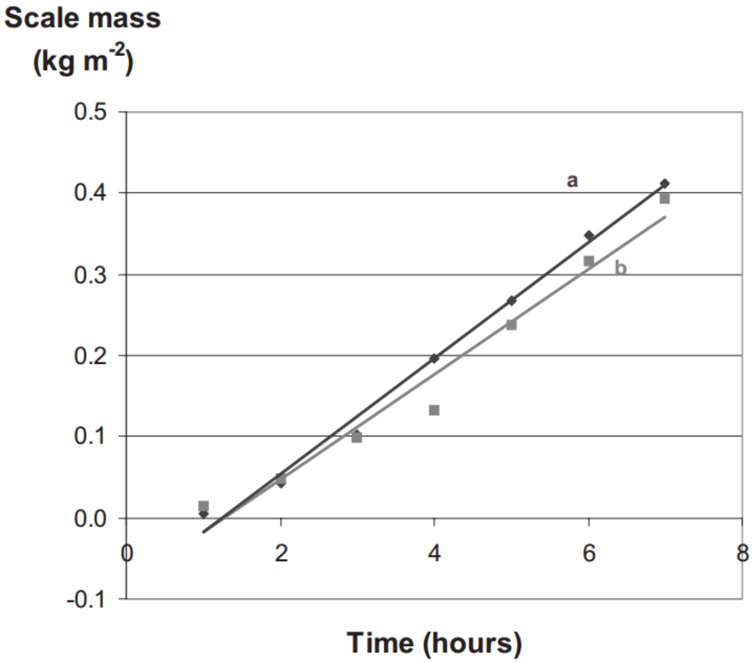

Figure 19. Mass of gypsum scale formed during the experiment regarding the run time. Flow rate: 30 mL/min; *S* = 3.75; T=20 ℃; pipe diameters: (a) 0.7 cm, (b) 1.3 cm (Hoang *et al.*, 2011).

d) Effects of flow rate and velocity

The effect of flow rate on the scale deposition was depicted in Figure 20. Higher flow rate causes greater scale deposition. This is assumed to be caused by the fact of more scale-forming material getting in contact with the surface. Moreover, the effect of pipe diameter was also significant, with larger diameters the scale mass deposition was relatively smaller. However, the total amount of scale was bigger due to the larger total surface area. A similar observation has been made for the relationship of scale amount deposited on the pipe walls vs. the velocity of flow. Scaling potential was greater for the faster solution flow. Also relationship to pipe diameter was observed.

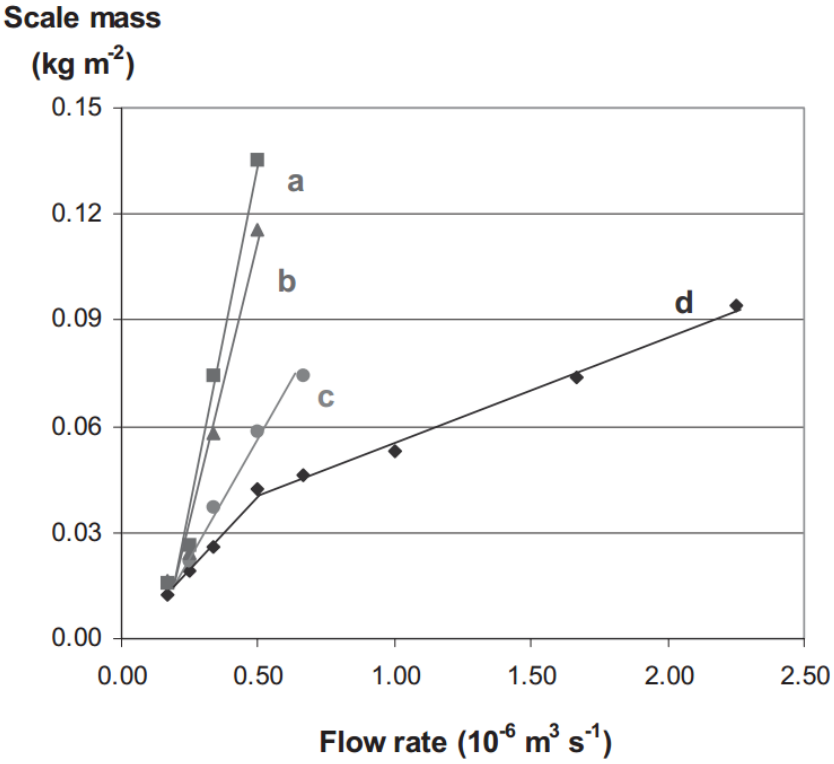

Figure 20. Mass of gypsum scale formed during the experiment regarding the solution flow rate. Run time: 3h; *S* = 3.05; T=20 °C; pipe diameters: (a) 0.3 cm, (b) 0.5 cm, (c) 0.7 cm, (d) 1.3 cm (Hoang *et al.*, 2011).

The results of this study are in contrary to conclusions from different research work. Ang *et al.* (2011) stated that the increase in solution velocity and thus higher flow rates, increase the shear and drag forces, exerted on the solid matter deposited on pipe walls. Watkinson and Martinez (1975), on the other hand, stated that the fouling resistance, for small flow velocities, increased with low velocities and decreased with higher ones. Therefore, it can be concluded, that the flow rate and velocity could cause higher scaling for small diameter pipes and low flows and could decrease it by forcing scale to detach in larger pipes and higher solution flows. However, due to the delivery of more scale-forming material it can have an opposite effect.

3.4. Emitter clogging

Drip irrigation technology also referred to as trickle irrigation, is a method commonly used in the agricultural practice and currently being employed in the mining industry for leaching purposes. Emitter clogging was identified as a major obstacle to development, maintenance, and operation of such irrigation systems.

3.4.1. Literature review

Most of the studies, regarding emitter clogging, are focused on irrigation systems in the agricultural world. The liquid distributed for those purposes is usually clean or reclaimed water (treated sewage effluent). Inspection of the flow properties of the drip irrigation system can be easily done simply by observing if there is any solution exiting the emitter. However, the external inspection alone is not sufficient as clogging starts inside the emitters and develops in time. Clogging influences the uniformity of the solution distribution greatly (F. Nakayama & Bucks, 1981). Moreover, F. S. Nakayama and Bucks (1991) pointed out that partial clogging is as bad as complete clogging due to the alternation of hydraulics in the entire irrigation cell. In agricultural world, this non-uniformity has a negative impact on plants growth whereas in case of bioleaching this leads to several processes limiting effects. Major causes of emitter clogging in such systems can be grouped into three categories (Taylor *et al.*, 1995):

a) physical plugging (caused by suspended solids),
b) chemical (caused by salts precipitation),
c) biological (caused by bacteria and algae).

Uys *et al.* (2000) identified two critical parameters determining the susceptibility of an emitter to plugging. The flow path size and the velocity of flow in the passage being those parameters. It is recommended by the authors to filter all particles larger than one-fifth to one-tenth of the smallest dimension of the emitter's flow path. Thus, classification of the sensitivity to clogging of emitters can be done by the size of labyrinth's flow path cross section. Emitters are sensitive to clogging once the cross section is smaller than 1.5 mm and above that value they are relatively insensitive. Furthermore, the discharge flow rate of an emitter was linked to clogging sensitivity by Ravina *et al.* (1992). Conclusion from their study was that emitters with smaller discharge values were always more susceptible to clogging. Liu and Huang (2009) listed filtering and flushing drip lines as simple and useful methods for clogging prevention. Whereas filtration will prevent solid particles of size from entering the drip line, the tool for detachment and removal of precipitated inorganic and organic material is flushing. Furthermore, the authors proposed acid injection as a tool for chemical precipitation control – not pertinent for Terrafame's process as the solution has very low pH already.

3.4.2. Emitter clogging in Terrafame

The review of existing literature, concerning emitter clogging subject, has shown that there is very little information about the chemical clogging and deposition of gypsum in the emitters. The physical plugging in the system is considered as a secondary factor which is triggered by the chemical precipitation first (for instance the precipitated solids can block the flow as they detach from the wall). Biological clogging, mentioned before, has not been identified in the system due to very extreme conditions which allow only the leaching bacteria to thrive. Although there is very little solid information about the formation of gypsum scale inside the emitters and clogging mechanism, some rough assumptions had to be made. These are based more on the overall comprehension of the scale formation in pipes, flow properties in the emitters and clogging mechanisms which were experimentally tested in the agricultural business, rather than on any experiments. Also, visual examination and practical insight gained from the Terrafame staff was factored in.

4. Experimental part

4.1. Characterization of the solids

The solid material had been collected from the drip lines and tested by the XRD and XRF analyses by the in-house chemical laboratory in Terrafame. The results obtained from the XRD were semi-quantitative (Figure 21). Calcium sulfate dihydrate – gypsum – was identified as the main phase, contributing to 82% of the sample. Moreover, jarosite along with other minerals was found; however, it should be stressed that the results come from the artificial process. Identified minerals, such as metamorphic cordierite, are formed in nature. It is unlikely that they were formed in the hoses. A better approach is to focus on the compound's composition rather than mineralogical formulas. Analysis of the XRD spectrum (Figure 22) was backed by the XRF test which helped to identify the composition of elements building the sample. It can be seen from the Table 4 that Ca/S ratio indicates Ca-sulfates. Moreover, iron hydroxides are also probable; judging by the potassium content, jarosite could represent them. Because gypsum was the dominant phase, it diminished the other elements. Summary of this analysis is that the main compounds found are gypsum, jarosite (different forms) and sulfur. Moreover, with some uncertainty, carbonates, silicates and aluminosilicates were also identified.

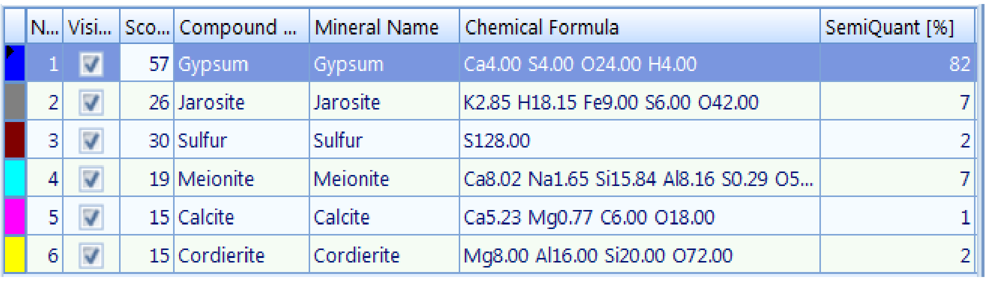

	N...	Visi...	Sco...	Compound ...	Mineral Name	Chemical Formula	SemiQuant [%]
■	1	☑	57	Gypsum	Gypsum	Ca4.00 S4.00 O24.00 H4.00	82
■	2	☑	26	Jarosite	Jarosite	K2.85 H18.15 Fe9.00 S6.00 O42.00	7
■	3	☑	30	Sulfur	Sulfur	S128.00	2
■	4	☑	19	Meionite	Meionite	Ca8.02 Na1.65 Si15.84 Al8.16 S0.29 O5...	7
■	5	☑	15	Calcite	Calcite	Ca5.23 Mg0.77 C6.00 O18.00	1
■	6	☑	15	Cordierite	Cordierite	Mg8.00 Al16.00 Si20.00 O72.00	2

Figure 21. XRD results table

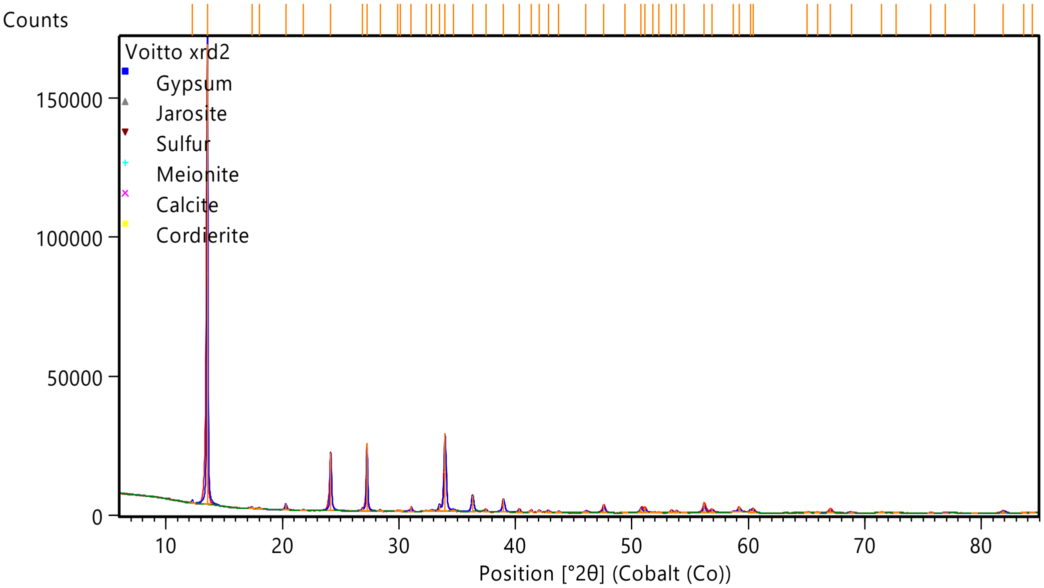

Figure 22. XRD spectrum image.

Table 4. XRF analysis results.

Element	**Value** [%]	**Element**	**Value** [%]
Na	0.16	Ti	0.05
Mg	0.32	Mn	0.55
Al	0.36	Fe	8.42
Si	1.20	Ni	0.26
P	0.03	Cu	0.02
S	24.25	Zn	0.21
K	0.83	Sr	0.01
Ca	30.53	Y	0.01

4.2. Calcium sulfate solubility tests

4.2.1. Motivation

Calcium sulfate has been identified to be the main solid found in the system. After an extensive review of the current state of the research, the conclusion was made that no one has yet tested the solubility of gypsum in similar thermal conditions and multi-component solution with a similar composition of metal ions, sulfate and acidity. Results of these tests have been identified as beneficial for the company. Knowledge of gypsum solubility curve in the PLS will allow for further considerations. Solubility tests were carried out using two different ways, described below.

4.2.2. Methodology for the initial tests

Sampling was done by collecting approximately 1 L sample of the PLS from selected points in the irrigation system (listed in Table 5). In addition to that a small sample of the PLS was taken and sent to the chemical laboratory for the ICP analysis to determine the composition of the PLS; temperature of the PLS was also recorded. Collected samples were kept refrigerated in the commercial refrigerator for approximately two months. This refrigerator provided the temperature of approximately +4 °C with a significant variance between the temperature on the top shelf and the bottom (~ 1 °C difference). Moreover, samples were shaken daily to prevent from large differences in concentration of the PLS in the bottle and provide agitation.

Table 5. Sampling points description for the initial solubility tests

Sampling point	Samples No.	Description	Comments
A1K1.1	7	Heap number 1 Inlet to irrigation cell 1	The oldest heap in leaching pad 4
A1K1.2	7	Heap number 1 Outlet from irrigation cell 1	
A5K2.1	7	Heap number 5 Inlet to irrigation cell 2	This cell consisted of the test drip lines from different manufacturers
A5K2.2	7	Heap number 5 Outlet from irrigation cell 2	
A6K1.1	4	Heap number 6 Inlet to irrigation cell 1	The youngest heap in leaching pad 4
A6K1.2	4	Heap number 6 Outlet to irrigation cell 1	
IP4	7	Irrigation Pond 4	–
PLS4	7	PLS Pond 4	–
Total	**50**		

Leaching pad number four had been chosen for these tests since, at the time, it was the youngest heap. Three irrigation cells were selected on three different heaps. Samples from both the inlet and outlet were collected. The average ambient temperature during the tests was 0 °C. Additionally, cell 2 on heap 5 contained the test irrigation drip lines described in Section 4.3.

4.2.3. Results and conclusions from the initial tests

After 65 days, a sample of PLS was taken from the cooled bottles and diluted with distilled water 1:10 to prevent changes in the solution. The analysis of 50 collected samples, resulted in creating a data set consisting of 30 variables. The concentrations of ions such as Al, Ca, Cd, Co, Cu, Fe, Mg, Mn, Na, Ni, Zn were tested as well as the redox potential and pH of the solution. Detailed information about the composition of PLS are confidential and cannot be published except for the concentration of calcium.

Table 6. Basic statistics of calcium concentration from the initial solubility test in mg/L.

Ion	Ca
MIN	651
Q1	674.5
MEDIAN	688
MEAN	686.5
Q3	694.5
MAX	724

Samples collected from the PLS pond 4 exhibited large iron oxidation (change of color from green to brownish) during the run-time of this test. Moreover, all samples collected from the outflow of the irrigation cells contained a layer of solid matter deposited at the bottom of bottles (1–2 mm thick).

The results obtained from this test had large variations. From Figure 23, it can be seen that there were practically no significant correlations obtained. However, some positive correlations could be seen from samples collected at the outflows of irrigation cells, located on heaps 1 and 5. It can be assumed that the solid matter deposited at the bottom was most probably gypsum. During the frequent mixing of those samples, the solid matter acted as seeds in the crystallization process, boosting the precipitation. However, those tests did not produce a clear answer that would lead to producing a viable solubility curve, several conclusions can be drawn. First, the average drop-down in calcium concentration over that period was approx. 95 mg/L (large variation in results should be accounted). Second, introducing seeds to the precipitation experiment, combined with frequent mixing, produced more accurate results. Moreover, iron (II) oxidation is something that cannot be prevented during such experiments and should be accounted in analyzing the results. Finally, more accurate experiment procedure is needed.

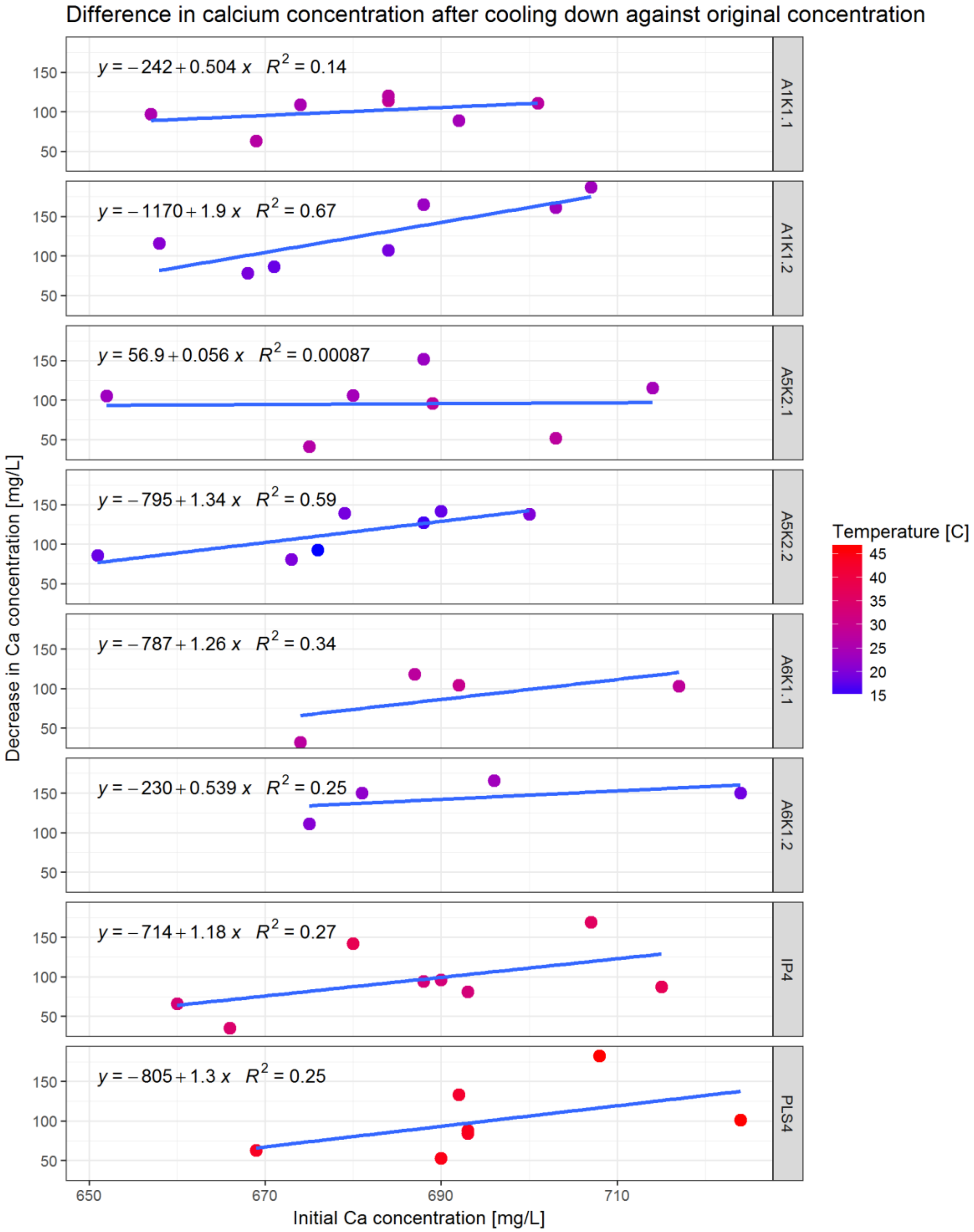

Figure 23. The decrease in calcium concentration against the initial concentration, grouped by sampling location, legend color corresponds to the PLS temperature during sampling, linear regression model used with parameters displayed on each plot.

4.2.4. Methodology for concise tests

The solubility test has been partially based on the research made by Wang *et al.* (2012). The procedure has been modified to mimic the conditions found in the system. However, due to delay in delivery of required equipment, results of these tests could not be produced within the time frame of this Thesis Project. Nonetheless, a know-how of best practice to perform such tests on Terrafame PLS was created. Moreover, the testing station was set up and prepared for the future tests.

Sampling

A Large sample of the PLS will be collected once from a selected point in the irrigation system. This procedure decreases the variability in ions concentration that could distort the results. The purpose of this experiment is to find out what is the calcium sulfate solubility in the irrigation system thus one of the irrigation ponds has been identified as the best place to sample since the collected material will mimic the reality best.

Experimental Apparatus

Solubility experiments were carried out in a large water bath (Memmert WNB 45) with the temperature control range of 10 °C – 95 °C. Additionally, Peltier cooler was installed aside to achieve temperatures below room temperature. Peltier cooler does not provide temperature control; it is entirely controlled by the water bath built-in thermostat. Samples of the PLS were saturated with Ca^{2+} using anhydrite powder ($CaSO_4$). The solution was mixed for equilibrium in glass bottles with screw caps, using the magnetic stirring plate (2MAG MIXDRIVE6). Both of those solutions were selected to protect the PLS from large iron oxidation caused by exposure to air.

Experimental procedures and conclusions

Although the tests using this approach were not carried out, some initial tests were performed to produce the best practice of doing such experiment.

The solution upon collection has approximately 30 – 35 °C and during storage it drops down to room temperature (~ 18 °C). This implies that part of the calcium might precipitate as gypsum. Therefore, the solution should be re-saturated (for approximately 24 hours) by heating and then cooled down (for another 24 hours) and agitated by stirring. After 24 hours of cooling, the stirring should be turned off and the solution should be allowed to settle down. After approximately 8 hours the supernatant should be formed on the top and the solids deposited at the bottom of the bottles. The sample for the ICP analysis should be taken from the supernatant.

During the initial tries of this approach, solution exhibited a significant oxidation of iron (all samples turned from green to brown which is a good indicator of ferric to ferrous iron oxidation) upon re-saturating. This could distort the results as the ionic strength of the solution is altered. However, the research review showed that gypsum solubility is influenced more by the anions present in the solution rather than the cations.

Another approach was also implemented, based on the seeded batch crystallization. This methodology could produce more important information than the calcium solubility as it will answer how much calcium can be precipitated from the solution in conditions mimicking the real-life situation. Four samples were prepared, 400 mL each, and placed in the water bath cooled down to approx. 4 °C. One sample was not seeded, two were seeded with anhydrite (approx. 0.5 gram) and the last one was seeded with a large amount of anhydrite (approx. 5 grams). All samples were kept stirred for a week. Sampling was done from the supernatant and the results showed a drop down in calcium concentration in the fourth sample of approx. 200 mg/L after one week. The samples with slight anhydrite saturation as well as the non-seeded sample exhibited similar calcium ions reduction of approx. 50 mg/L. This shows that seeding and introducing appropriate agitation (mixing) can produce positive results in the removal of calcium ions from solution. However, it is still upon testing to use the different material as seeds (for instance sand) to decrease the amount of calcium added.

4.3. Dripline tests

The clogging phenomenon was addressed from the technical perspective as well. Drip lines of different manufacturers were tested in the system and compared to the ones currently in use. Names of manufacturers and models of tested drip lines are hidden – this information is not important for this work. The place selected for these tests was in the leaching pad 4, on heap 5, within the lower cell of the second irrigation section. Driplines were laid next to each other and connected to the system as follows in Figure 24. The available technical parameters of each drip line were listed in Table 7. All used drip lines had the in-line emitters, embedded in or on the hoses. Driplines manufactured by Azud and both Type B and C had cylindrical emitters (see Figure 7), whereas Type A, D and E drip lines used emitters embedded in the wall of the hose – the emitter stands in the way of the flowing solution (Figure 25).

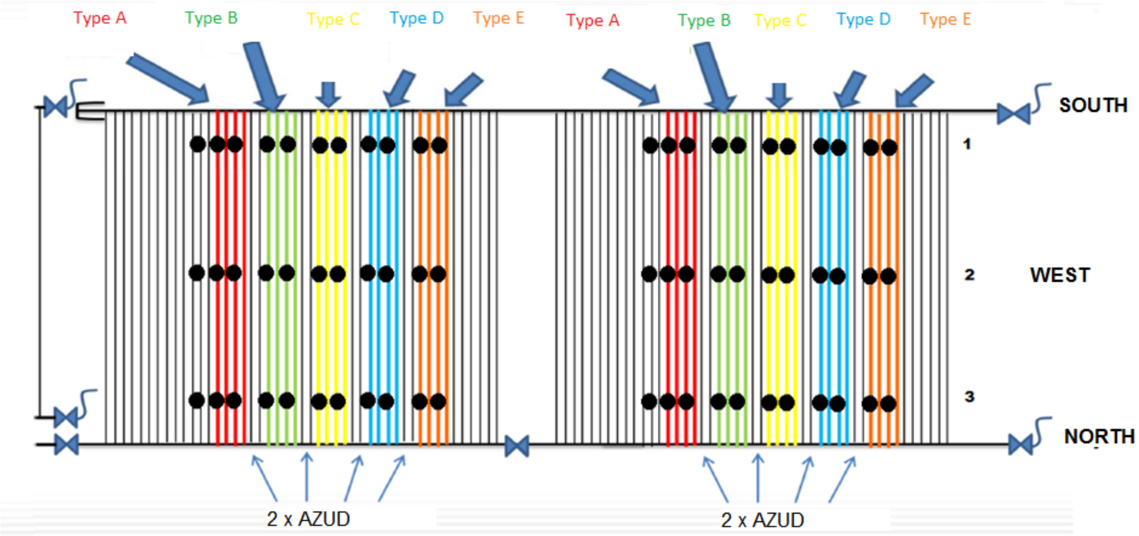

Figure 24. Layout of the driplines test; different types marked according to color. Source: Terrafame's materials.

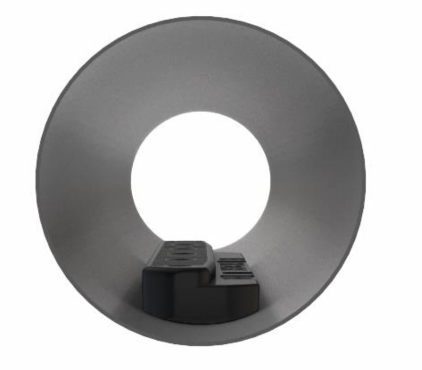

Figure 25. In-line emitter placed on a wall of the hose (cross sectional view of the Netafim Aries drip line). Source www.netafimusa.com.

Table 7. Technical parameters of tested drip lines.

Drip line:	**AZUD**	**A**	**B**	**C**	**D**	**E**	**Unit**
Emitter type	Cylindrical	On-wall	Cylindrical	Cylindrical	On-wall	On-wall	
Nominal flow:	4	4.2	4	8	4	6	L/h
Min. emitter spacing:	60	20	60	75	100	100	cm
Nominal thickness:	0.9 – 1.0	1.2	1.14	1.14	1.0	1.0	mm
Inner diameter:	13.6	14.2	14.0	14.0	14.0	14.0	mm
Outer diameter:	16.0	16.6	16.0	16.0	16.0	16.0	mm
Max. pressure:	3 – 3.5	4.0	3.45	3.45	4.0	4.0	bar
Discharge coef. (k):	1.34	1.455	N/A	N/A	N/A	N/A	–
Discharge exponent (x):	0.47	0.46	N/A	N/A	N/A	N/A	–

The test ran from week 7 until week 15 of 2017 and was based on measuring the dripping flow rate, Q, from selected emitters (marked by black dots in Figure 24). The value which was measured was the time needed to collect 10 mL of solution from the emitter and after that recalculated to L/h as follows in the Eq. 19.

$$Q = \frac{10}{recorded\ time}\left[\frac{mL}{s}\right] \cdot 3.6 \rightarrow \left[\frac{L}{h}\right] \tag{20}$$

Data were obtained from 33 sampling points using the following methodology:

- weekly measurements (initial assumption was to measure twice per week but it has changed to 1 over time)
- Two measurements per hose type (2 different hoses considered, for Azud – 1)
- Three measuring points per each hose
- In total: 6 measurements per hose type per cell
  12 measurements per hose brand

Obtained figures were plotted against time and results analyzed. The flow rate from emitters had an increasing trend in time. From Figure 26 we can observe that at the beginning of the operation, between weeks 7 – 10, most of the drip lines met the target flow properties. After that time, we could see a rapid increase in the flow rate from the drip lines A and D – possibly caused by pressure increase due to clogging of other emitters in the drip line. Whereas the increase in flow was observed from all drip lines, Azud and Type B drip line remained close to their target value for the longest period. In the Western part of the comb, the variation in flow rates was significantly larger. Especially during week 9, where for the Type B drip line measured flow rate was above 20 L/h (probably measurement error). From Figure 28 we can conclude that until week 12 all drip lines, except for Type E, remained close to their target values – neglecting the outlying value measured in week 9 for Type B. After that time, we can observe that the most stable drip lines were again Azud and Type B. This conclusion is also visible when average value of flow rate from two is taken (Figure 30).

Another aspect of these tests is the analysis of the no-flow instances, obtained during sampling. For the part of irrigation cell located in the East, many no-flow instances were observed for the Type A, Type D and Azud drip lines whereas, in the opposing cell, Type E, D and B are the drip lines which failed most frequently to deliver the solution, consecutively. These results give opposing information from two parts of the irrigation cell. Nonetheless, considering a few sampling points (3 per drip line where the number of emitters is approx. 60), it can be assumed that those differences could occur. The no-flow instances were most likely caused by solution freezing or some temporary blockage; precipitation is also considered to play a significant role.

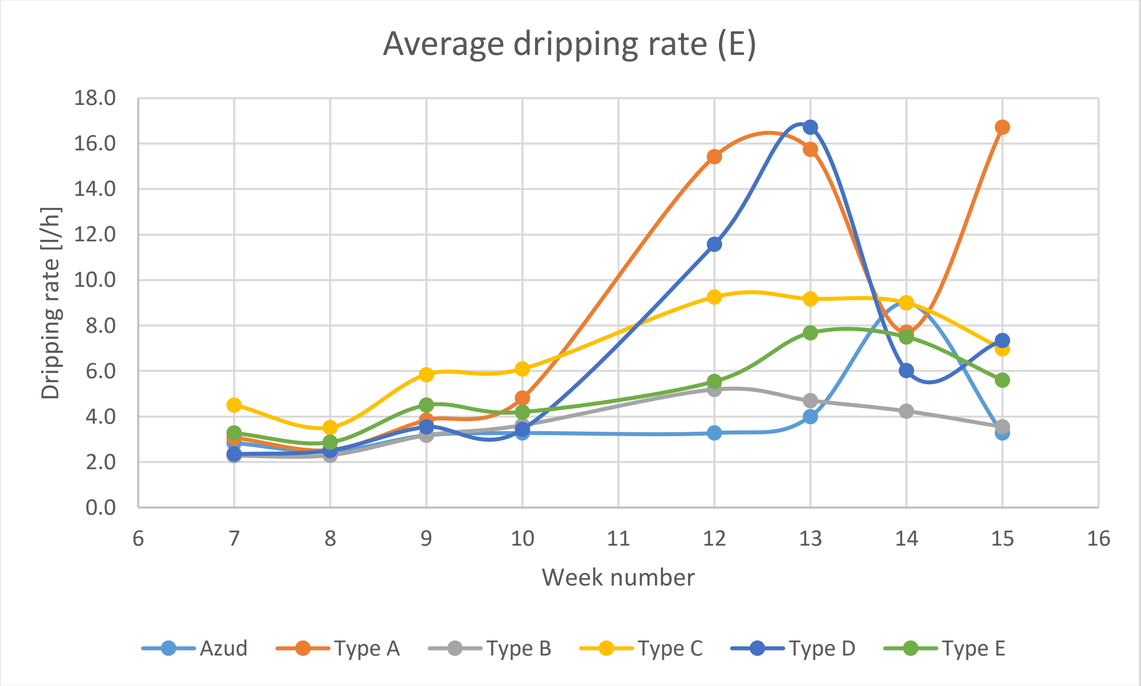

Figure 26. The average dripping rate in the Eastern part of the test cell.

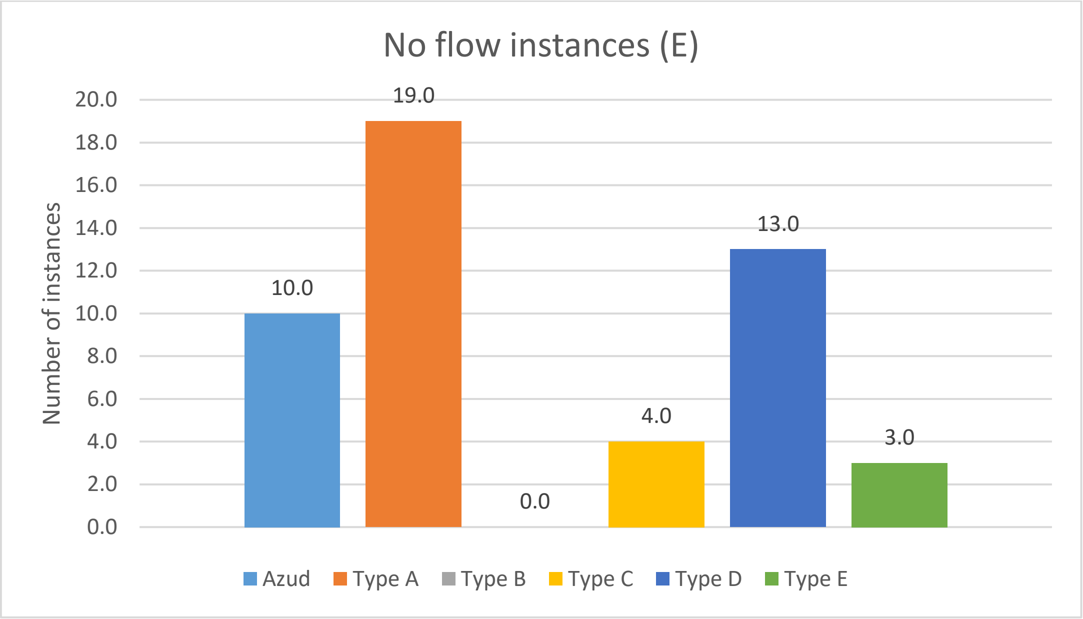

Figure 27. The number of no flow instances in the Eastern part of the test cell.

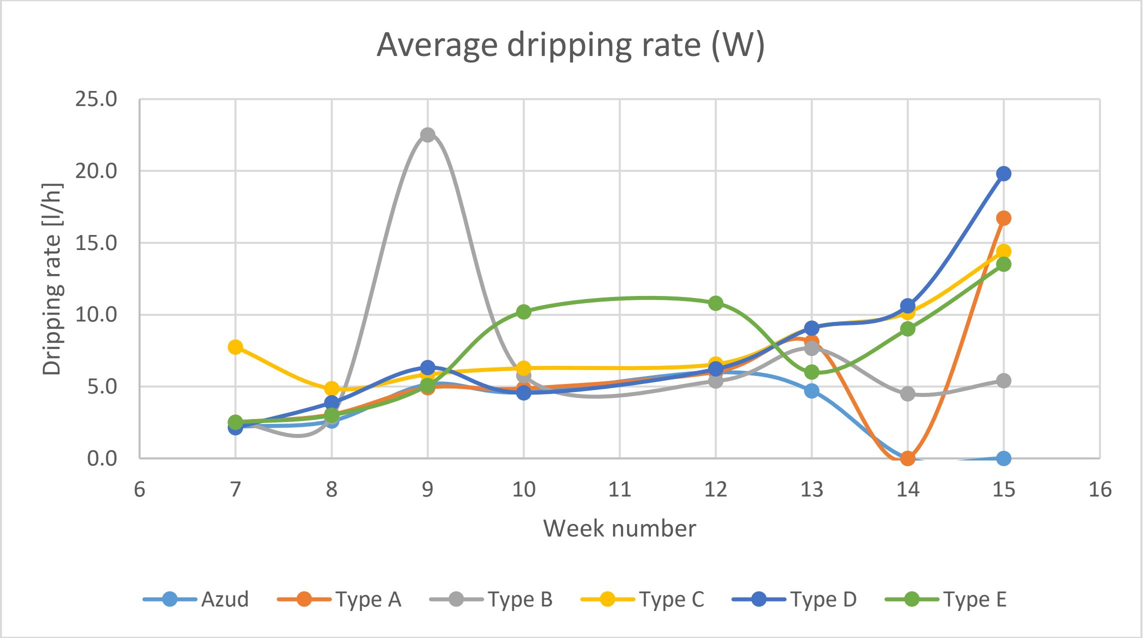

Figure 28. The average dripping rate in the Western part of the test cell.

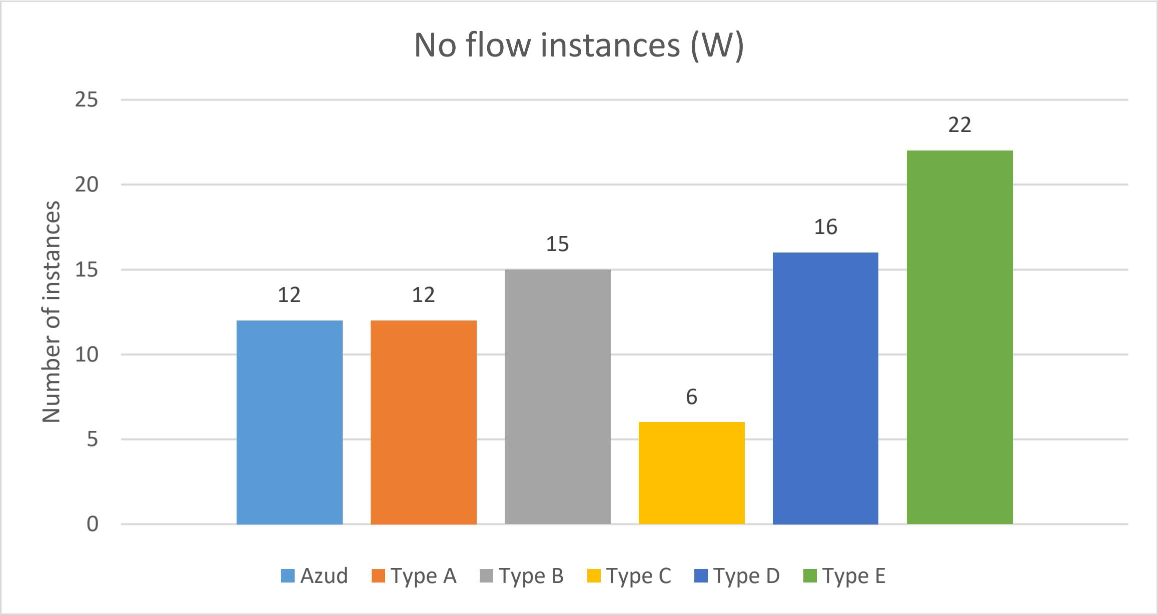

Figure 29. The number of no flow instances in the Western part of the test cell.

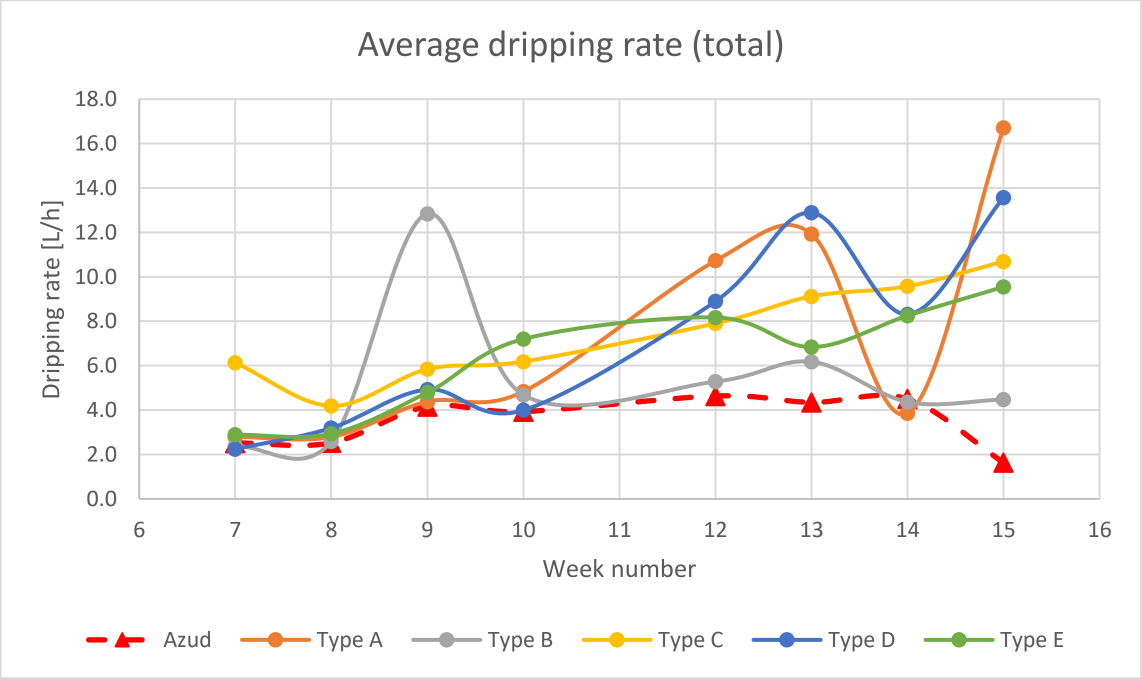

Figure 30. The average dripping rate in the test cells.

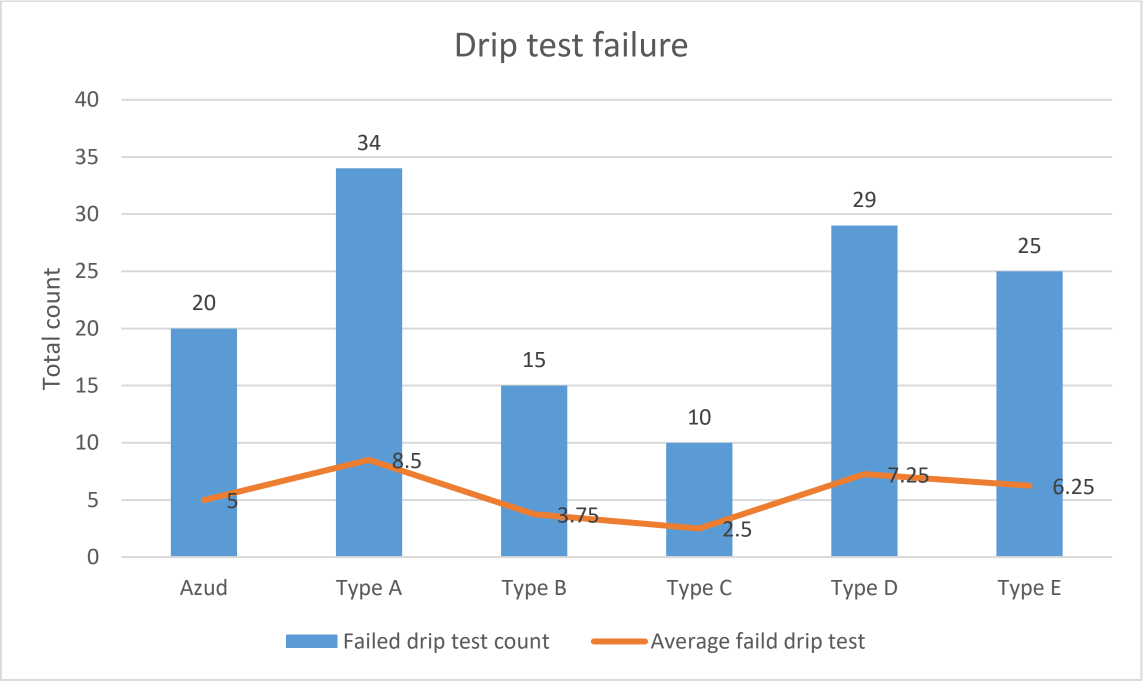

Figure 31. The total number of no-flow instances with the average value per hose.

When looking at the problem in the domain of one irrigation cell, some pattern had been discovered. Namely, the flow rate hindering was much more visible in the regions away from the inlet to the cell. Furthermore, the lower cell exhibited more no-flow instances in comparison with the first one. The increase in flow rate which is observed in time can be explained by the increasing pressure inside the laterals as more and more emitters begin to clog. Moreover, it can be concluded that the drip lines with emitters embedded on the walls are performing less effective in comparison with the cylindrically shaped type emitters. It is believed that gypsum scale can easily build up on the emitter since it is placed in the way of the flowing solution, obstructing it. From tested drip lines, Type B and C performed best. The model with 8 L/h solution yield was most resistant to clogging. However, the flow rate was too high for the parameters of the bioleaching process and heap parameters (to prevent from clogging the heap by fine particles, large distances between emitters should be applied, causing significant parts of the ore being excluded from irrigation). Setting aside the Type B and Azud drip lines, similarities in performance can be observed, especially in maintaining the flow rate at a constant rate which can be an indicator of clogging. The question arises if it is necessary to replace the existing irrigation system with a different manufacturer’s equipment when no significant difference is seen. Unfortunately, the results obtained from these tests don’t provide a clear answer. One of the parameters that could bias the decision is the cost difference between the drip lines; however, such calculation is not within the scope of this work.

4.4. Drip line inspections

During this project, irrigation system had been investigated both from the data analysis point-of-view and visual inspections of the irrigation system on the field. Some drip lines had been collected and examined. The emitters were stripped from the plastic housing to see the labyrinth flow path and inspect the precipitation and how it forms. The following statements can be concluded from observations, although they cannot be assumed as a rule due to the relatively small number of samples collected:

Conclusion 1: Precipitation forms first either around the orifice or at the inlet to the emitter (mesh) or in both of those spots, obstructing or completely blocking the flow.

Conclusion 2: Once the discharge is blocked, more and more solid matter is being accumulated within the emitters, causing complete sealing of the flow path.

Conclusion 3: After the number of clogged emitters rise, the discharge from already working ones increase significantly. Eventually speeding up clogging within their structure.

Conclusion 4: Distribution of clogged emitters is denser further away from the inlet to the irrigation cell.

Sections of drip lines with emitters were collected from the area of leaching pad 4 from laterals changed 7, 10 and 14 days before sampling. Emitters were stripped, opened and photographed (see Appendix C). The important thing to stress is that examined emitters were clogged (no flow was observed from them).

Visual inspection of the 7-days-old sample showed that the precipitation was concentrated around the orifice mostly. There was no significant accumulation of solid matter found in the labyrinth flow path or the entrance to the emitter (mesh). The 10 and 14-days-old sample had much larger precipitate content, concentrated both at the entry mesh (which was completely sealed) as well as around the orifice. Moreover, the solid matter was seen along the flow path, deposited in the hollows. The overall pattern of precipitation magnitude was observed as depicted in Figure 32. Close to the inlet to the irrigation cell, there was very little solid matter observed, and the flow from emitters could be seen. On the opposite side of the irrigation cell, however, there was visually much more precipitates (inside the hoses). Also, the flow from drip lines located in that area was either less uniform (most clogged) or there was completely no flow. Interesting observation, supporting this hypothesis, can be observed on the border line of two irrigation cells. Drip lines at the end of the first one are clogged whereas the next drip line, which belongs to the second cell, exhibits flow from the orifices.

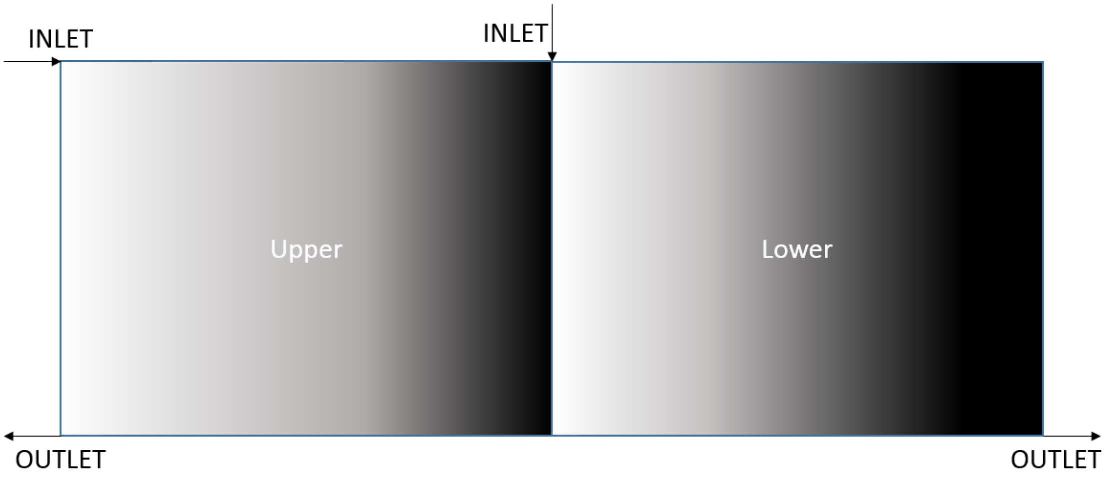

Figure 32. The observed distribution of clogged emitters within the section of irrigation (white color represents working emitters; black color represents clogged emitters).

This observation can be explained by the decrease in pressure head inside the irrigation cell, further away from the inlet. Based on the technical properties of emitters, lower pressure inside the lateral will cause smaller discharge rate from an emitter and thus make it more prone to clogging. This has been partially countered by influencing the design of several irrigation cells. In the new approach, the sub-main pipe has a decreasing diameter, starting with 110 mm at the inlet and finishing on 63 mm at the end of the cell. The decrease in cross-section of the flow path will increase the pressure and make it more uniform along the sub-main line.

Gypsum precipitates on the walls of the sub-main pipes as well. The methodology of sub-main pipes' diameter reduction, mentioned above, leads to another obstacle which is a complete sub-main pipe clogging due to scale deposition. Recently, it has been observed at the very end of irrigation cells. This issue is currently countered by flushing the sub-main pipes with pressurized water by an external company. This task is not performed along with every drip line replacements.

4.5. Conclusions

Calcium sulfate dihydrate was confirmed to be the primary solid found in the irrigation system. The experimental part revealed that the solubility of gypsum should be tested in more controllable conditions to produce a meaningful solubility curve. The initial trials, carried out using the second testing method, showed very promising results – know-how information were left at the company for these tests to be continued.

The drip lines with a cylindrical embedded emitter exhibited a better performance compared to the ones with an emitter attached to the wall of the hose. Moreover, a clear pattern of clogging distribution was observed on heaps – clogging more prominent away from the inlet to the irrigation cell.

5. Data analysis

Terrafame has inherited many historical process data from its predecessor – Talvivaara Mining Company. Bioleaching has been monitored since the commencement of operation. Since the acquisition, new owners decided to continue this approach. During the few recent years, leachate sampling system has been expanded and developed to deliver more accurate information about the performance of bioleaching process. New sampling points were added, allowing the company to quantify and assess nickel leaching rates. Precise knowledge of the efficiency is very important as it conveys significant information from the point-of-view of mining company operations; metals recovery plant can plan metal production and the officials can improve their business decisions. Moreover, leaching itself can be improved by exploring and analyzing the data.

One of the main targets for this project was to perform a detailed analysis of these data sets, collected during the period of almost ten years (2008 – 2017). This research aimed mostly on tracking the patterns promoting gypsum precipitation. Moreover, the exact composition of the PLS is the company's secret and cannot be published.

5.1. Data sets

5.1.1. Leachate composition

5.1.1.1. Sampling points and methodology

The leachate is sampled at multiple points from the system, and the great majority of data come from the primary leaching stage. Samples are collected regularly and recorded. Each leaching pad has its label which can be used for its assessment. Starting from the irrigation, we can obtain data collected from the top of the heap (straight from the irrigation pipes). After that, we can monitor the PLS composition that exits the heaps. Wells allocated on each drainage side (the one which the drainage layer is tilted towards) allow for the insight into the performance of each heap separately. Additionally, we can also obtain information from the inlet to the PLS pond which is an average of the data from the wells. The available data also contains information on the PLS composition at different places along the circulation pathway (secondary leaching, different ponds, etc.).

At first, the overall situation is viewed, containing full data set. For the purpose of this Thesis though, only primary leaching data are considered. This constraining assumption has been taken due to very complicated relationships of leachate circulation and the fact that clogging problem is most prominent in the primary stage of leaching. This approach might imply that the overview of the system will not be understood correctly. However, the effects observed in the primary leaching leachate composition are a result of components of the entire system acting together (because the circulation system is closed).

PLS collection and testing

PLS is collected from the system regularly, twice per week, sent to the chemical laboratory and analyzed. The methodology of sampling varies between the sampling points. In most cases leachate is collected into plastic containers attached to a long stick, allowing to reach the liquid, i.e., in the wells. After the sample is collected temperature measurement takes place and the sample is placed in a special plastic bottle. Temperature values can be significantly different from the reality; the time between collecting and taking the temperature measurement varies greatly and depends on the person taking the measurement. This can have a negative effect, especially during the winter period when the ambient temperature drops down to over -30 °C. Furthermore, the time between sample collection and delivery to the laboratory can also distort real values; temperature change can trigger gypsum precipitation thus lower the value of dissolved Ca^{2+} ions. Nonetheless, it must be stressed that the underlying reason of leachate sampling is the assessment of metals extraction efficiency.

The concentration of ions in the PLS is assessed by the inductively coupled plasma mass spectrometry method. The samples are filtered before going into the machine thus only dissolved ions are factored in. Unfortunately, there has been no indication of the TDS content in the PLS; however, for some samples, total solids are calculated.

5.1.1.2. Data set description

The total number of observations selected for the analysis was over 59 000, collected over the course of 9 years from 2008 up until mid–2017. Most of those observations contained the following variables with the unit used for reporting indicated in the brackets:

- Date of collection
- Sulfate concentration [mg/L] – rarely assessed
- Leachate temperature [°C]
- pH value [-]
- Redox potential [mV]
- Dissolved oxygen [mg/L]
- Concentrations of the following ions [mg/L]: Al^{3+}, As^{3+}, Ca^{2+}, Cd^{2+}, Co^{2+}, Cr^{3+}, Cu^{2+}, Fe, K^{+}, Mg^{2+}, Mn^{2+}, Na^{+}, Ni^{2+}, Si, U, Zn^{2+}, Fe^{2+} and Fe^{3+} which is back calculated as a difference of total iron and iron (II)

The information about Uranium and Silicate concentrations in the PLS were excluded due to errors in reported values.

5.1.2. Ambient temperature

Weather conditions are monitored at the site since September 2015. Both precipitation and temperature data are recorded daily. Missing historical data can be obtained from the Finnish Meteorological Institute weather station, located in Sotkamo – Kuolaniemi (approx. 20 km north–east of the site).

5.1.3. Operational information

The data and information gathered from the operational practice on site could be one of the most valuable pieces of knowledge, giving a non-numerical insight into the system.

5.1.3.1. Heap construction and irrigation logs

Set of historical information about the heap construction progress, completion and commencement of irrigation are available. These data give a good overview of when the leaching was started and can be used as a starting point for some further observations.

5.1.3.2. Dripline replacement logs

This important set of information, containing logs of drip line replacement events, is a great tool to assess the lifetime of laterals and the magnitude of clogging phenomenon. The dataset is rather small, compared to previously described, since those kinds of information have been collected since 2015 with variable conscientiousness. Most data had been collected from the leaching pad 3.

5.1.3.3. Experience and observations

Much important information was obtained from the personal experiences and practice of the staff. This is a valuable piece of non-numerical insight into the operations of the system. Moreover, the know-how that Terrafame has created during the years of its operation allowed for better comprehension of observed values.

5.2. Methodology

The data were imported from the Terrafame system. Due to many variables, R programming language was employed to make the analysis feasible. This step involved familiarizing with the software and learning new methods of data analysis. After all data points were reshaped, analysis of outliers was performed. These values are defined as observations significantly standing out from the rest of the observations. Outliers analysis is one of the most important tasks during the data analysis. The process of identifying outlying data points is a purely mathematical problem whereas recognizing them as untrue values and removing from data set is rather based on an overall data comprehension and common sense. We can distinguish two types of outliers: statistical and technical/data entry. The statistically identified outlier might be a valid data point whereas a mistyped value cannot. This especially applies to the process data which in this case (as described previously) are erroneous due to, for instance, inaccurate sampling or hand data input.

Technical outliers can be initially eliminated by the visual analysis of plotted data (i.e. by using the scatter plots). Every observation which seems way off from what it is supposed to be can be eliminated. For the statistical outlier search, boxplots (Tuckey's method) are a very useful tool. Despite the outlier detection, their structure is also capable of presenting information about the data set in a condensed form. This type of plot consists of the box whose upper and lower line inform about the 3rd (Q3) and 1st (Q1) quartile of the whole set respectively. The distance between those lines is understood as the interquartile range ($IQR = Q3 - Q1$). Line within the box represents the median. Whiskers extend to the maximum and minimum values in the set, excluding outliers (Cox, 2017). One of the most commonly used methods for outliers identification is the IQR method. Values outside of the range written in Eq. 20 are treated as outliers.

$$Outliers \notin [Q3 + 1.5 \cdot IQR; Q1 - 1.5 \cdot IQR] \quad (21)$$

5.3. Results

5.3.1. Outliers analysis of the process data

Analysis of the outliers was initially focused on identifying both technical and data-entry outliers. This step has been performed by visual observation of the variability in the plotted data. Each variable, from every sampling point, was a subject to this examination. The decision had been made to remove the identified values as they distorted the data interpretation greatly. Criteria for removal were based both on the process knowledge and common sense. For instance, values of temperature exceeding 100 °C or pH > 7 were considered as untrue and impossible, thus removed. Consequently, the analysis in search of the statistical outliers was performed by introduction of boxplots with 1.5IQR coefficient applied. Statistical outliers have been identified for most of the variables. In Figure 33 we can observe that the temperature of PLS leaving leaching pad number 4 has many outlying values present. However, those values are treated as outliers by the Tuckey's boxplot, they can be considered as realistic data. For instance, looking at the temperatures observed in the outflow from the third leaching pad, we can observe that the values which are marked as extremely outlying in pad 4, here are considered as a viable piece of information. Therefore, a conclusion might be drawn that for process data from such complicated system, with many variables and interconnections, it is justified to either ignore the statistical outliers or increase the range of the outer fences of the box plot, for example to 2.5IQR. The boxplot with an increased range of tolerance, presented in Figure 34, shows that none of the previously identified outliers are still in that group of data. Similar comparison can be seen between boxplots depicted both in Figure 35 and Figure 36.

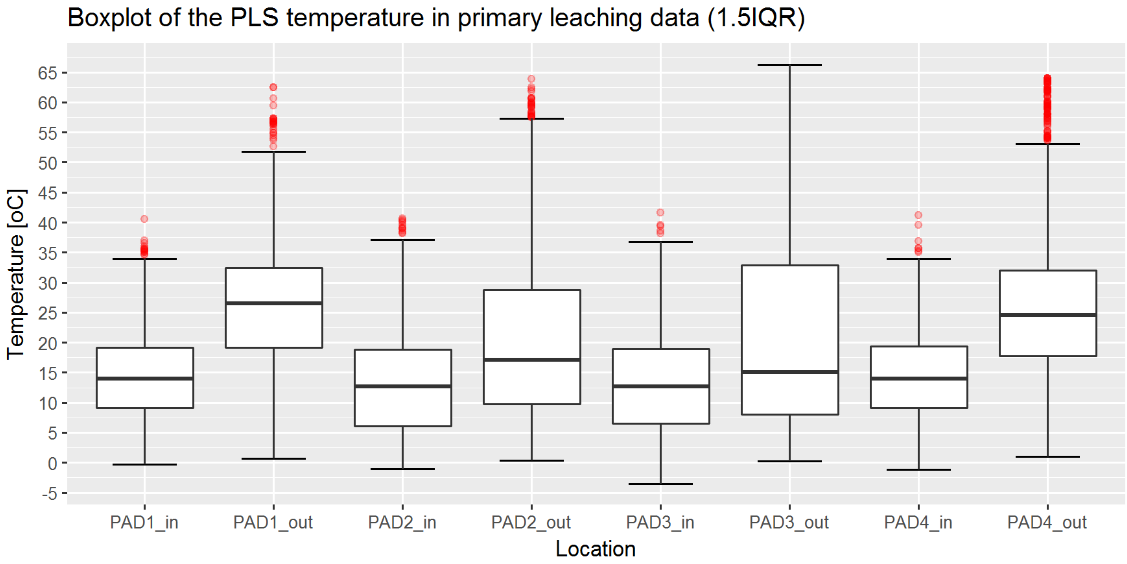

Figure 33. Boxplots of the PLS temperature in primary leaching stage with 1.5IQR tolerance applied.

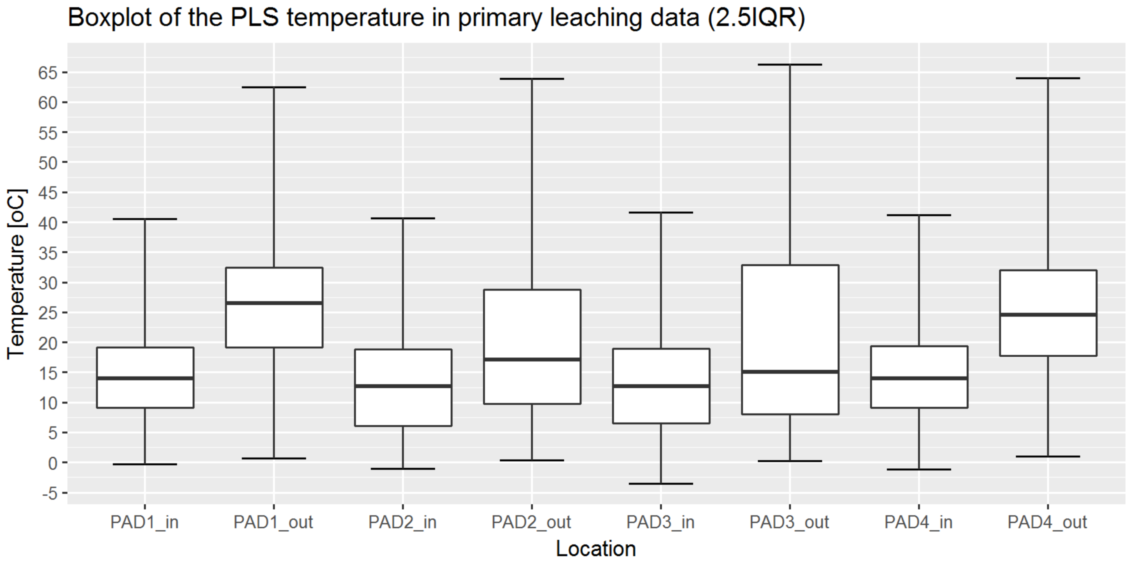

Figure 34. Boxplots of the PLS temperature in primary leaching stage with 2.5IQR tolerance applied.

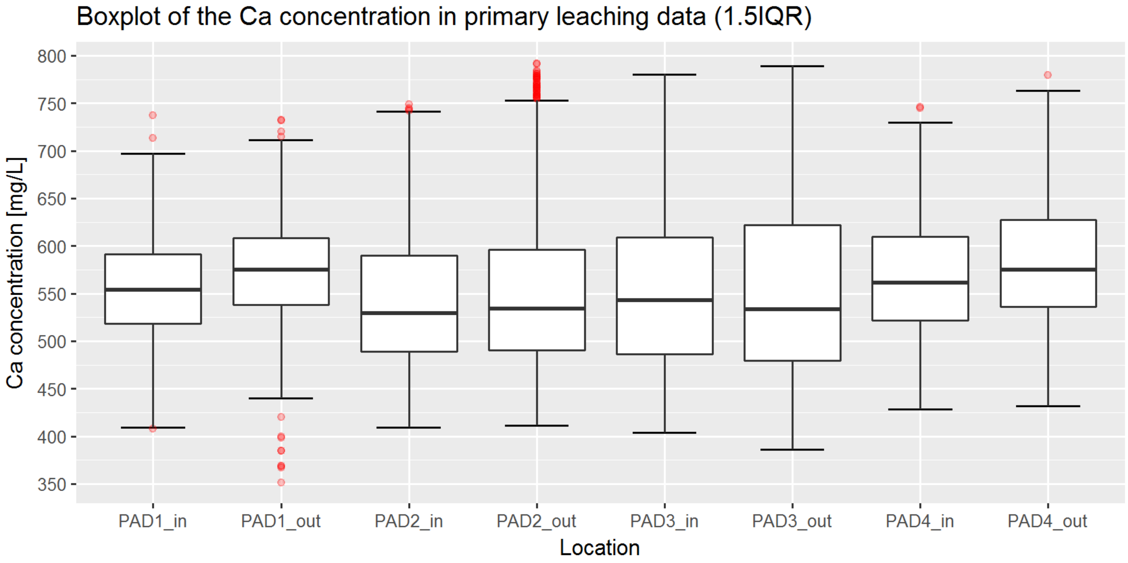

Figure 35. Boxplots of the calcium concentration in primary leaching data with 1.5IQR tolerance applied.

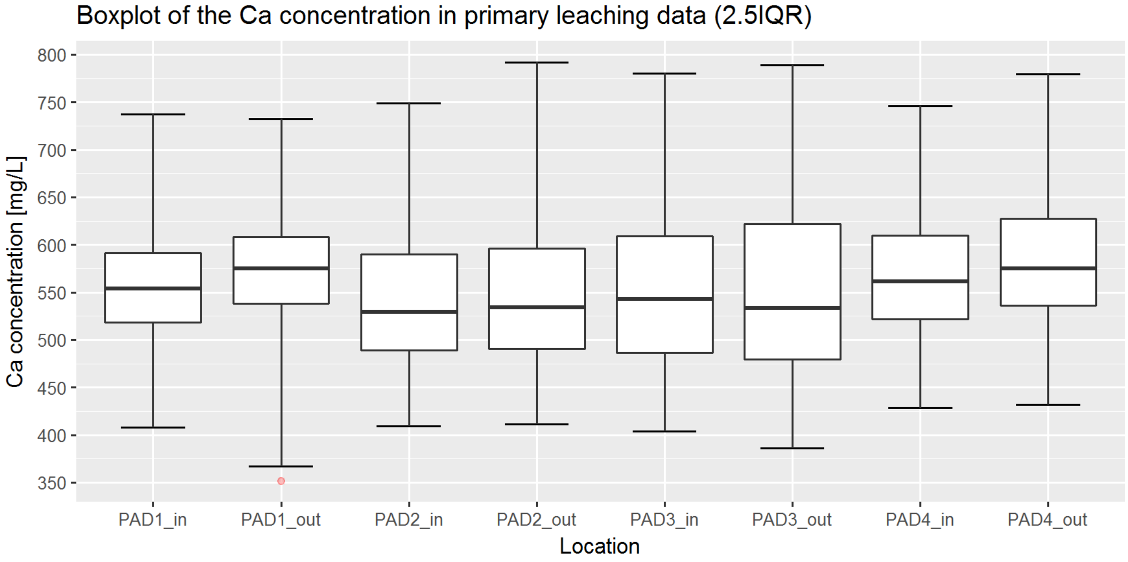

Figure 36. Boxplots of the calcium concentration in primary leaching data with 2.5IQR tolerance applied.

Basic statistics of every analyzed variable in the data set were calculated, but due to confidentiality, these values cannot be published. For the full data set, the standard deviation of calcium ions concentration was calculated to be 66. This means that most of the values are concentrated around the mean. There was a large standard deviation observed for iron ions of over 4 000, informing about significant variability in the data. Similar observation has been made for the aluminum, magnesium, manganese and zinc ions. When analyzing entire system, we are counting in data from different sampling points with dissimilar characteristics (such as primary and secondary stages of leaching). This is the reason why large variability can be observed in some of the data. Nonetheless, such information gives a good insight into how the entire system operates and what the possible values are.

For the primary leaching data, we observe similar dependencies since most of the data came from this stage of production. In here, we can see a similar situation as in the entire dataset with some differences. Calcium has a little larger variation – standard deviation is equal to 69.5 – and the iron concentration observations are again the most scattered.

5.3.2. Correlation analysis

Correlation between variables in the system is very strong for some pairs. Results of the correlation in the entire dataset, depicted in Figure 37 have shown that the most prominent dependency can be seen between concentrations of nickel and zinc. Both of those ions presented strong, positive relationships to the concentrations of cobalt, cadmium, and iron and a little weaker to manganese, magnesium, calcium and sodium, for which a correlation was negative. From the gypsum precipitation perspective, close attention should be paid to the relationships of calcium ions. As predicted previously, it is mostly dependent on the temperature of PLS. Strong correlations with iron, manganese, magnesium and a weaker, negative with aluminum ions are also visible. Moreover, a very weak negative dependency between the pH value and other ions have also been noticed.

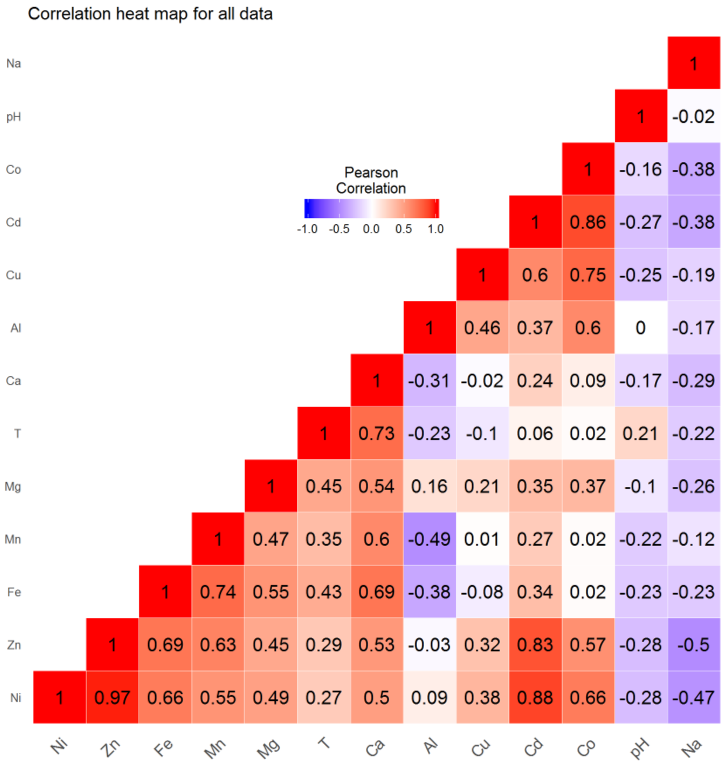

Figure 37. Correlation heat map of all process data. Values in boxes represent the Pearson's correlation coefficient value, based on 28640 observations, with corresponding shades applied.

Correlation of observations from the primary leaching stage showed slightly different and more concise results due to less noise. From Figure 38 we can observe that zinc and nickel still hold the tightest correlation value. Both of those ions presented strong, positive relationships to the concentrations of Cd, Fe and Co and a little weaker to Mn, Mg, Ca and temperature. Again, close attention should be paid to the correlation of calcium ions. The highest value of Pearson's coefficient has been identified for the calcium – temperature pair. Strong correlations with iron, manganese, magnesium and a weaker, negative with aluminum and sodium ions are also visible.

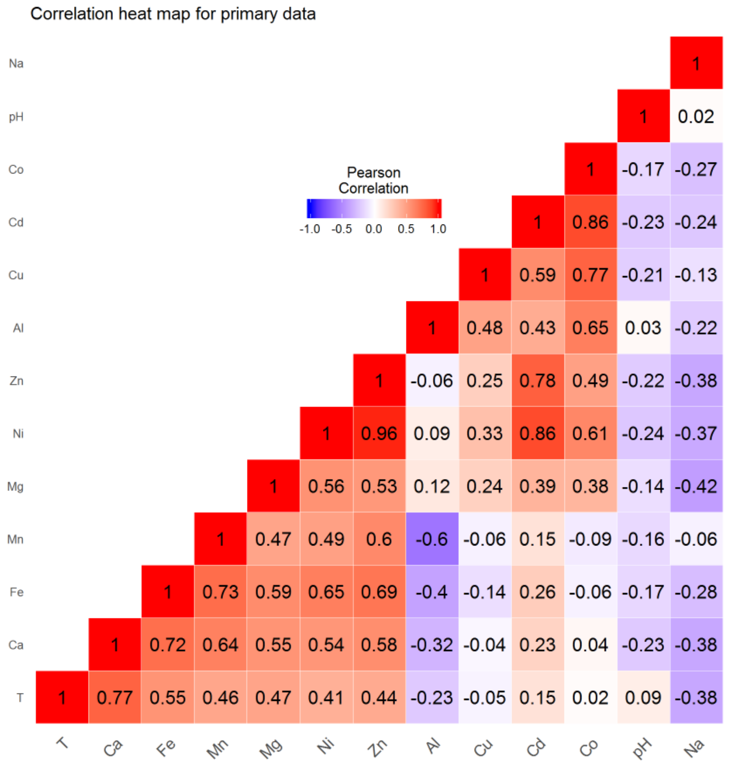

	T	Ca	Fe	Mn	Mg	Ni	Zn	Al	Cu	Cd	Co	pH	Na
Na													1
pH												1	0.02
Co											1	-0.17	-0.27
Cd										1	0.86	-0.23	-0.24
Cu									1	0.59	0.77	-0.21	-0.13
Al								1	0.48	0.43	0.65	0.03	-0.22
Zn							1	-0.06	0.25	0.78	0.49	-0.22	-0.38
Ni						1	0.96	0.09	0.33	0.86	0.61	-0.24	-0.37
Mg					1	0.56	0.53	0.12	0.24	0.39	0.38	-0.14	-0.42
Mn				1	0.47	0.49	0.6	-0.6	-0.06	0.15	-0.09	-0.16	-0.06
Fe			1	0.73	0.59	0.65	0.69	-0.4	-0.14	0.26	-0.06	-0.17	-0.28
Ca		1	0.72	0.64	0.55	0.54	0.58	-0.32	-0.04	0.23	0.04	-0.23	-0.38
T	1	0.77	0.55	0.46	0.47	0.41	0.44	-0.23	-0.05	0.15	0.02	0.09	-0.38

Figure 38. Correlation heat map of the primary leaching process data. Values in boxes represent the Pearson's correlation coefficient value, based on 19339 observations, with corresponding shades applied.

5.3.3. Calcium concentration data

The analysis performed so far was based on the data obtained by two owners of the mine site. This implies few interpretation difficulties such as a significant difference in the process efficiency which can be depicted in the change of temperature exiting the system (depicted in Figure 39). Moreover, the old data has less reliability due to change in ownership and personnel. Therefore, further analysis was based on data collected since acquisition by Terrafame Group in August 2015.

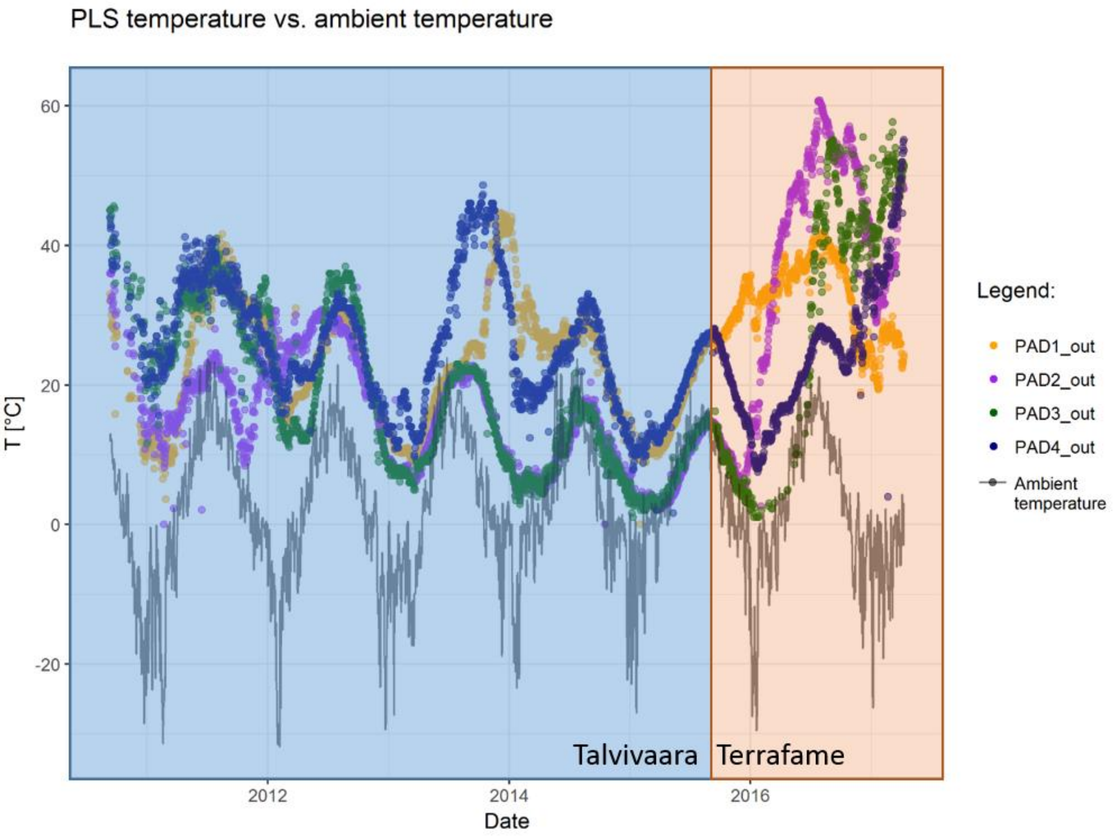

Figure 39. Ambient temperature obtained from the weather station in Sotkamo (~ 20 km NE from the site) and relationship to PLS temperatures in the outflow from the heaps. The distinction between two mine owners indicated on the graph.

Since the PLS circulation system is mostly exposed to the external factors such as weather conditions, a tight correlation between the ambient temperature and the temperature of PLS in irrigation ponds can be expected. The values from irrigation ponds 3 and 4 were set against the average daily ambient temperature, obtained from the weather station in Terrafame.

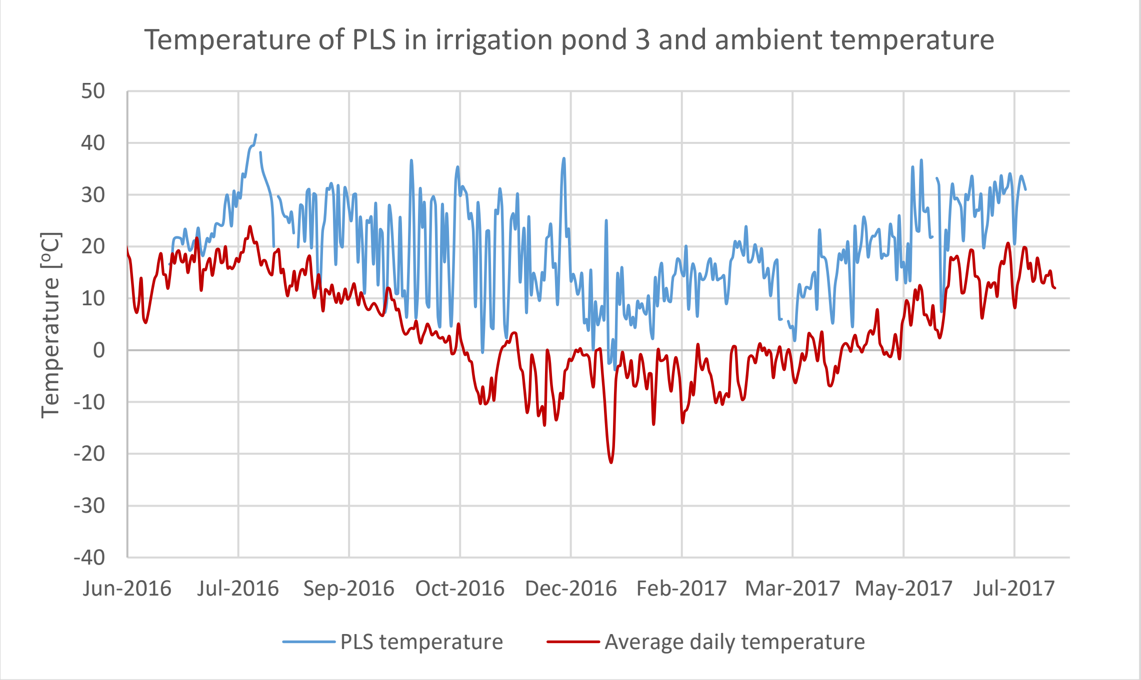

Figure 40. PLS temperature in the irrigation pond 3 and the average ambient temperature.

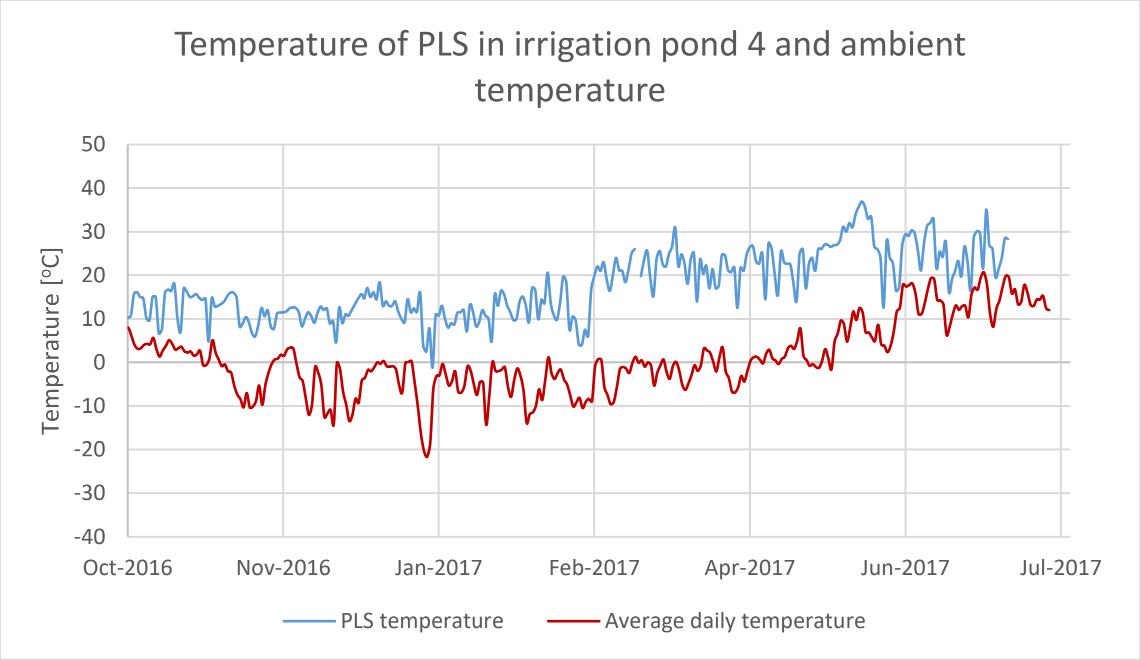

Figure 41. PLS temperature in the irrigation pond 4 and the average ambient temperature.

Figure 40 and Figure 41 both represent such relationship. It can be clearly seen that the PLS temperature follows the ambient conditions. Nevertheless, significant variation in the PLS temperature in irrigation pond 3 has been observed for the second half of 2016. After that incident, the temperature of PLS follows the outside temperature. For the irrigation pond 4 there has been less variation observed and generally those two variables are tightly connected. When describing such relationship, it should be kept in mind that irrigation ponds are fed with PLS from various sources and thus temperature variations can be expected; however, the incident in the second half of 2016 was unexpected.

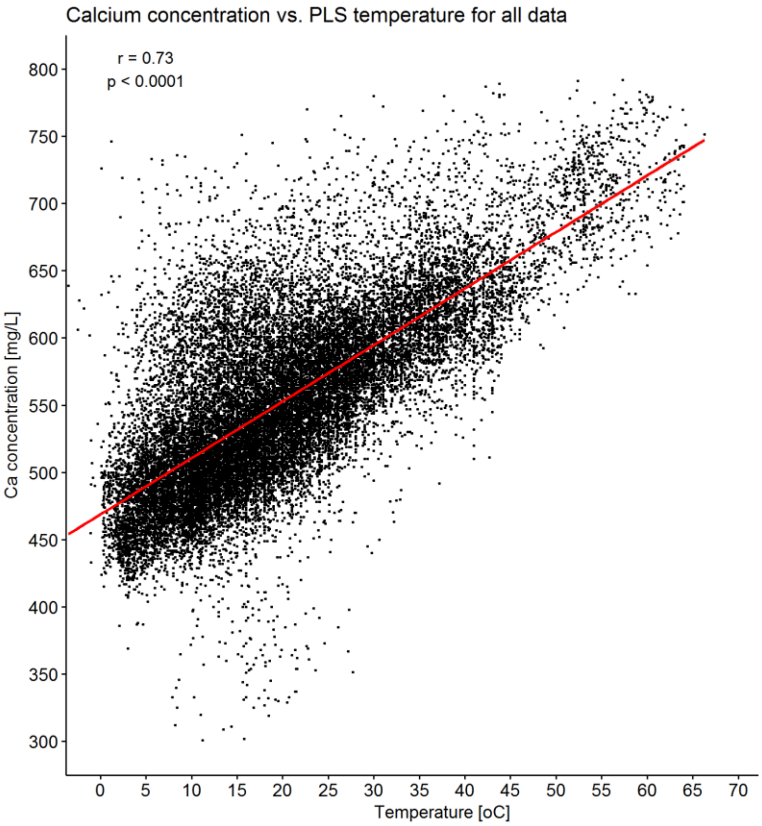

Figure 42. Calcium concentration relationship to the PLS temperature for all process data. Regression line indicated with a red color; Pearson's coefficient and p-value in top left corner.

Calcium concentration has been plotted against the PLS temperature value in Figure 42. The Linear regression line has been fitted to the data with previously determined Pearson's correlation coefficient $r = 0.73$ and the p-value lower than 0.05, indicating statistical significance of this regression. We can observe that the distribution of observations above the regression line seems to be much more dispersed that below. However, for low temperatures we can see the inconsistency in calcium concentrations below that line.

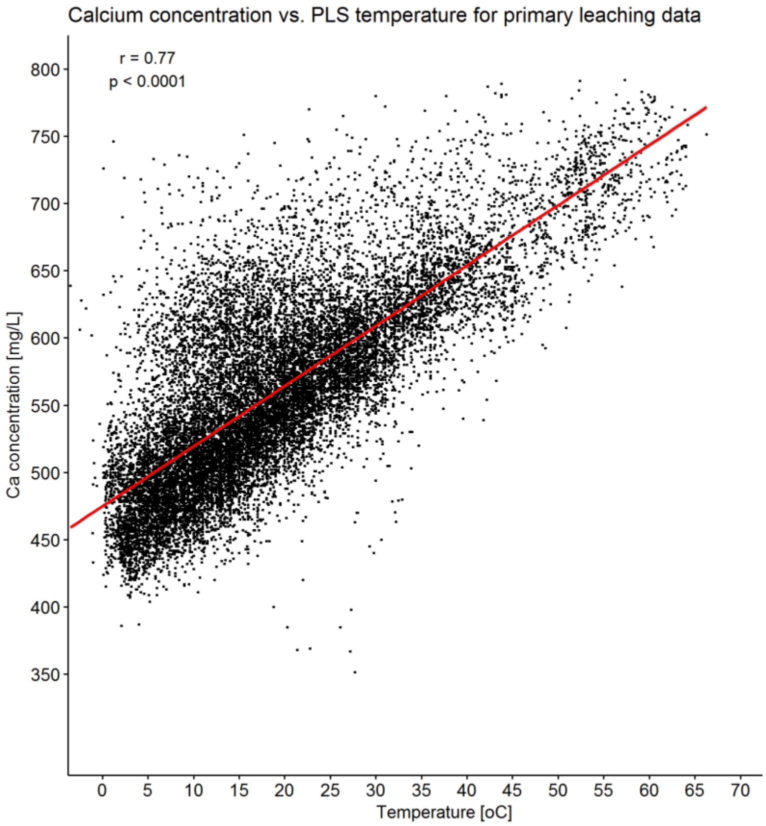

Figure 43. Calcium concentration relationship to the PLS temperature for primary leaching data. Regression line indicated with a red color; Pearson's coefficient and p-value in top left corner.

Calcium concentration has been plotted against the PLS temperature value in Figure 43. The Linear regression line has been fitted to the data with previously determined Pearson's correlation coefficient $r = 0.73$ and the p-value lower than 0.05, indicating statistical significance of this regression. We can observe that the distribution of observations above the regression line seems to be much more dispersed that below. However, for low temperatures we can see the inconsistency in calcium concentrations below that line.

The total concentration of other ions dissolved in the solution influence calcium concentration in the PLS (Figure 44). This tight trend has been observed for the leaching pad 4. Higher concentration of ions in solution translates to higher ionic strength. More ions present in the solution block other ions – in this case, calcium and sulfate – from interacting and thus creating crystalline forms. Therefore, we can observe this trend.

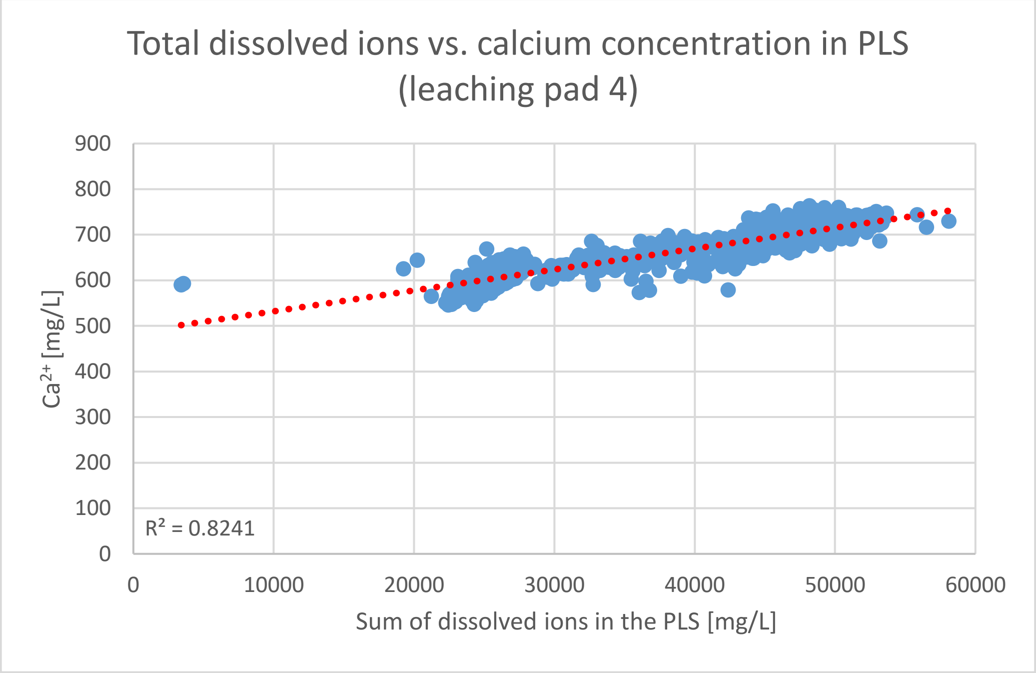

Figure 44. Total dissolved ions influence on calcium concentration in the solution (for leaching pad 4).

5.3.4. Operational data analysis

The operational data analysis included the drip line replacement logs, dates of the heap construction and the beginning of the irrigation as well as the history of flow rates in the system.

Firstly, all the information about the drip line replacements were used to estimate the average life time of one lateral. Most of the drip line replacements were logged for the leaching pad 3 and 4. These areas consist of the heaps having the new design and were built during the Terrafame's ownership thus close attention will be paid to those data points. Consecutively, the frequency of replacements was related to parameters of the solution such as temperature and calcium concentration in search for patterns promoting clogging phenomenon.

Table 8. Average drip lines lifetime on leaching pad 3. Values in italic represent an average lifetime of changed drip line on each heap. The last row represents average drip line lifetime per one hose change on all heaps; the last column represents average drip line lifetime on each heap.

Average lifetime (days)	**Drip line**							**Average lifetime per heap**
Location	1st	2nd	3rd	4th	5th	6th	7th	
Heap 1	*47*	*57*	*42*	*15*	*68*	*76*	*48*	**50**
Heap 2	*47*	*44*	*39*	*25*	*41*	*74*	*55*	**46**
Heap 3	*71*	*29*	*25*	*22*	*61*	*38*	*70*	**45**
Heap 4	*51*	*20*	*21*	*37*	*80*	*48*	*30*	**41**
Heap 5	*41*	*23*	*47*	*69*	*48*	*45*	-	**45**
Heap 6	*26*	*22*	*49*	*80*	*46*	*27*	-	**42**
Average lifetime per change	**47**	**33**	**37**	**41**	**57**	**51**	**51**	**All average: 45**

From Table 8 we can see that the overall average drip line lifetime was calculated to be 45 days for leaching pad 3. The shortest lifetime was noted for the 2nd and 3rd hose replacements which took place between August and November 2016. The longest run was noted during the 5th change and hoses lasted on average 57 days and happened between December 2016 and April 2017. However, it is important to recognize large differences in the drip lines lifetime, varying from 8 to over 80 days.

The analysis of data on leaching pad 4 was performed on a smaller number of observations because this is a younger heap and hoses replacement data were not yet produced. From Table 9 it can be concluded that the average drip line lifetime is 55 days. So far, this is 10 days longer than on the leaching pad 3 but might change as more data will be collected. The variation of data in this set was also observed. The first hoses on heaps 1 – 3 lasted for approx. 100 days whereas on heap 6 this period reduced almost by half. This phenomenon could be explained by the lag between construction and irrigation of the first and last heap (usually that period is 4 – 5 months) and thus different parameters under which those drip lines worked.

Table 9. Average drip lines lifetime on leaching pad 4. Values in italic represent an average lifetime of changed drip line on each heap. The last row represents average drip line lifetime per one hose change on all heaps; the last column represents average drip line lifetime on each heap.

Average lifetime (days)	**Drip line**			**Average lifetime per heap**
Location	1st	2nd	3rd	
Heap 1	*113*	*48*	*46*	**69**
Heap 2	*111*	*49*	*26*	**62**
Heap 3	*95*	*50*	*26*	**57**
Heap 4	*76*	*52*	*30*	**53**
Heap 5	*72*	*40*	-	**56**
Heap 6	*57*	*40*	*24*	**40**
Average lifetime per change	**87**	**47**	**31**	**55**

All drip line replacement events on leaching pad 3 were plotted in Figure 45 with their average lifetimes on X-axis. Moreover, the average daily temperature reading (from the weather station at Terrafame) was included. The lifetime decreased at the beginning until November 2016. After that, during the winter period, we can observe a rise in lifetime, until

February 2017. There is no clear correlation with the ambient temperature; however, the lifetime seems to be longer during the winter period. Currently, during summer when average ambient temperatures rose well above 0 °C, a decrease in the lifetime can be seen from the data.

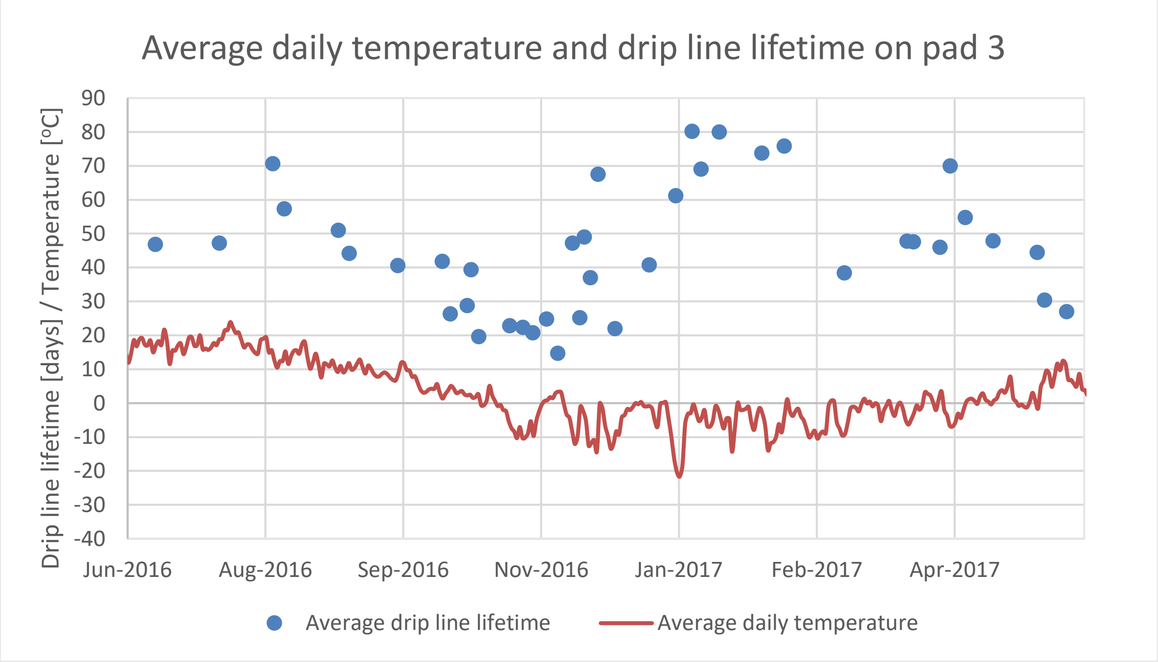

Figure 45. Average daily temperature and drip line lifetime on leaching pad 3.

Furthermore, both PLS temperature and calcium concentration were related to the hose replacement data. After the average lifetime was calculated, the average PLS temperature and calcium concentration during the runtime of each hose was calculated and the results plotted in Figure 46 and Figure 47. Unfortunately, there was no clear pattern observed, relating those parameters to the lifetime. However, some of the short living hoses were dealing with 15 – 20 °C PLS whereas the longer lasting ones were associated with lower temperatures.

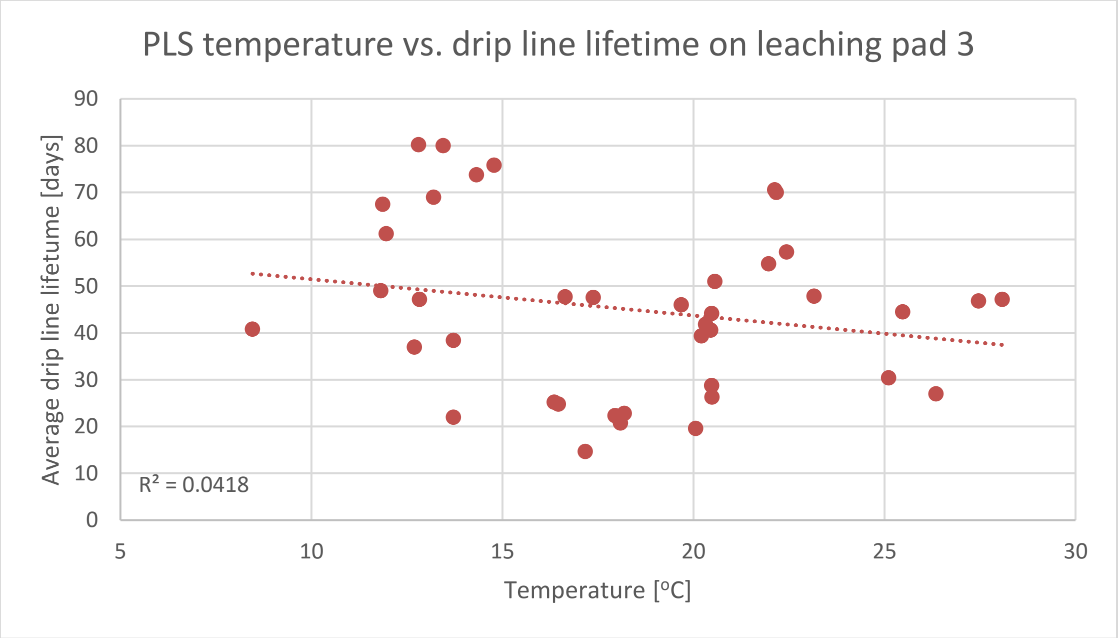

Figure 46. Average drip line lifetime on leaching pad 3 in relation to the average PLS temperature during the lifetime period of that drip line.

When looking at the relationship of average calcium concentration to the lifetime, again no clear conclusion can be drawn. Hoses can last either 80 days or 40 at similar calcium exposure. Nevertheless, it can be seen that very high calcium concentration (above 700 mg/L) was associated with much shorter lifetime. From the analysis of data collected from leaching pad 3 large variations were observed. No clear and viable correlations were observed; however, lower leachate temperatures, associated with the period of a year and ambient temperature seem to extend the lifetime of drip lines.

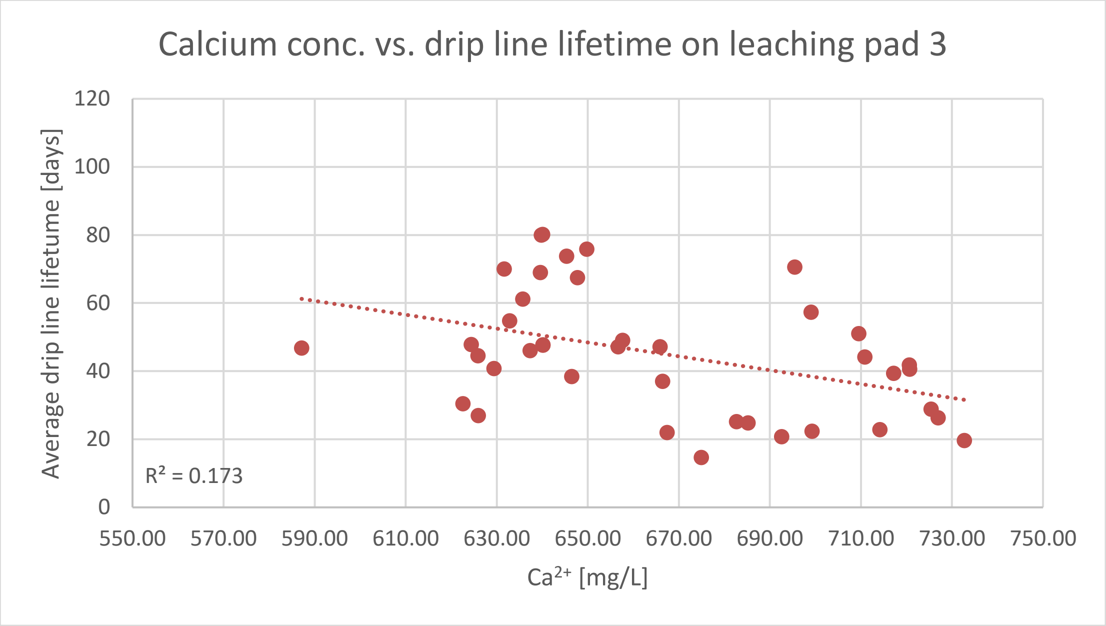

Figure 47. Average drip line lifetime on leaching pad 3 in relation to the average Ca^{2+} ions concentration in PLS during the lifetime period of that drip line.

All drip line replacement events on leaching pad 4 were plotted in Figure 48 with their average lifetimes on X-axis. Moreover, the average daily temperature reading (from the weather station at Terrafame) was included. From the analysis of this data set, a constant decrease of the lifetime in time can be observed. The relationship with the ambient weather could be that higher temperatures increase the likelihood of clogging. From Figure 48 we can read that the first drip lines, installed at the end of autumn, lasted for the longest time. This period decreased significantly for the hoses replaced at the end of the winter (they were exposed to higher ambient temperatures).

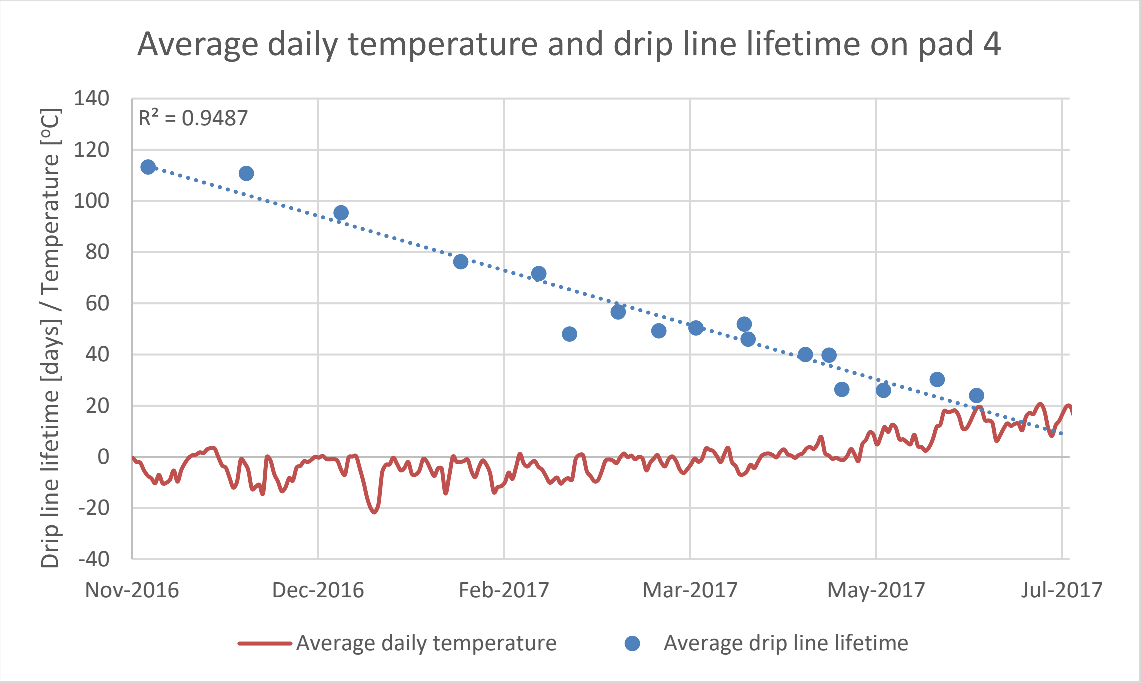

Figure 48. Average daily temperature and drip line lifetime on leaching pad 4.

A similar trend can be observed when relating the length of operation to the average temperature of PLS over that period (Figure 49). The most favorable temperature of leachate is around 10 – 15 °C, causing the drip lines to work for approx. 100 days. The increase of this temperature causes a constant decrease in the lifetime to approx. 25 days for 28 °C PLS.

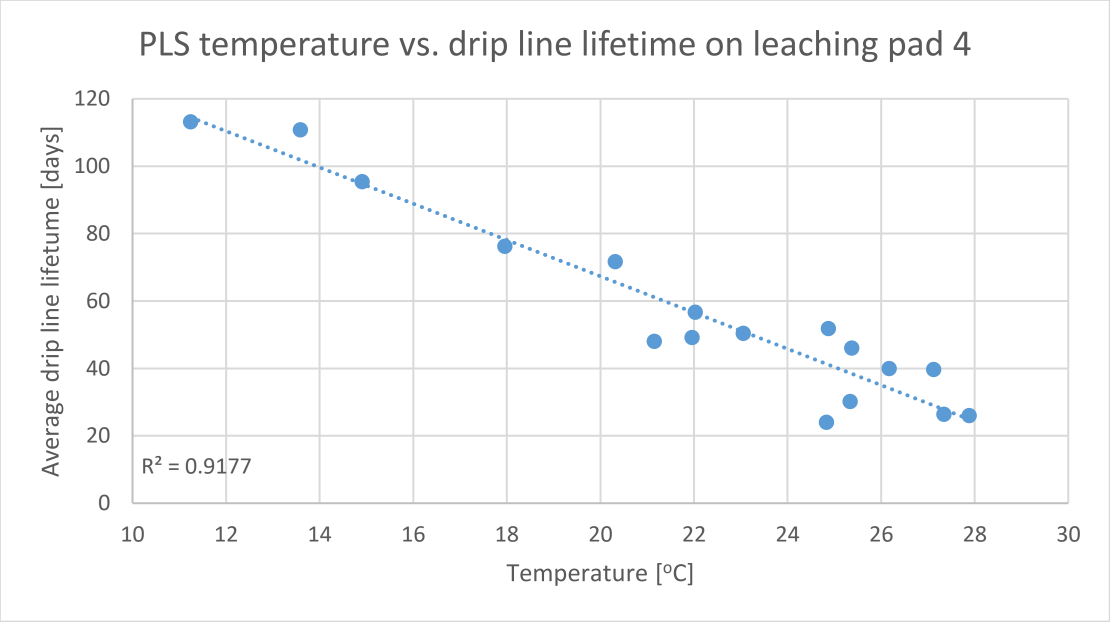

Figure 49. Average drip line lifetime on leaching pad 4 in relation to the average PLS temperature during the lifetime period of that drip line.

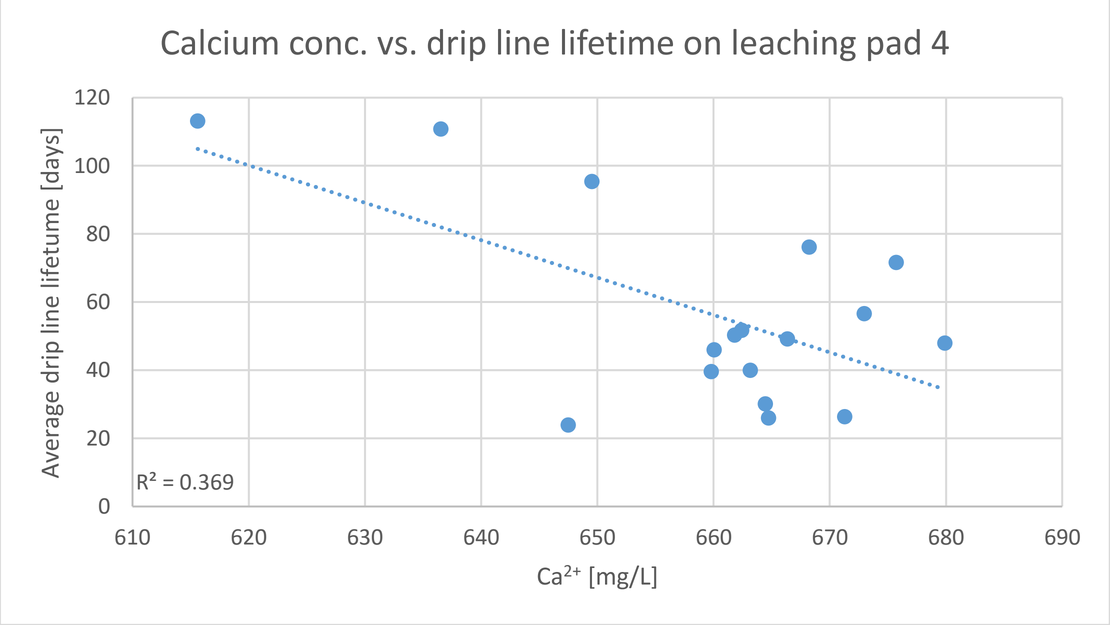

Figure 50 Average drip line lifetime on leaching pad 4 in relation to the average Ca^{2+} ions concentration in PLS during the lifetime period of that drip line.

Calcium concentration did not have as significant influence on the hoses as temperature (Figure 50) although, some mild correlation could be also seen. Increase in calcium concentrations caused the lifetime to decrease. It seems like concentrations below 650 mg/L of calcium ions caused the least clogging and lifetime was around 100 days; however, there is one value which fulfilled this condition, but hose lasted only for approx. 20 days.

5.4. Conclusions

Analysis of the process data revealed several important dependencies that helped with formulating the conclusions. Outliers' analysis is an important step during data analysis and should be done carefully, especially for process data bearing large variances and errors. For the purpose of this Thesis, a threshold value determining an outlier was set to 2.5IQR.

Calcium concentration is tightly connected to the PLS temperature. For the hot solution, we could observe high dissolved calcium content whereas, for a colder solution, the concentration was decreasing. Lower temperature forces calcium ions to precipitate, following the solubility curve, and due to large availability of sulfate ions (150 – 200 g/L) most likely those ions bond together, forming calcium sulfate. This correlation would suggest that heating circulating solution (or in this case preventing it from cooling down) would help to prevent calcium sulfate from precipitating. This is in contrary to the results obtained from correlating the drip line lifetime to the PLS temperature on leaching pad 4. The hoses were usable for the significantly longer period for a colder solution and with increasing temperature, that period decreased (tight linear correlation obtained). Similar results were obtained from leaching pad 3 data; however, variability in data was great thus there was no clear correlation obtained. Those results are in accordance with the conclusions obtained by Hoang *et al.* (2011) and described in Section 3.3.2. Another reason for a decrease in the drip lines lifetime could be related to the sulfide oxidation and the age of the heap. As the oxidation increases, it produces more acidity in a heap and influences the dissolution of Ca^{2+}. Furthermore, the number of ions dissolved in the solution determines the solubility of calcium sulfate – positive correlation.

6. Clogging control strategy

There is a clear need for the formulation of drip line clogging prevention strategy. After familiarizing with the production process in Terrafame, including bioleaching and metals recovery stages and in-depth process data analysis, a set of recommendations and solutions was created. The problem of gypsum precipitation within the irrigation system has been addressed from various angles.

6.1. Gypsum constituent influx control

Leachate circulation system was examined from the point-of-view of gypsum constituents addition. The primary sources of calcium were found both within the ore's mineral composition and metals recovery process. Bioleaching of the sulfide minerals generates large amounts of sulfur and sulfate. Additionally, sulfate is introduced along with the pH control, done by addition of sulfuric acid. The process of metals recovery requires different acidity levels for precipitating targeted metals. This creates the need for increasing the pH of the solution and is done by adding lime stone and milk of lime. Currently, due to the ramp-up, it is predicted that the value of calcium added to the process will double. Furthermore, during the pre-neutralization stage in the metals recovery process, a large amount of gypsum is formed, containing valuable metals within its structure. This material is sent for additional leaching at the secondary leaching stage. The total volume in the second quarter of 2017 was already exceeding 50 000 t of dry weight and is predicted to be over 100 000 t by the end of the year.

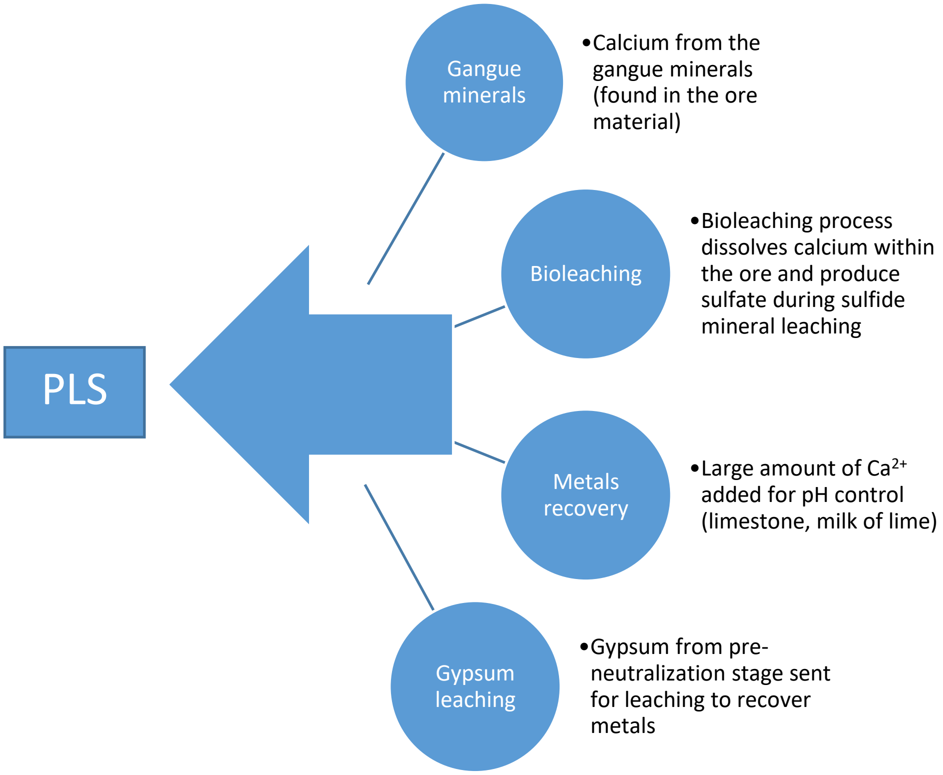

Figure 51. Main sources of calcium sulfate constituents in the system.

Eventually, calcium added to the system will make it to the solution sent to the irrigation system and might precipitate as calcium sulfate. The only way of decreasing this influx could be a separation of the leached gypsum from the pre-neutralization stage. Unfortunately, no other means of preventing calcium and sulfate addition to the system were identified. Both bioleaching and metals recovery are the most crucial stages of production and any changes to their functionality might bring negative effects to the metals production.

6.2. Reduction of calcium ions concentration

The constant influx of calcium sulfate constituents to the circulating solution leads to reaching the supersaturation state. The system balances the oversaturation of calcium ions by precipitating gypsum (due to the large availability of sulfate ions). Precipitation rate follows the solubility line of calcium sulfate which for the solution in Terrafame has been described previously. The PLS exiting leaching pads have high temperature and thus a high concentration of calcium ions. During its transportation, back to the irrigation ponds and distribution around the heaps, the temperature drops significantly. This induces precipitation of the excess calcium content. Therefore, for the efficient irrigation system operation, it is necessary to remove the excess amount of calcium from the solution and by doing that decrease gypsum formation.

6.2.1. Chemical precipitation

Chemical precipitation of calcium sulfate and its constituents have been identified as unfit for the Terrafame's process. Although there are several methods for chemical precipitation of calcium sulfate available, introducing a foreign chemical to the solution can have a negative effect on bacteria and thus on metals production. Additionally, the chemical added to the solution could have some negative environmental effects. Chemical precipitation methods generally involve entrapping the calcium ions in an insoluble form – making it easier for removal – by ion exchange. Nonetheless, the only chemical that could be added to the solution is calcium sulfate itself; it would work as seeds for the precipitation process described in the next section.

6.2.2. Physical precipitation

Precipitation of calcium sulfate can be based on changing the physical conditions of a solution such as the temperature or concentration of ions. Previous literature study and data analysis have shown that the solubility of calcium sulfate is mostly dependent on the temperature. The driving force for precipitation – supersaturation state – is present in the solution. There are several methods that could be used for the physical precipitation. Two of those methods are listed and described below.

a) Precipitation pond

Although gypsum is currently precipitating in the entire irrigation system, including PLS and irrigation ponds, the rate of that process is not sufficient. An approach is proposed to construct and use a special pond for precipitating gypsum and thus to counter the excess of calcium ions in the PLS. The general idea behind this solution is to decrease the temperature of the PLS and by doing that, shift the allowable calcium concentration downwards, defined by the solubility curve, forcing the precipitation. However, it is important to note that nucleation does not occur so quickly by just decreasing the temperature. Additional stirring and introduction of seeds should be delivered to speed up the crystallization process. Seeding can be done either by adding gypsum to the solution or sand (which could be more suitable for the process).

The total daily PLS volume, flowing through the primary irrigation system, is approx. 130 000 m^3. Within this volume, there is approximately 9 – 10 tons of calcium ions (assuming the average concentration of 700 mg/L). Processing the entire flow rate of the PLS is purely impossible due to a large amount of material and need for constant irrigation. Therefore, the pond should facilitate only a part of the total flow. Moreover, the residence time of the PLS treated in the precipitation pond should be extended so that more gypsum could be precipitated.

From the technical perspective, few issues should be addressed. First, an efficient system of precipitates removal is of importance. This step could be fulfilled by incorporating a special scraper, designed exclusively for ponds cleaning. The solid matter scraped from the bottom of the pond could be lifted upwards and deposited in a special ditch from which the precipitated material could be moved for further processing. Another approach could be to use a small sized dredger. This solution though would be viable only in a very large pond. Ideally, the precipitates are going to concentrate at the bottom of the pond and a sup-layer will form in the upper part. There, a special pipe should be fixed, connected to a pump that would suck in treated solution from the sup-layer and direct it back to the system.

b) Cooling tower

Cooling towers are tall structures, usually used in nuclear power plants for removing the waste heat and cooling process water. Cooling is done either by evaporation or air. Currently, the Finnish industrial machinery producer developed a forced-draught solution cooling tower which is focused on gypsum removal from process liquids. Pressurized solution is fed from the top of the tower through spray nozzles, with the cold air flow coming from the bottom. The air flow is generated by a fan located in the lower section of the tower. The cooled solution is collected at the bottom of the tower and directed to the thickener via a launder or special piping system. In the thickener, the solid precipitated material is removed via the underflow whereas overflow is redirected to the leachate circulation system as a treated solution. One cooling tower can process up to 750 m^3/h of the solution. The cooling fan power is from 15 – 110 kW (depending on the model). However, this equipment provides very high efficiency in gypsum removal and easy separation of solid matter from the liquid; it is a very expensive solution. The large capital expenditure on such equipment and need for additional thickeners would have a very long payback time, causing the investment to be unviable. Additionally, precipitated gypsum would probably contain a certain amount of valuable metals and thus needed to undergo further treatment. Unless using this solution will bring some substantial process optimizing benefits, it might be considered for the Terrafame process. Moreover, Outotec claims to have already built and launched several cooling towers around the world.

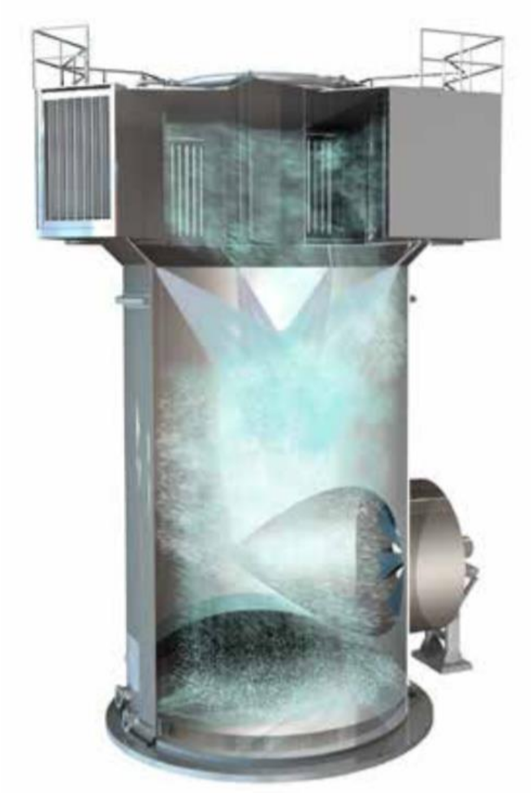

Figure 52. Outotec's forced draught cooling tower. Source: www.outotec.com

c) Dilution with water

Diluting the PLS with fresh water is by far the easiest and fastest way of reducing the mass concentrations of ions in the PLS. This technique brings immediate results; however, it cannot be treated as a permanent solution. Very little capital expenditures are needed to utilize this method as most of the pipework is already existing and is fully operational.

First, fresh water availability is limited. Currently, it is delivered either as water from the mining pit dewatering or from adjacent water reservoirs as raw water (partially contaminated with organic matter). Future developments of the mining pit will lead to partial dewatering of a lake (ore body is located underneath the lake) which will greatly contribute the availability of fresh water. Another aspect is, of course, the environmental concern that a lot of clean water will be contaminated. Diluting the PLS will bring down the concentration of calcium. However, it will only treat the symptoms but not cure the disease. The constant addition of fresh water will inevitably increase the overall volume of PLS, and it might happen that the system will reach its maximum capacity. Nevertheless, it is important to view this solution as one of the best means of preventing and controlling the clogging magnitude. Once the concentration of calcium reaches a certain value, in one of the irrigation ponds, the decision can be made to start pumping fresh water and dilute the feed, reducing the critical concentration and thus preventing excessive gypsum precipitation.

6.3. Process related solutions

Despite the techniques, listed in the previous section, clogging phenomena could be decreased by introducing few process related solutions.

6.3.1. Irrigation section design

Current irrigation system design was described in detail in Section 2.3. After combining the visual inspection of the clogging phenomena, backed with the experiences of the staff members (described in Section 3.4.2), the conclusion can be drawn that perhaps changing the dimensions of the irrigation cells could have a positive impact on decreasing the solution flow blockage due to gypsum formation. This solution assumes that the pressure head loss at the end of the irrigation cell is large, causing the decrease in flow rate; precipitates deposition is much more probable.

The new design of an irrigation section would include 4 irrigation cells. Therefore the length of one cell should be reduced from approx. 82 m to 41 m. Each of the cells should have its own connection to the main PLS delivery pipe. This will include additional pipes to be installed. The cost of this solution shouldn't be much higher than the operation of the old design cells as it only requires two additional sub-main pipes installed and the same number of additional valves on the main pipe – those elements can be cleaned and reused.

6.3.2. Alternative drip lines

The results of different drip lines tests showed that drip lines with cylindrical emitter performed best – Type B. However, the difference between Type B drip line and currently used was not so significant. The main difference between those two manufacturers is in the emitter design. Type B seems to have larger screening section compared to Azud. This means that more solution can enter to the emitter. Moreover, Type B drip line can also be produced with four exit orifices. This could effectively decrease the probability of fast clogging as there are more ways for the solution to exit. Nevertheless, it is recommended to build an entire irrigation cell with Type B drip line and compare its efficiency to Azud.

6.3.3. Solution temperature control

The temperature control of the solution is one of the steps that could be taken to decrease the calcium precipitation problem. However, increased PLS temperatures have been found to decrease the lifetime of drip lines, it is believed that overall higher PLS entry temperature is better for the bioleaching process. One of the reasons causing large precipitation in the system is the temperature drop of the solution. When it exits the heaps temperature is usually high, approx. 60 °C and by the time it reaches the irrigation cells drops down to approx. 20 °C in the summer and even lower during the winter time.

To prevent the PLS from losing the heat, several solutions could be implemented in the system:

a) pipeline insulation – insulating the pipes in which PLS is transported from the PLS ponds to the irrigation ponds and the main pipe to irrigation cells, will decrease the temperature loss along that way. Especially during the winter time when ambient temperature can be as low as –30 °C,

b) pond covers – covering the surface of ponds will decrease the overall heat loss of the PLS. There are many solutions available on the market for covering ponds. For instance, the American "Shade balls" or Danish "Hexa-Cover" floating plastic covers are easily applicable solutions for heat loss prevention on large ponds (Figure 53a and b).

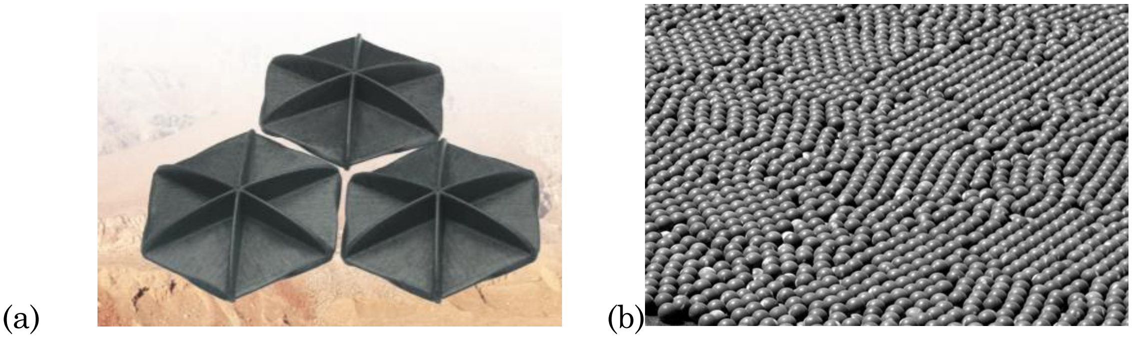

Figure 53. Floating pond covers: hexagonal (a) Hexa-Cover® and spherical (b) Shade Balls. Sources: (a) www.hexa-cover.dk; (b) www.shade-balls.com.

Controlling thermal conditions of the PLS could be easily done by applying floating pond covers. These are easily installed and removed which gives a large flexibility in temperature control. This solution could bring a positive effect on decreasing gypsum precipitation in the drip lines. However, according to the analyzed data, it might also promote it as higher PLS temperatures were connected to shorter lifetime of drip lines. The key condition for applicability of this approach is a significant decrease in calcium concentration first and after that increasing the PLS temperature to boost the bioleaching process, especially during the winter period.

6.3.4. Pulsating pressure and dripline flushing

The positive effects of pulsating pressure on labyrinth emitter clogging have been confirmed by Zhang *et al.* (2017). The researchers compared the efficiency of the system with constant pressure head and pulsating one. Variation in the of the pressure values was approx. between 1 – 7 m and the frequency as follows from the Figure 54. The overall difference between two was that the emitters working under constant pressure head started to clog after 8th irrigation whereas pulsating pressure extended that period to 14th irrigation cycle. The overall criterion for clogging was a decrease of average flow to 75% of the initial flow. After the 15th irrigation, the average flow rate from constant pressure cells has reached the clogging criterion whereas for pulsating pressure it decreased to 92% – still operational.

However, the experiment involved examination of preventing plugging due to the presence of sand particles in solution and involved emitter type with low nominal discharge rate (design comparable to the one presented in Figure 25) it can be assumed that this type of solution could have a positive influence on removal the early signs of precipitation. Periodical pressure increase, cause the flow in emitter channel to be more turbulent, providing additional energy that can literally flush out solids through the emitter. Nevertheless, the correlation between flow rate and gypsum scale formation in pipe systems should be kept in mind (described in Section 3.3.2).

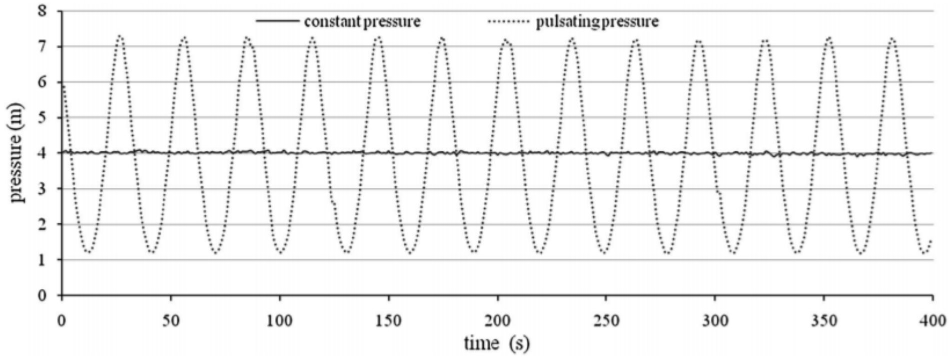

Figure 54. Irrigation pressure against time (solid line – constant pressure; dashed line – pulsating pressure), used in the experiment by Zhang et al. (2017).

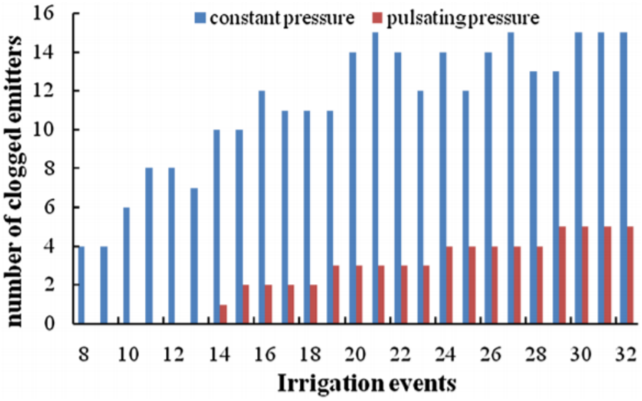

Figure 55. Comparison between the number of clogged emitters in relation to the number of irrigation events. Blue color – constant pressure, red color – pulsating pressure Zhang et al. (2017).

Conclusions from the research done by Zhang *et al.* (2017) suggests that incorporating such solution in the design of irrigation system at Terrafame could increase the average lifetime of the drip lines.

From the technical point-of-view, pulsating pressure could be delivered either by manual flow control (opening and closing valves) or by installing special valves on the connection between the main and sub-main pipes that deliver a solution to each irrigation cells. Such valves allow for pressure control in the cell as well as provide automated periodical flushing to the irrigation system. Currently, Netafim Company offers such solution for pressure control and automated flushing (Figure 56 and Figure 57).

Figure 56. On the left – battery operated control valve, on the right – programmable controller. Source: www.netafimusa.com

Flushing of the system should be firstly focused on removing the solids from the pipes; open the outflow valve from the irrigation cell and increase the inflow pressure – this will flush out all loose particles and possibly contribute to detachment of scale. After the pipes have been flushed, the pressure should be decreased to normal, outflow valve closed and the pulsating pressure should be introduced. The solution flow will push out solids through the labyrinth since the outflow from the cell is closed.

Figure 57. Netafim's flushing and pressure control valve installed on the sub-main pipe. Source: www.aquaroyalspring.com.

6.3.5. Solution management

Solution management is currently implemented in the company's structure. It is based on mixing the solution between ponds. Frequent monitoring of calcium concentration in various points of the system gives a good insight into the current situation. Once the particular level of calcium content is reached in one of the ponds, the decision can be made to start pumping the solution from another pond (with lower concentration). However, this solution might bring a negative effect. As it was seen previously in Figure 44, the ionic strength of solution has a direct impact on the concentration of calcium ions and thus calcium sulfate. Mixing of high ionic strength solutions with lower ionic strength solution might lead to decrease in gypsum's solubility instead of increasing it. Therefore, solution management should be performed carefully.

6.4. Molecular Oscillation Technology

The molecular oscillation technology is a relatively new way of water treatment. This solution doesn't impact the solution physically or chemically, but it incorporates so called, molecular or lattice oscillations (Barati *et al.*, 2014).

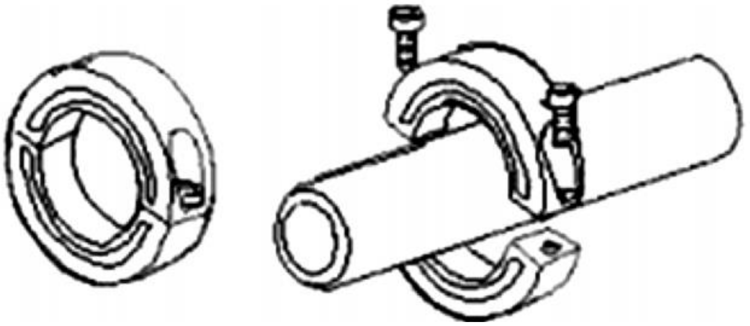

Figure 58. Installation of Merus ring on the pipe (Barati et al., 2014).

Every chemical element has its own molecular oscillation that compares to a human fingerprint. German company Merus, the manufacturer of the Merus ring depicted in Figure 58, claims to have isolated, recorded and stored the oscillations of elements. The ring itself influences the original oscillations that alter the physical properties of the targeted elements – for instance, calcium. This equipment operates solely on energy provided by the environment (warmth). Figure 59 shows the mathematical results of active oscillation interference with the fundamental oscillation of the substance. If those two oscillations have the same amplitude and are 180° phase-delayed, resulting oscillation will be zero (Figure 59a); however, once they are in-phase, resonance effect will occur (Figure 59b) (Barati *et al.*, 2014).

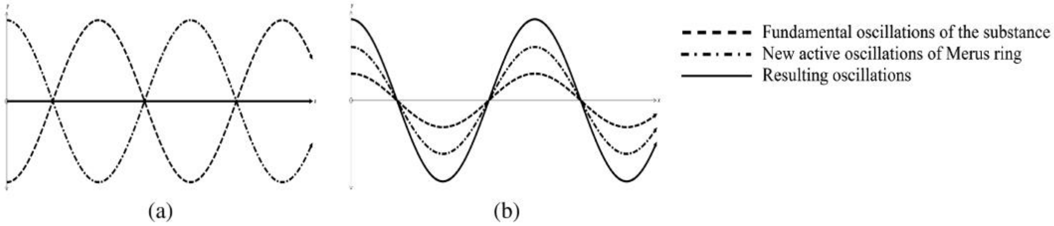

Figure 59. Effect of the molecular oscillation ring on substance fundamental oscillation (a) 180° phase-delayed, (b) in-phase (Barati et al., 2014).

Barati *et al.* (2014) experimentally tested the influence of Merus ring on emitter clogging by setting aside two systems: one with the ring and another without. The results of this study showed that application of the ring contributed to lower precipitation of Ca^{2+} in the emitters.

However, the theory behind this solution is very vague – company itself admits that it is not entirely understood by them – the positive effects on scale reduction from other plants are convincing. Given the low costs of purchase and operations, as well as simplicity in installation and no contact with the PLS, Merus rings should be considered for further testing at Terrafame.

6.5. Summary

Removal of calcium sulfate is inevitable as more and more of its constituents are introduced to the system due to ramp-up. Failing to do so will result in increased and faster precipitation in the irrigation system.

Dilution with clean water is the best short-term solution with an immediate effect on decreasing calcium concentration. Nevertheless, forced precipitation, either in ponds or cooling towers, is considered as the best long-term approach. Additionally, a set of operational techniques should be implemented that could possibly prolong the lifetime of drip lines (pulsating pressure, irrigation cell size decrease). Substituting existing drip lines with others could bring some positive results; the best way to assess this is by building a test irrigation cell with new drip line and comparing it with currently used.

7. Conclusions and recommendations

7.1. Conclusions

The objective of this project was to investigate causes of irrigation system blockages in the heaps bioleaching process, extend the knowledge about this phenomenon and ultimately propose a solution to counter it.

To answer the question of how does the production system work at Terrafame, full conceptual model of the site was created. Emphasis was put on the solution circulation routes as well as tracking of the gypsum constituents sources. Metal sulfides bioleaching process was found to produce sulfur and ultimately sulfate. The primary sources of calcium ions were found to be in the ore itself. However, the metals recovery stage also contributed to the addition of calcium significantly.

The solid matter found in the irrigation system was tested with the XRD and XRF – calcium sulfate dihydrate was identified as a primary precipitate. Gypsum solubility was then a critical parameter to check. Preliminary solubility tests showed that, on average, calcium concentration decreased by approx. 93 mg/L when solution was cooled down to 4 °C. The discrepancy in obtained results led to designing of a new approach, which should produce more concise results. Due to delay in the delivery of required equipment only initial trials were performed. The results showed positive effects on precipitating gypsum with seeds, in the form of anhydrite powder and agitation (decrease in Ca^{2+} ions concertation by 200 mg/L in 7-days). In the future, further tests should be carried out to produce better data.

Detailed analysis of the process data collected by Terradame revealed that calcium ions are well correlated with the leachate temperature. Based on that information rough solubility line was drawn. Moreover, total dissolved solids (TDS) showed a positive correlation with calcium concentration in leaching pad 4 data.

Lifetime of each hose was approximated to be from 45 to 55 days – based on hose replacement data. Leachate temperature and thus calcium concentration was found to have a tight correlation with the likelihood of drip line clogging. Hoses exposed to colder leachate exhibited a longer lifetime whereas warmer solution shortened the operational period. These findings are in contrary with the experiences of the staff. To confirm validity of this trend more data should be collected from the upcoming winter season.

Set of technical solutions was proposed to counter the clogging phenomena, backed with the literature study, visual observations and conceptual model of the site (not published in this work). The strategy of clogging control was proposed.

Firstly, the focus was put on gypsum removal from the solution. Physical precipitation was identified as safest and most efficient way to decrease calcium content in the solution. For an immediate decrease of calcium ions in the solution, dilution with clean water seems like best way to go. Nevertheless, in the long run, there is a need to remove calcium from solution. Gypsum precipitation in a specially designed pond or in cooling towers could be an option to consider. Both solutions have a high CAPEX and thus an extended payback period.

Along with the physical removal of calcium, a set of operational solutions should be incorporated. First, changing the pressure conditions in the irrigation cells could be benefitial. Drip lines flushing and using pulsating pressure was found to decrease the clogging of emitters. Higher periodical flow rates could break the structure of the precipitated gypsum (inside the emitter) and push it out, clearing the labyrinth pathway and allowing the solution to flow at a constant rate. Moreover, drip lines of different manufacturers should be tested furtherly; however, the differences in the design of emitters and drip lines are not great – cost can be a decisive factor. In addition to all the proposed solutions, molecular oscillation ring could be installed on one of the irrigation cells for testing; however, no significant effect should be anticipated.

The topic of emitter clogging due to gypsum precipitation in the biohydrometallurgical processes has not been studied in the literature. This report broadens the comprehension of this phenomenon found in the Terrafame process and sets a new direction to solve it. Although not all of the initial goals were achieved, this research identified weak points in the system and proposed viable solutions to counter it.

7.2. Recommendations

Recommendations for the future research are to test the solubility of gypsum in the PLS with the proposed methodology to establish the solubility line. Parallelly to these tests laboratory scale experiments as well as small scale field tests should be carried out regarding gypsum crystallization. The initial attempts made by the author exhibited positive effects on precipitating calcium sulfate in the seeded crystallization test. Having this set of data could be beneficial to look again at the correlation analysis and try to find better dependencies in the system. Furthermore, the solution should be tested and described in detail (exact composition, total solids, total dissolved solids, density, etc.). It would be beneficial for the entire operation to implement a particular software, dedicated for hydrometallurgical plants – OLI Software.

From an operational point-of-view, solution testing methodology should be changed to obtain better and more reliable data. Firstly, the PLS temperature should be tested at the collection location – for instance inside the sampling well instead of from the bottle, after collection. Secondly, it should be considered if data obtained from sampling, calcium concentration specifically, can be used as a viable source of assessing calcium sulfate solubility. As it was stated in this work, there is a tight correlation between temperature and solubility of gypsum. Between sampling and delivery to the laboratory, thermal conditions in which samples are present change drastically and that could drastically change dissolved calcium content in the sample.

Appendix A

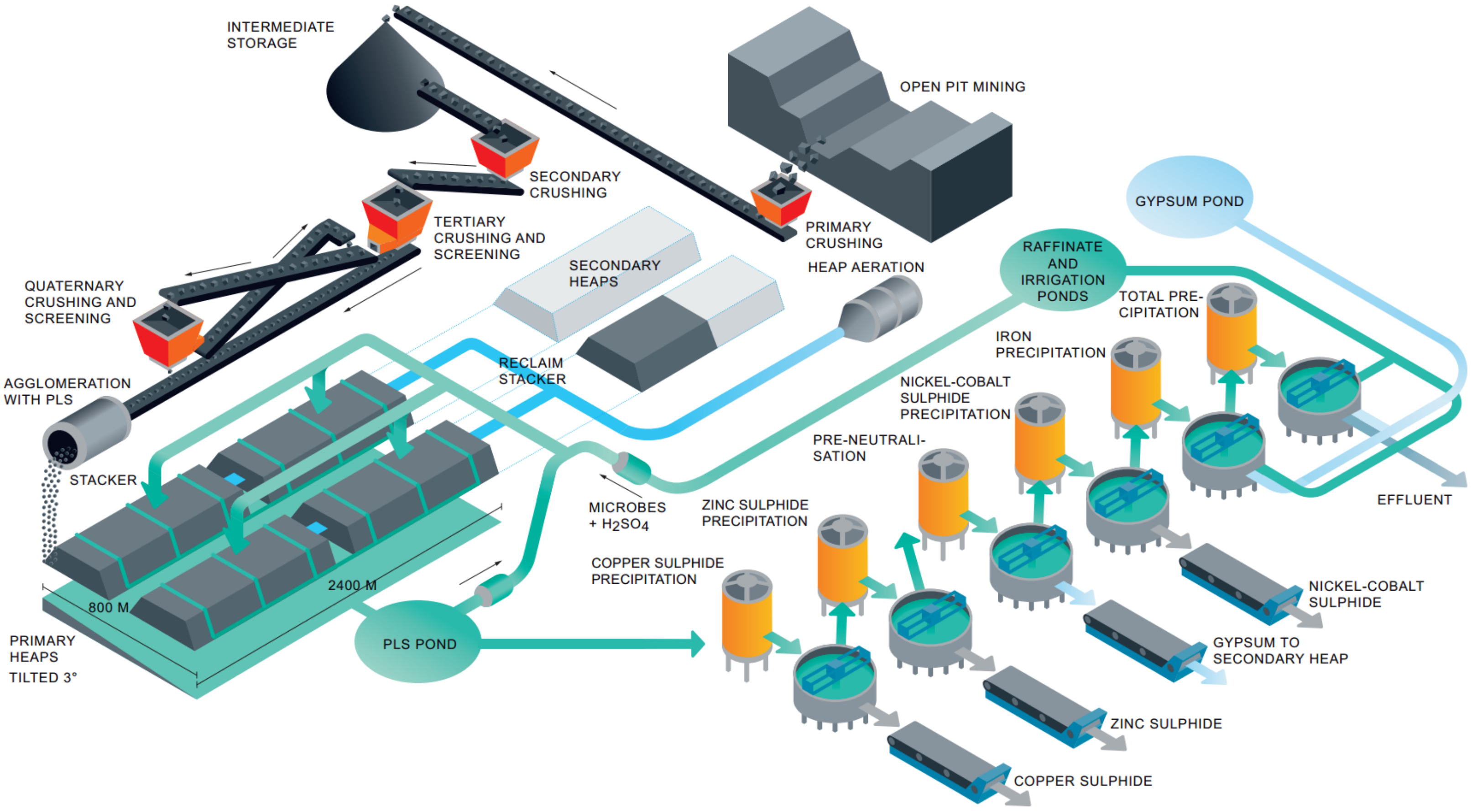

Figure 60. Terrafame production flowchart. Source: Terrafame Oy.

Appendix B

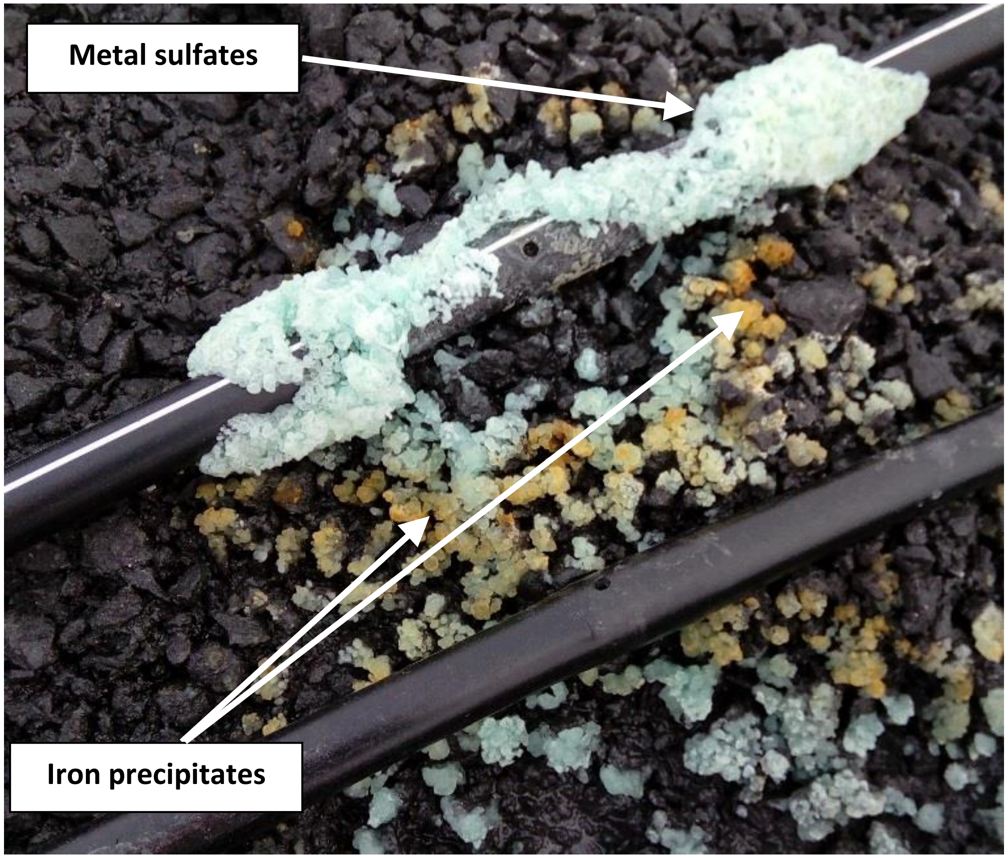

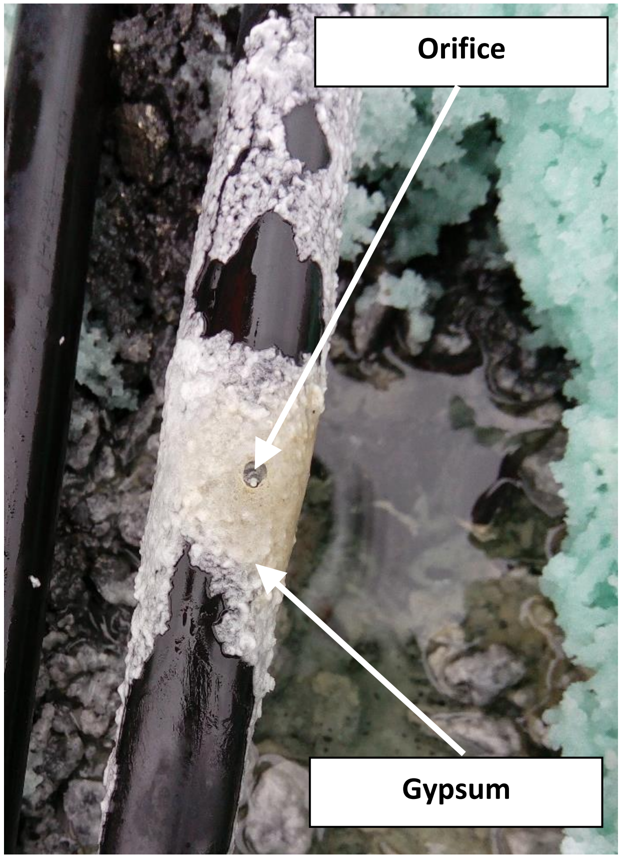

Appendix C

7 days old emitter

No significant precipitation in the labyrinth path

Blocked flow at the orifice by thin ”wall” of gypsum

~14 days old emitter

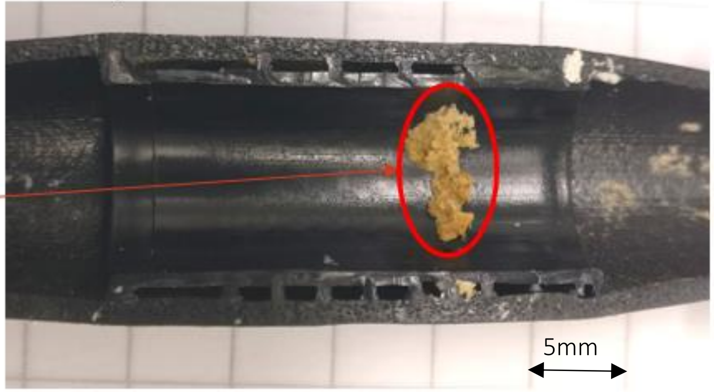

Emitter entry point blocked

Old emitter

Appendix D

SELF-EVALUATION

The work performed during this Master's Thesis project involved studying and understanding several different topics.

Conceptual model

First stage of this project involved creating a conceptual model of the site to fully understand all process associated with the production. The following topics were studied:

Fundamentals of bioleaching on heaps were studied:

- ✓ unsaturated flow conditions
- ✓ redox chemistry of sulfides leaching
- ✓ bacterial growth

Production system:

- ✓ desk study (PLS flow tracking, production processes)
- ✓ field study (field observations, obtaining information from the staff)

Data analysis

This knowledge allowed for appropriate comprehension of the process data which were exported from Terrafame's database. To process such large amount of data, author had to use the R programming language. This task involved learning the language itself and linked software. Having acquired the skill of data manipulation in R, statistical analysis of the data was performed. Such analysis has never been done in the company and was very helpful for further problem formulation. Moreover, costs calculation of hoses replacements was performed (not published in this work).

Gypsum precipitation study

Field study:

- ✓ collection of solid samples from the irrigation system
- ✓ collection of drip lines and stripping the emitters to observe how the precipitates form
- ✓ field observations

Desk study:

- ✓ precipitation from solutions (theory study)
- ✓ literature study on gypsum solubility in hydrometallurgical processes
- ✓ literature review of gypsum scaling in pipe flows

Solubility experiments:

- ✓ gypsum solubility experiment design
- ✓ gypsum seeded crystallization experiment design

Gypsum control strategy:

- ✓ review of the technical solutions to remove gypsum from solutions
- ✓ design of the conceptual gypsum precipitation pond

- ✓ proposed set of work related improvements that could be inexpensively incorporated in the system (irrigation cell redesign, pulsating pressure, drip lines flushing)

Results obtained during this research project were very helpful for the company and lead to setting a new direction towards effective countering of the clogging problem. However, the precipitation of gypsum from Terrafame solution should be described more accurately, incorporating the state-of-the-art science.

Bibliography

Anderko, A., Wang, P., & Rafal, M. (2002). Electrolyte solutions: from thermodynamic and transport property models to the simulation of industrial processes. *Fluid Phase Equilibria, 194*, 123-142.

Ang, M., Muryanto, S., & Hoang, T. (2011). Gypsum scale formation control in pipe flow systems: A systematic study on the effects of process parameters and additives.

Appelo, C. A. J., & Postma, D. (2005). *Geochemistry, groundwater and pollution* (2nd ed. ed.). Leiden ;: Balkema.

Azimi, G., & Papangelakis, V. G. (2010). Thermodynamic modeling and experimental measurement of calcium sulfate in complex aqueous solutions. *Fluid Phase Equilibria, 290*(1), 88-94.

Azimi, G., Papangelakis, V. G., & Dutrizac, J. E. (2007). Modelling of calcium sulphate solubility in concentrated multi-component sulphate solutions. *Fluid Phase Equilibria, 260*(2), 300-315.

Azud Sistema S.A. (2017). Azud Drip catalog.

Barati, K., Mostafazadeh-Fard, B., & Sheikhbahaei, A.-A. (2014). Molecular Oscillation Technology: New Phenomenon to Reduce Emitter Clogging in Trickle Irrigation. *Journal of Irrigation and Drainage Engineering, 140*(11).

Bartlett, R. W. (1997). Metal extraction from ores by heap leaching. *Metallurgical and Materials Transactions B, 28*(4), 529-545.

Campbell, A. N., & Yanick, N. S. (1932). The system NiSO4—CaSO4—H2O. *Trans. Faraday Soc., 28*, 657-661.

Cox, V. (2017). *Translating statistics to make decisions : a guide for the non-statistician*

Dasberg, S., & Or, D. (1999). *Drip Irrigation*. Berlin, Heidelberg: Springer Berlin Heidelberg.

Dohring, H., & Dixon, J. (2012). *Precipitation: Prediction, Formation and Environmental Impact*. Hauppauge, UNITED STATES: Nova Science Publishers, Inc.

Donati, E. R., & Sand, W. (Eds.). (2007). *Microbial processing of metal sulfides* (Vol. 130): Springer.

Dutrizac, J. E. (2002). Calcium sulphate solubilities in simulated zinc processing solutions. *Hydrometallurgy, 65*(2), 109-135.

Fitts, C. R. (2013). *Groundwater science* (Second edition. ed.). Waltham, MA ;: Academic Press is an imprint of Elsevier.

Free, M. (2013). *Hydrometallurgy : fundamentals and applications*. Hoboken, New Jersey: Wiley.

Havli□k, T. (2008). *Hydrometallurgy : principles and applications*. Cambridge: Woodhead Publishing Ltd.

Hoang, T. A., Ang, H. M., & Rohl, A. L. (2008). Effects of temperature on the scaling of calcium sulphate in pipes. *Powder technology., 179*(1), 31.

Hoang, T. A., Ang, H. M., & Rohl, A. L. (2011). Effects of Process Parameters on Gypsum Scale Formation in Pipes. *Chemical Engineering & Technology, 34*(6), 1003-1009.

Karmeli, D. (1977). Classification and flow regime analysis of drippers. *Journal of Agricultural Engineering Research, 22*(2), 165-173.

Lewis, A. E. (2010). Review of metal sulphide precipitation. *Hydrometallurgy, 104*(2), 222-234.

Liu, H., & Huang, G. (2009). Laboratory experiment on drip emitter clogging with fresh water and treated sewage effluent. *Agricultural Water Management, 96*(5), 745-756.

Lu, N., & Likos, W. J. (2004). *Unsaturated soil mechanics*. New York :: Wiley.

Nakayama, F., & Bucks, D. (1981). Emitter clogging effects on trickle irrigation uniformity. *Transactions of the ASAE, 24*(1), 77-0080.

Nakayama, F. S., & Bucks, D. A. (1991). Water quality in drip/trickle irrigation: A review. *Irrigation Science, 12*(4), 187-192.

Petersen, J. (2010). Modelling of bioleach processes: Connection between science and engineering. *Hydrometallurgy, 104*(3), 404-409.

Petersen, J., & Dixon, D. G. (2007). Modelling zinc heap bioleaching. *Hydrometallurgy, 85*(2–4), 127-143.

Qingsong, W., Gang, L., Jie, L., Yusheng, S., Wenchu, D., & Shuhuai, H. (2008). Evaluations of emitter clogging in drip irrigation by two-phase flow simulations and laboratory experiments. *Computers and Electronics in Agriculture, 63*(2), 294-303.

Ravina, I., Paz, E., Sofer, Z., Marcu, A., Shisha, A., & Sagi, G. (1992). Control of emitter clogging in drip irrigation with reclaimed wastewater. *Irrigation Science, 13*(3), 129-139.

Rawlings, D. E., & Johnson, B. D. (2007). *Biomining*. Berlin: Springer.

Riekkola-Vanhanen, M. (2013). Talvivaara mining company - From a project to a mine. *Minerals Engineering, 48*, 2-9.

Rohwerder, T., Gehrke, T., Kinzler, K., & Sand, W. (2003). Bioleaching review part A. *Applied Microbiology and Biotechnology, 63*(3), 239-248.

Ryan, P. C. (2014). *Environmental and low temperature geochemistry*

Saari, P., & Riekkola-Vanhanen, M. (2012). Talvivaara bioheapleaching process. *Journal of the Southern African Institute of Mining and Metallurgy, 112*(12), 1013-1020.

Savva, A., & Frenken, K. (2001). Irrigation manual: planning, development, monitoring and evaluation of irrigated agriculture with farmer participation. Vol. 3, module 8. Sprinkler irrigation systems: planning, design, operation and maintenance. *Sprinkler irrigation systems: planning, design, operation and maintenance., Vol. 3, module 8.*

Schwertmann, U. (1991). Solubility and dissolution of iron oxides. *Plant and Soil, 130*(1), 1-25.

Taylor, H., Bastos, R., Pearson, H., & Mara, D. D. (1995). Drip irrigation with waste stabilisation pond effluents: Solving the problem of emitter fouling. *Water Science and Technology, 31*(12), 417-424.

USGS. (2016). Irrigation techniques. Retrieved from https://water.usgs.gov/edu/irmethods.html

Uys, W., Koegelenberg, F., & Engineering, A. R.-I. f. A. (2000). *The performance and care of drip irrigation emitters*. Silverton, South Africa: ARC-Institute for Agricultural Engineering.

Wagman, D. D., United, S., & National Bureau of, S. (1982). *The NBS tables of chemical thermodynamic properties : selected values for inorganic and Cb1s and Cb2s organic substances in SI units*. New York: Published by the American Chemical Society and the American Institute of Physics for the National Bureau of Standards.

Wang, W., Zeng, D., Yin, X., & Chen, Q. (2012). Prediction and Measurement of Gypsum Solubility in the Systems CaSO4+ HMSO4+ H2SO4+ H2O (HM = Cu, Zn, Ni, Mn) at 298.15 K. *Industrial & Engineering Chemistry Research, 51*(14), 5124-5134.

Watkinson, A., & Martinez, O. (1975). Scaling of heat exchanger tubes by calcium carbonate. *ASME J. Heat Transfer, 97*, 504-508.

Wollmann, G., & Voigt, W. (2008). Solubility of gypsum in MSO4 solutions (M = Mg, Mn, Co, Ni, Cu, Zn) at 298.15 K and 313.15 K. *Journal of Chemical and Engineering Data, 53*(6), 1375-1380.

Zeng, D., & Wang, W. (2011). Solubility phenomena involving CaSO4 in hydrometallurgical processes concerning heavy metals. *Pure and Applied Chemistry, 83*(5), 1045.

Zhang, L., Wu, P., Zhu, D., & Zheng, C. (2017). Effect of pulsating pressure on labyrinth emitter clogging. *Irrigation Science, 35*(4), 267-274.